Department of Biotechnology, Chemistry and Pharmacy

University of Siena

DOCTORAL THESIS IN

Biochemistry and Molecular Biology

Cycle XXXVI

Title of thesis

Identification of molecules acting as inhibitors of members of the aldo-keto reductase superfamily

Scientific-disciplinary sector: BIO/10

Supervisor Prof. Francesco Balestri

PhD Student Lucia Piazza

Academic Year 2022/2023

List of Abbreviations

- AGEs: Advanced Glycating End-products
- RAGEs: AGEs-receptors
- AKRs aldo-keto reductases
- AKR1B1: aldose reductase
- AKR1B10: aldose reductase like
- AP-1: activator protein 1
- ARE: Antioxidant Response Element
- ARIs: Aldose Reductase Inhibitors
- ARDIs: Aldose Reductase Differential Inhibitors
- BSA: albumin serum bovine
- COX-2: Cyclooxygenase-2
- DAG: diacylglycerol
- DEAE: Diethylaminoethyl
- DMSO: dimethyl sulfoxide
- DHN: 1,4-dihydroxy-2-nonene
- DTT: D,L-dithiotreitol
- EDTA: Ethylenediaminetetra acetic acid
- EGCG: Epigallocatechin Gallate
- EVs: extracellular vesicles
- F α-PNP: α-pyrrolidinononanophenone
- GSDHN: 3-glutathionyl-1,4-dihydroxynonane
- GSHNE: 3-glutathionyl-4-hydroxynonanal
- HCC: hepatocarcinoma
- HNA: 4-hydroxynonenanoic acid
- HNE: 4-hydroxy-trans-2-nonenal
- iNOS: inducible nitric oxide synthase
- IkB-α: NF-kappa-B inhibitor alpha
- IKK: nuclear factor-κB (IκB) kinase
- IPTG: Isopropyl-β-D-thiogalactopyranoside
- MAPK: mitogen-activated protein kinase
- MONAL-41: 4-methoxy-1-naphtaldehyde
- MONOL-41: 4-methoxy-1-naphtalenemethanol

- MNK-R cells: cisplatin-resistant gastrointestinal cancer cells
- MVs: Microvesicles
- MVBs: multivesicular bodies
- NADPH reduced nicotinammide adenine dinucleotide phosphate
- NF-kB: nuclear factor κB
- NSCLC: non-small cell lung cancer
- Nrf-2: nuclear factor erythroid 2–related factor 2
- LC3-II: Microtubule-associated protein 1A/1B-light chain 3
- LPS: lipopolysaccaride
- PAH: polycyclic aromatic hydrocarbon
- PGE: prostaglandin E2
- PMSF: Phenylmethylsulfonyl fluoride
- PKC: protein kinase C
- PTFE: Polytetrafluoroethylene
- RAR/RXR: retinoic acid receptors or retinoid X receptors
- ROS: reactive oxygen species
- SDH sorbitol dehydrogenase
- SDS-PAGE: sodium dodecyl sulfate/polyacrilamide gel electrophoresis
- SsBb: soyasaponin Bb
- TEMED: N,N'-metilen-bis-acrylamide, N,N,N'N'- Tetramethylethylenediamine
- VSMC: vascular smooth muscle cell

Abstract

AKR1B1 and AKR1B10 are NADPH-dependent reductases belonging to Aldo-Keto Reductase superfamily. AKR1B1 and AKR1B10 act as detoxicant enzymes. However, plenty of evidence suggest the involvement of both enzymes in pathological conditions. AKR1B10 emerged as a cancer biomarker since its overexpression in several non-gastrointestinal cancers. AKR1B10 activity supports cancer progression through several mechanisms including cytotoxic aldehydes detoxification, chemoresistance, regulation of retinoids homeostasis, and polycyclic aromatic hydrocarbon (PAH) derivatives metabolism. Therefore, AKR1B10 is considered a target for antineoplastic treatments. However, AKR1B10 shares kinetic and structural features with AKR1B1. Inhibitors that discriminate between AKR1B10 and AKR1B1, and minimize the interference with the detoxifying ability of the ubiquitous AKR1B1, may be relevant to develop novel treatment for cancer. Several natural products were proven to be inhibitors of AKRs. In this regard, *zolfino* bean extract is known for being rich in AKR1B1 inhibitors. Here results on isolation and characterization of selective inhibitors of AKR1B10 from *zolfino* bean extract are reported. The workflow includes fractionation of a crude extract of *zolfino* bean on a C18 column, evaluation of inhibitory ability of the fractions, and LC-MS characterization of relevant sets of fractions. Correlation between results from LC-MS and kinetic analyses allowed the identification of promising candidates for selective enzyme inhibition.

In addition, this study was focused on the detrimental effects of AKR1B1 in diabetes. The role of AKR1B1 as the first enzyme of the polyol-pathway is generally accepted as the responsible of several cell damaging processes including oxidative stress and accumulation of both glycating agents and sorbitol, which contribute to the onset of secondary diabetes complications. However, several inhibitors of AKR1B1 failed clinical trials because of side effects. AKR1B1 is a multispecific but non-permissive enzyme, i.e. it reduces a variety of aldehydes with different chemical properties still discriminating between compounds belonging to the same chemical class. This peculiar feature of AKR1B1 paved the way for differential inhibition (DI), an alternative inhibition strategy based on compounds able to inhibit AKR1B1 depending on the substrate it is working on. These compounds, namely differential inhibitors, have to intervene on AKR1B1 glucose-reductase activity leaving unaffected or affecting at lesser extent its detoxifying activity. In this study, novel synthetic compounds were screened for their ability to act as differential inhibitors of AKR1B1. In addition, these compounds were tested for their ability to discriminate between AKR1B1 and AKR1B10.

Finally, this study aimed to optimize a fluorescent assay for the detection of AKR1B10. The characterization of a substrate with fluorescent properties and preliminary tests for its application to detect AKR1B10 reductase activity in biological samples are also reported.

1 Introduction

1.1 Aldo-keto reductases family 1 members B10 and B1: structure and catalytic mechanism

AKRs-superfamily is a group of about 190 enzymes, which are mainly involved in the metabolism of endogenous and xenobiotic carbonyl compounds. AKRs-superfamily consists of 16 families, which are further divided into several subfamilies based on a >60% of amino acid sequence identity [1]. To date, fifteen AKRs have been identified in humans, which belong to the AKR1A, AKR1B, AKR1C, AKR1E, AKR6A, and AKR7A subfamilies. AKR1B subfamily includes member 1 (AKR1B1, also known as Aldose Reductase) and member 10 (AKR1B10, also known as Aldose Reductase-like protein), two enzymes of special interest for their involvement in the physiopathology of secondary diabetes complications and cancer, respectively [1].

AKR1B1 and AKRB10 are NADPH-dependent cytosolic reductases with 71% aminoacidic sequence homology [2]. As common features of AKRs, AKR1B1 and AKR1B10 show a $(\alpha/\beta)_8$-barrel core motif and a highly conserved catalytic tetrad in the active site, which is composed by residues Asp43, Tyr48, Lys77, and His110 (the reported numbers indicate the positions of amino acids in AKR1B1 and correspond to those +1 in AKR1B10) [3]. The active site, the neighbouring Trp111 (Trp112 in AKR1B10), and the nicotinamide moiety of the cofactor delimit a rigid portion named “anion-binding pocket”, which provides a stable region for tight anchoring substrates functional groups [4]. Like other AKRs, both enzymes show a Bi-Bi ordered catalytic mechanism, in which the cofactor enters the active site before the aldehyde binding and leaves after alcohol removal (Figure 1).

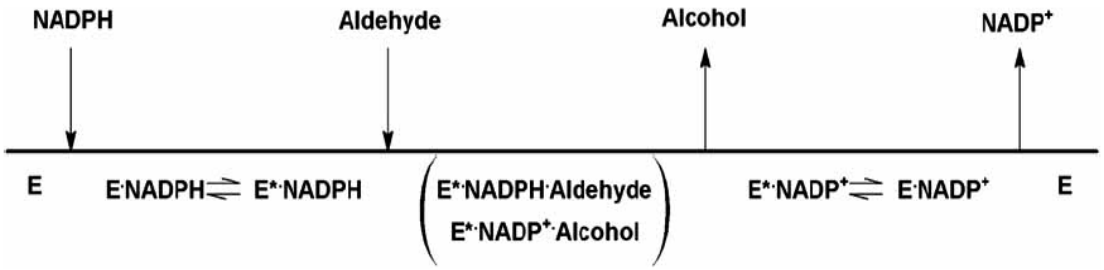

Figure 1 AKR1B1 and AKR1B10 catalytic mechanism (Del Corso et al. 2008).

The reduction of the aldehyde occurs through the stereospecific transfer of the 4-*pro-R* hydride of NADPH to the carbon of the carbonylic group and the transfer of the proton of Tyr48 to the carbonyl oxygen [5].

In addition, there are three external mobile loops named A, B, C (residues 112–136, 216–227, and 298–310, respectively) which show high variability among AKRs and contribute to protein flexibility, substrate specificity, and inhibitor selectivity. Residues in loop B located between strand and helix 7 of the α/β-barrel are part of a region named "safety belt", which delimits the cofactor binding-site. The binding of the cofactor induces a conformational change of the safety belt, which locks the cofactor into place [6]. Loop A and C residues compose a region named "specificity pocket" next to the active site. This region undergoes to induced-fit adaptations depending on the binding of specific ligands, generally inhibitors with hydrophobic moiety. Specificity pockets of AKR1B1 and AKR1B10 are highly different: Thr113, Phe-115, Phe-122, Leu-300, Ser302 and Cys303 compose the specificity pocket of AKR1B1, whereas the specificity pocket of AKR1B10 includes Gln114, Phe116, Phe123, Val301, Gln303, and Ser304 residues [7]. The variability of the specificity pockets is markedly involved in inhibitor selectivity of AKR1B1 and AKR1B10, as discussed in section 1.6.3.

1.2 AKR1B1 and AKR1B10 detoxifying activity: role in HNE metabolism.

Electrophilic carbonyl compounds such as 4-hydroxynonenal (HNE), malondialdehyde, crotonaldehyde, and acrolein are able to induce cytotoxicity as result of their high reactivity towards macromolecules such as DNA and proteins. Cytotoxic aldehydes are usually produced by the intracellular metabolism of lipids, steroids, amino acids and vitamins, in particular under oxidative stress conditions [8]. In addition, gastrointestinal tissues are intensely exposed to cytotoxic aldehydes produced by lumen microbiota or provided through diet [8]. Intracellular levels of cytotoxic aldehydes are regulated through several metabolic mechanisms, which can be summarized as Phase I and II reactions. Briefly, in Phase I reactions, cytotoxic aldehydes functional groups are modified mostly by redox enzymes. Phase II reactions promote the conjugation of cytotoxic aldehydes or products of Phase I reactions to endogenous compounds such as glutathione (GSH), which facilitate their excretion.

AKR1B1 and AKR1B10 are highly efficient Phase I enzymes because of their ability to reduce cytotoxic aldehydes at physiological levels [9-12]. In this context, it is worth mentioning that AKR1B10 is primarily expressed in colon, stomach, intestinal tissues, and at low levels in liver,

while AKR1B1 is ubiquitous [2, 13]. This may reflect the additional requirement of the gastrointestinal tract to be protected from the persistent exposure to cytotoxic aldehydes.
AKR1B1 and AKR1B10 show overlapping substrate specificity, but differential ability in eliminating free or GS-conjugated (glutathione-conjugated) carbonyl compounds, as reported in Table 1 [8].

		1B1			1B10		
	C_n	K_m (mM)	k_{cat} (min^{-1})	k_{cat}/K_m (min^{-1} mM^{-1})	K_m (mM)	k_{cat} (min^{-1})	k_{cat}/K_m (min^{-1} mM^{-1})
D,L-Glyceraldehyde	3	0.065 ± 0.010	33	507	0.563 ± 0.045	29	52
Acrolein	3	0.884 ± 0.280	11	12	0.110 ± 0.012	116	1070
Crotonaldehyde	4	9.643 ± 0.929	31	3	0.086 ± 0.014	103	1200
Trans-2-hexenal	6	0.878 ± 0.151	41	47	0.061 ± 0.019	96	1580
Trans-2, 4-hexadienal	6	0.905 ± 0.299	43	47	0.096 ± 0.056	78	813
4-Hydroxynonenal	9	0.716 ± 0.046	50	70	0.031 ± 0.007	119	3839
GS-propanal	3	0.158 ± 0.025	56	355	0.533 ± 0.071	2	4
GS-butanal	4	0.021 ± 0.009	25	1153	0.246 ± 0.021	68	278
GS-hexenal	6	0.007 ± 0.002	16	2345	0.146 ± 0.020	74	506
GS-trans-4-hexenal	6	0.122 ± 0.075	36	297	0.078 ± 0.019	144	1858
GS-4-hydroxynonanal	9	0.005 ± 0.001	13	2600	ND	ND	ND

C_n, carbon chain length.

Table 1. Kinetic parameters of AKR1B1 and AKR1B10 to carbonyl compounds and glutathione conjugates (Shen et al. 2011).

Among the cytotoxic aldehydes metabolized by AKR1B1 and AKR1B10, 4-hydroxy-2,3-nonenal (HNE) is one of the most relevant for its role in pathological conditions. HNE is a common marker of lipid peroxidation, which is the result of oxygen radicals-mediated injury of cell membranes. HNE is very reactive due to an α,β-unsaturated aldehydic moiety and a hydroxyl group on C-4.
HNE reacts readily with various cellular components, such as DNA, proteins and other molecules containing nucleophilic thiol or amino groups. In Michael additions a nucleophilic thiol or an amino group can react with the C2-C3 double bond resulting in the covalent bond between HNE and the nucleophilic compound. The C1 aldehyde group can react with primary amines, e.g. lysine, and form Schiff bases. [14, 15]. Accordingly, high cellular levels of HNE-

adducts are a common denominator of several diseases including neurodegenerative disorders, diabetes, atherosclerosis, and many types of tumours [16-18].
Therefore, cells strictly regulate the intracellular levels of HNE through Phase I and Phase II reactions:

Phase I reactions: The aldehyde group of HNE can be either oxidated by aldehyde dehydrogenases to form 4-hydroxy-2,3-nonenoic acid (HNA) [19] or reduced by AKRs to produce 1,4-dihydroxy-2-nonene (DHN) [9-11, 20, 21].

Phase II reactions: HNE and DHN can be converted to their glutathionylated adducts glutathione 4-hydroxynonenal (GSHNE) and 3-glutathionyl-1,4-dihydroxynonane (GSDHN), respectively, through either spontaneous or glutathione-S-transferase-mediated glutathionylation of the carbon-carbon double bond [22]. Furthermore, AKR1B1 can reduce GSHNE to form GSDHN [10], with a marked preference toward the 3S,4R-GSHNE diastereoisomer [23].

Several studies suggested the pivotal role of AKR1B1 and AKR1B10 in HNE detoxification in human tissues and cell lines. AKR1B10 reduces cytotoxic aldehydes including HNE at subtoxic concentrations which mimic the daily exposure in humans [11]. Accordingly, the downregulation of AKR1B10 has been reported in several gastrointestinal disease such as ulcerative colitis, Crohn's disease, and colorectal cancer [24, 25]. Moreover, the protective role of AKR1B10 in the digestive system was further supported by the silencing and the ectopic expression of AKR1B10 in colon cancer cells, which increased and reduced both the HNE levels and the HNE-induced cytotoxicity, respectively [25]. Similarly, the overexpression of AKR1B1 reduced HNE levels and the HNE-mediated cell-damage in SK-N-SH cells treated with the 4'-fluorinated analog of α-pyrrolidinononanophenone (F-α-PNP) [26]. Accordingly, pre-treatment with Tolrestat, a well-known AKR1B1 inhibitor (ARI), enhanced the cytotoxic effect of the F-α-PNP in SK-N-SH cells [26]. In addition, HNE and its GS-conjugates are involved in several signalling pathways [27]. Accordingly, GS-DHN could be considered a mediator of the mitogenic effect of HNE in VSMC through the activation of PKC, which results in the induction of the transcription factors NF-kB and AP-1. Consistently, AKR1B1 can modulate this signalling pathway, since ARIs reduced cell growth and the induction of NF-kB and AP-1 in VSMC [28]. Besides their role in cell growth, PKC, NF-kB, and AP-1 are involved in proinflammatory signalling. Accordingly, ARIs suppressed the LPS-induced activation of both NF-kB and AP-1 through the inhibition of phosphorylation of IkB-α, PKC, and IKK [29]. Moreover, ARIs prevented the LPS-induced release of PG-E, nitric oxide, proinflammatory

cytokines and chemokines, and the expression of the inflammatory markers iNOS and COX-2 in peritoneal murine macrophages [29]. In addition, the reduction of NF-*k*B activity in human leukemic cells following treatment with artichoke leaf extract, which is rich in ARIs, further supports the involvement of AKR1B1 in HNE cell-signalling [30].

1.3 AKR1B10 role in cancer

Besides its role as detoxifying enzyme, AKR1B10 emerged as a cancer biomarker. Accordingly, the overexpression of AKR1B10 was reported in several cancer tissues including those originating in lung, pancreas, liver, breast, and nasopharynx [31-36]. Several evidence reported in literature demonstrate that AKR1B10 supports cancer progression through several mechanisms including cytotoxic aldehydes detoxification, chemoresistance, regulation of retinoids homeostasis, and polycyclic aromatic hydrocarbon (PAH) derivatives metabolism. The following paragraphs will discuss the abovementioned mechanisms.

1.3.1 Cytotoxic aldehydes detoxification

As outlined above, a basal expression of AKR1B10 is strictly required for the detoxification system of the gastrointestinal tract in physiological conditions. Similarly, AKR1B10 detoxicant ability is believed to protect cancer cells from toxic aldehydes produced under oxidative stress. ROS-levels behave as a double sword in cancer: low concentrations promote tumorigenesis and cancer progression, but high levels can be detrimental. Accordingly, the silencing of AKR1B10 enhanced the colorectal cancer cells sensitivity to the exposure of acrolein and crotonaldehyde and inhibited both cell growth and DNA synthesis [37]. Accordingly, Liu et al. demonstrated that the silencing and the ectopic-induced expression of AKR1B10 in liver cancer cells enhanced and decreased both ROS-induced injury and malondialdehyde intracellular levels, respectively [38]. In addition, AKR1B10 expression was upregulated in HCC tumour tissues with respect to their controls [38]. In line with these results, AKR1B10 overexpression was significantly associated with poor survival in hepatocarcinoma (HCC) patients [32, 38].

Furthermore, the antioxidant defence role of AKR1B10 is supported by the activation of the transcriptional factor Nrf-2 in AKR1B10-overexpressing cancer cells [38-40]. Under oxidative stress Nrf-2 can activate the expression of proteins through a *cis*-acting element termed ARE (Antioxidant Response Element), whose sequence has been found in AKR1B10 promoter region [41]. This is consistent with the AKR1B10 overexpression in cancer cell lines that are resistant to oxidative stress inducer drugs. In cisplatin-resistant gastrointestinal cancer cells (MNK-R cells) the up-regulation of AKR1B10 contributed to the suppression of HNE-adducts accumulation following cisplatin treatment, but the co-administration of a AKR1B10 selective

inhibitor reverted the condition to the parental control phenotype. Accordingly, MNK-R cells showed higher viability following both HNE and cisplatin treatments compared with the parental cell line [39]. Moreover, the administration of a selective inhibitor of AKR1B10 restored the sensitivity of colorectal cancer cells resistant to mitomycin c. Consistently, the ectopic overexpression of AKR1B10 protected nontolerant-mitomycin c cells from injury following the exposure to mitomycin c and cytotoxic aldehydes treatments [42]. The AKR1B10 modulation of oxidative stress-induced pathways was further supported in studies in which the effect of anthracycline treatments was investigated. Doxorubicin treatment elicited ROS-mediated activation of autophagy in colorectal cancer cells. However, this pathway was downregulated by the ectopic overexpression of AKR1B10 as demonstrated by the decreased levels of LC3-II, a marker of autophagy [43]. Accordingly, AKR1B10-overexpressing cells exposed to HNE showed decreased LC3-II levels compared to the controls [43]. By contrast, both the silencing and the selective inhibition of AKR1B10 in doxorubicin-resistant colorectal cancer cells enhanced the expression of LC3-II following doxorubicin treatment [43]. All together, these data strongly support a pivotal role of AKR1B10 in ROS-injury defence in cancer cells.

1.3.2 Retinoids metabolism

Retinoids are a group of compounds assimilated by humans through products of animal origin and vegetables [44]. Among the numerous retinoids-mediated signalling pathways, the RAR/RXR (retinoic acid receptors or retinoid X receptors) gene-signalling pathway is one of the most reported. The binding of retinoic acid (RA) to RAR/RXR receptors results in a conformational change. These activated receptors form RAR-RXR heterodimers or RAR-RAR and RXR-RXR homodimers, which bind RARE (Retinoic acid response element) leading to the recruitment of transcriptional repressors of cancer genes [45]. RA is the final product of the metabolic pathway of retinol. Briefly, NAD^+- dependent enzymes oxidize retinol to retinaldehyde (i.e., all-*trans*-retinaldehyde), which is further oxidized to retinoic acid by NAD^+-dependent enzymes. However, several NADPH-dependent reductases including AKRs can catalyse the reversible conversion of retinaldehyde to retinol, therefore hampering the anticancer activity of RA [46].

Both AKR1B10 and AKR1B1 are reported to metabolize the retinaldehyde but with different efficiency. Although the K_m values are similar (0.6-1.1 μM), the K_{cat} value of AKR1B10 is 80-fold higher than that of AKR1B1 [47]. Accordingly, the overexpression of both AKRs in HeLa cells resulted in a decrease of the *trans*-activation of RA receptors compared to controls,

meaning that a lower amount of RA is produced [48]. Thus, the overexpression of AKR1B10 can support cancer progression through the suppression of RA-signalling.

1.3.3 Isoprenoid metabolism

AKR1B10 is part of the metabolic recycle of isoprenoids since it efficiently reduces geranylgeranial and farnesal in their corresponding alcohols [49, 50]. Farnesol and geranylgerianol are involved in cholesterol synthesis and proteins prenylation. Several proteins including Ras need to be prenylated to activate their functions. Mutated Kras seemed to drive the progression of several type of tumours including pancreatic cancer. Accordingly, the knockdown or inhibition of AKR1B10 resulted in the decrease of prenylated KRas and its downstream effectors in pancreatic cancer cells [35, 51]. Moreover, the shutdown of AKR1B10 caused apoptosis and the decrease of cell migration, invasion, and proliferation [35, 51].

1.3.4 Anthracyclines metabolism

As outlined above, AKR1B10 is involved in cancer progression through the suppression of ROS-mediated injury elicited by anticancer drugs. However, AKR1B10 can promote anthracyclines chemoresistance through the reduction of the C-13 carbonyl group [52]. Accordingly, the overexpression of AKR1B10 was detected in anthracyclines-tolerant cell lines, which therefore showed increased anthracycline metabolism compared to their drug-sensitive counterparts [43, 53]. Moreover, both the ectopic and the drug tolerance- induced overexpression of AKR1B10 in cancer cells increased the viability and the accumulation of anthracycline metabolites following anthracycline treatment [52, 54]. These findings suggested both a reduced efficacy of anthracycline corresponding alcohols as anticancer drugs and the pivotal role of AKR1B10 in anthracycline-chemoresistance. Accordingly, the co-administration of anthracyclines and AKR1B10 inhibitors was effective in several studies [52, 54-56]. In addition, side effects consistently contributed to limit the clinical success of anthracyclines in cancer therapy. The corresponding alcohols of both doxorubicin and daunorubicin exert pro-oxidative iron dependent and independent insults, apoptosis, and calcium dysregulation in cardiomyocytes, which can lead to cardiovascular diseases and heart failure [57, 58]. Accordingly, the co-administration of inhibitors of AKR1B10 expression and anthracyclines not only reduced the tumour growth but also ameliorated cardiotoxicity in A549 tumour-bearing mice [59].

1.3.5 PAHs derivatives metabolism and lung cancer

Polycyclic aromatic hydrocarbons (PAHs) are a class of chemical carcinogens present in tobacco smoke, heavily subjected to conversion into their highly mutagenic *o*-quinone

metabolites. In this regard, it has been demonstrated that AKR1B10 can oxidize several PAH *trans*-dihydrodiol substrates to PAH *o*-quinones *in vitro* [60]. Moreover, smoking *per se* is able to up-regulate the expression of AKR1B10 in airway epithelium of healthy current smokers [61, 62] and in human epithelium cell lines [62]. By contrast, AKR1B10 is downregulated in former smokers [61]. Consistently, AKR1B10 mRNA is over-expressed in smokers' squamous cell NSCLC (non-small cell lung cancer) compared to non-smokers [63, 64]. Therefore, AKR1B10 is considered a promising diagnostic marker specific to smokers' NSCLC with squamous cell cancer or adenocarcinoma [36].

1.4 AKR1B10 as a secretory protein: a moonlighting function

While the AKR1B10 reductase-activity has been deeply investigated, there are some non-catalytic functions of the protein which need to be carefully examined for their involvement in cancer progression. In this regard, it has been demonstrated that AKR1B10 is secreted in serum of breast cancer and HCC patients [31, 65, 66]. Pathways of protein secretion can be classified in classical and non-classical: the first one is Endoplasmic Reticulum/Golgi-dependent and requires a specific signal sequence at N-terminus of the protein; the second one is Endoplasmic Reticulum/Golgi-independent and includes several mechanisms such as secretory lysosome exocytosis, extracellular vesicles release, and specific membrane transporters-mediated transfer. It has been demonstrated that AKR1B10 is secreted as an active biocatalyst by cancer cells through a lysosome-mediated non-classical pathway [67]. This secretion is mediated by the association to the molecular chaperone HSP90α, which interacts with residues in helix 10 located at the C-terminus of AKR1B10 [68]. Besides its secretion through lysosome-mediated non-classical pathway, proteomic analyses detected AKR1B10 in extracellular vesicles (EVs) derived from several tissues and cell types [69].

There are two major classes of EVs, namely Microvesicles (MVs) and small EVs, which are classified based on their size and biogenesis. MVs have a range size of 200-800 nm. MVs are generated as cellular membranes microdomains enriched in lipid rafts, cholesterol and phosphatidylserine, which progressively protrude from cell surface until a thin neck is formed and cleaved, resulting in vesicles release. Several signalling proteins involved in cytoskeletal remodelling such as EGF receptors and RAS superfamily members as well as regulators of lipid remodelling promote MVs biogenesis. By contrast, small Evs are 30-150 nm vesicles, which are generated in a process named endolysosomial degradation. Briefly, cell membrane invaginates and forms early endosomes, which undergo a process of maturation resulting in multivesicular bodies (MVBs) formation. Among proteins involved in MVBs formation there are ESCRTs, tetraspanins and RABs proteins, which act as key regulators of proteins sorting,

endocytic trafficking and membrane fusion and fission, respectively. During maturation, MVBs undergo membrane invagination to form intraluminal vesicles. The intraluminal vesicles have several fates: i) MVBs are typically directed to lysosome and subsequently degraded, ii) MVBs can be directed to Golgi for redistribution or recycling, iii) MVBs can fuse with cell membrane and eventually release the intraluminal vesicles, now termed small EVs, in the extracellular space, iv) the intraluminal vesicles can refuse with MVBs membrane and release their content in the cytoplasm [70].

EVs are produced from both normal and tumour cells, although the latter show higher efficiency. Cargo of EVs is various and includes DNA, non-coding RNA, RNA, and proteins. EVs showed multiple roles in cell processes including cancer progression [71, 72]. First, EVs can be used by cancer cells for intercellular communications by regulating their own and recipient cancer cells phenotype. Second, EVs can regulate the metabolism of stromal cells, therefore promoting a protumour microenvironment. For example, EVs can induce endothelial proliferation and release proangiogenic factors, therefore supporting cancer growth especially in hypoxic conditions. Third, EVs have an impact in several mechanisms involved in cancer metastasis. Cargoes of cancer EVs can modulate cell polarity, cell adhesion, the remodelling of the extracellular matrix and can induce epithelial-mesenchymal transition in recipient cells. Fourth, EVs regulate the immunity system by facilitating immune surveillance escaping. And finally, drug-resistant cells can use EVs to induce drug-resistance in their drug-sensitive counterparts. Therefore, considering the crucial role of EVs in several aspects of cancer development, the deep understanding of EVs content is considered crucial for cancer therapy.

As above mentioned, AKR1B10 was detected in EVs in several cell types and tissues, including cancer. In addition, the EVs-mediated transfer of AKR1B10 between cell lines was demonstrated [73]. Therefore, since AKR1B10 is considered a cancer biomarker, to clarify the role of its systemic delivery could provide new insights for cancer treatment.

Moreover, there is an increasing interest for using EVs as important sources of information for cancer diagnosis, monitoring, and prognosis. Cancer diagnostic classic procedures are often invasive, painful and infection risk prone. Therefore, analyses performed on liquid biopsies such as serum, saliva, and blood were proposed as an alternative tool.

As regard lung cancer, several liquid biopsy technologies could be applied to clinical practice. Among them, microRNAs secreted via small EVs were mentioned as possible biomarkers for lung cancer diagnosis and tumour type classification [74]. However, to date, the use of small EVs is limited to research purposes and specific as well as sensitive biomarkers are needed.

Therefore, the AKR1B10 pro-cancer role and application as a NSCLC biomarker, together with the detection of AKR1B10 in cancer patients' serum and EVs, encourage an in-depth analysis of this moonlighting function.

1.5 AKR1B1 and polyol-pathway: role in secondary diabetes complications

AKR1B1 is considered a multi-specific non-permissive enzyme, i.e., a ductile biocatalyst able to convert a broad range of related substrates [75] but discriminating among compounds belonging to the same chemical class and even between enantiomeric forms [23]. Accordingly, besides its ability to catalyse the conversion of hydrophobic as well as hydrophilic aldehydes, AKR1B1 reduces several aldoses including D-glucose.

D-glucose is poorly recognized by AKR1B1 compared to other substrates (K_m= 205 ± 20 mM for *h*AKR1B1). Since AKR1B1 does not reduce the cyclic forms of aldoses [76], the low affinity is reasonably due to the low percentage of the free aldehydic form of D-glucose in solution (approximately 1.28 x 10^{-3}% of total glucose at 25 °C) [77]. This is further supported by the higher affinity of AKR1B1 for L-Idose [78], the C_5 carbon epimer of D-Glucose, whose percentage of the free aldehydic form in solution is 60-80 fold higher than glucose [77]. Moreover, besides its inability to recognize cyclic aldoses, AKR1B1 is inhibited by cyclic hemiacetals as suggested by the biphasic behaviour of the enzyme when long chain aldoses (the only ones able to produce cyclic forms) are used as substrates [79].

The reduction of glucose catalysed by AKR1B1 is the first step of the polyol pathway. This is a two-step metabolic route, in which the conversion of glucose to sorbitol catalysed by AKR1B1 is followed by the oxidation of sorbitol to fructose catalysed by the enzyme sorbitol dehydrogenase via a NAD^+-dependent reaction [80]. Since AKR1B1 affinity for glucose is low, glucose preferentially enters the glycolysis and its conversion to sorbitol only accounts for the 3% of the total glucose metabolism in euglycemic conditions [81]. However, the saturation of hexokinase occurring under hyperglycaemia results in the increase of glucose metabolism through the polyol pathway up to 30-35% [81]. The activation of polyol pathway leads to multiple cells damaging processes which contribute to the onset of nephropathy, neuropathy, retinopathy, and cataract in diabetes patients [80].

Since sorbitol is an active osmolyte, the sorbitol-synthesis activity of AKR1B1 affects the proper osmolarity in a variety of cells in physiologic conditions [82-84].

The sorbitol-polyol hypothesis suggested that the intracellular accumulation of sorbitol plays a role in hyperglycaemic injury. Once formed, sorbitol degradation proceeds slowly, especially

in tissues where SDH expression is low [85]. Since polyols are unable to permeate cell membranes, the excessive intracellular accumulation of sorbitol could lead to osmotic stress, followed by cell swelling and lesion [86]. Accordingly, several studies demonstrated that the accumulation of polyols in lens triggers the development of cataract in animal models [87-90]. However, sorbitol accumulation plays a minor role in other diabetes tissues since its intracellular levels are not high enough to induce osmotic stress [85]. In addition, the ability of antioxidants to prevent cataract formation without reducing sorbitol content in lens cells suggested that the osmotic stress is a co-causative damaging process [91, 92]. Accordingly, oxidative stress is considered a leading factor in the onset of secondary diabetes complications. In this regard, the polyol-pathway contributes to the oxidative stress in diabetes tissues because its activation decreases the intracellular amount of NADPH, which is a cofactor of several antioxidant enzymes such as Glutathione Reductase (GR) [93, 94]. The competition between AKR1B1 and GR for the cofactor may hamper the activity of GR, resulting in the decrease of the intracellular levels of GSH [95] and consequently in an impaired redox status in diabetes patients [96]. The impact of AKR1B1 activity on GSH content was further supported by the ability of AKR1B1 inhibitors (ARIs) to restore the normal levels of GSH in diabetic tissues [97-99]. Furthermore, the increased intracellular levels of fructose and its metabolites results in accumulation of Advanced Glycating End-products (AGEs). Briefly, the formation of AGEs is induced when the electrophilic carbonyl groups of reducing sugars such as glucose or fructose form a Schiff base with the free amino groups of proteins, lipids or nucleic acids, which finally rearrange in stable end-products. The binding of AGEs to AGEs-receptors (RAGEs) induces inflammation, oxidative stress, and endothelial disfunction [100, 101]. In addition to fructose accumulation, also the NADPH/NAD^+ imbalance can promote the formation of AGEs through the accumulation of triose phosphates, which are precursors of the AGE methylglyoxal [100, 101]. Moreover, the accumulation of triose phosphates leads to elevated intracellular levels of DAG. DAG is an inducer of PKC, which promotes cell growth, membrane permeability, endothelial dysfunction, inflammation, and apoptosis mainly through the activation of MAPKs signalling [102, 103].

1.6 AKR1B1 and AKR1B10 inhibition strategies

1.6.1 Classic Aldose Reductase inhibitors

Due to its implication in diabetes, AKR1B1 inhibition strategies have been deeply investigated. Classic Aldose Reductase Inhibitors (ARIs) usually show two common structural features: a polar group which allows the anchoring to the anion-binding pocket of the active site, and a

hydrophobic moiety which interacts with the hydrophobic portion of the active site. ARIs can be classified in: i) acid acetic derivatives, ii) cycle imides, and iii) natural compounds.

i. Cyclic imides. These molecules are characterized by either a spyroidantoin or a spirosuccimide moiety. The best-known molecules belonging to this class are analogues and derivatives of *Sorbinil*. *Sorbinil* was one of the first compounds with a spyroidantoin moiety to be tested as a AKR1B1 inhibitor [104]. Despite its inhibitory efficacy, clinical trials showed no improvements of diabetic complications [105]. Moreover, the administration of *Sorbinil* was followed by several side effects such as skin rash, fever, and myalgia [106]. Analogues and derivatives of *Sorbinil* have been deeply investigated for their ability to ameliorate diabetic complications, but most of the clinical trials failed because of side effects.

ii. Acid acetic derivatives. Compounds belonging to this class are *Ponalrestat, Zopolrestat, Epalrestat, Alrestatin* and *Tolrestat* [80]. However, these molecules show poor bioavailability because of the low pKa of the acetic acid moiety, which causes ionization and limits their flux through cellular membranes at physiologic pH. Indeed, most of these molecules failed the phase III in clinical trials [80]. To date, *Epalrestat* is the only commercially available ARI for the treatment of diabetic neuropathy. However, *Epalrestat* administration is authorized only in Japan.

iii. Natural compounds. In accordance with the recent trend to focus on the pharmaceutical properties of natural compounds, several ARIs were isolated from natural sources such as flowers, plants, and marine organisms including natural products commonly present in diet or in traditional medicine [107, 108]. These molecules show a variety of chemical structures including flavonoids, terpenoids, alkaloids, tannins and coumarins [108]. Natural compounds have some advantages in drug development. Firstly, the toxicological properties of several natural molecules are already known in humans. In addition, natural sources often offer new chemical scaffolds which are useful for drug-design. Although the *in vitro* efficacy of natural ARIs is well-known, there are few clinical studies which show the effective targeting of AKR1B1 in diabetes patients. In this regard, dietary supplementation with Vitamin C reduced sorbitol accumulation in diabetic patients' erythrocytes [109, 110]. Moreover, the administration of Silymarin (an ARI isolated from *Silybum marianum* [111]) in patients with diabetic nephropathy reduced serum malondialdehyde, urinary TNF-α (a marker of inflammation) and albumin excretion [112]. However, as stated above, to date no ARI is effectively used in diabetes therapy.

1.6.2 Aldose Reductase Differential Inhibitors (ARDIs):

Side effects of classic ARIs in clinical trials arose legitimate doubts about the benefit of AKR1B1 inhibition. However, clinical failure of ARIs could be the result of several factors including the total block of AKR1B1 functions as well as its detoxifying activity, which should be preserved. Therefore, the administration of ARDIs (Aldose Reductase Differential Inhibitors), i.e., inhibitors able to target specifically AKR1B1 Glucose-reductase activity, was proposed to overcome the undesirable effects of Classic ARIs [113].

The possibility of a differential inhibition derives from the peculiar feature of AKR1B1 of being both a multi-specific and a non-permissive biocatalyst, i.e., it reduces substrates with different chemical properties such as aldoses and hydrophobic aldehydes but discriminates among members belonging to the same chemical class. These findings together support the occurrence of a very specific range of interactions between different substrates and AKR1B1 active site. Therefore, taking advantage of different substrate-dependent interaction patterns, ARDIs can effectively intervene on the ongoing reaction through an intra-site differential inhibition [75].

A "complete" ARDI should be able to prevent the reduction of glucose without affecting the conversion of cytotoxic aldehydes such as HNE. As classical inhibitors, ARDIs inhibitory action can be described through different kinetic models. Kinetic models suggested that competitive ARDIs are the most effective and theoretically the only ones able to realize a complete DI [75]. As shown in Figure 2, the competitive ARDI targets the free biocatalyst and inhibits the transformation of substrate B (i.e., glucose). Conversely, the transformation of substrate A (i.e., HNE) is completely unaffected by the presence of the inhibitor in terms of both kinetic constants of dissociation of complex EA and EIA to products (i.e., k_{+2} and k_{+6}) and affinity of substrate A to the free enzyme and the complex E.

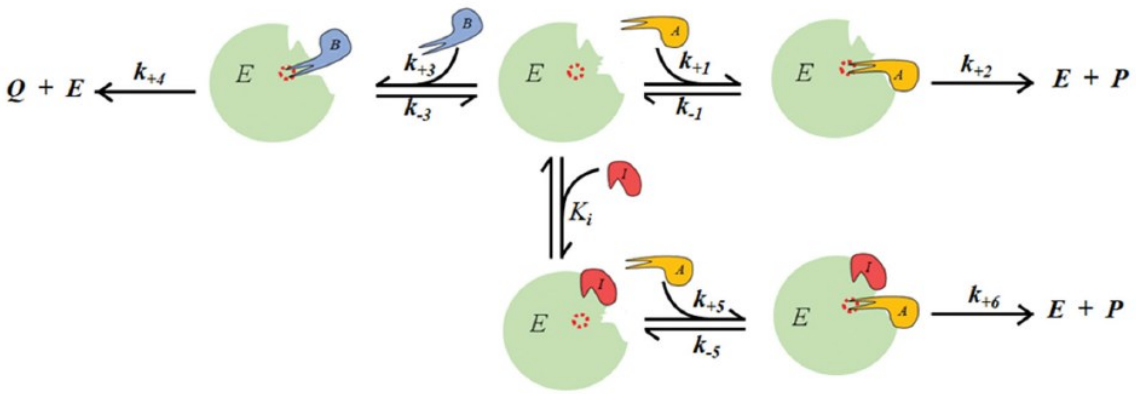

Figure 2. Competitive inhibition model of ARDIs. *The inhibitor I acts as an ARDI and binds to the free form of AKR1B1affecting the conversion of the substrate B (i.e., glucose) but not the reduction of the substrate A (i.e. HNE). Kinetic constants k_{+1}, k_{-1}, k_{+2}, k_{+3}, k_{-3}, k_{+4}, k_{+5}, k_{-5} and k_{+6} are related to the formation and dissociation of the complex EB EA, and EIA; K_i represents the dissociation constant of the EI complex. (Cappiello* et al., *2020).*

When analysed in steady-state conditions, the model of competitive DI reported in Figure 2 can be described by the rate equations 1 and 2 expressing the generation of product P (i.e., DHN) and product Q (i.e., sorbitol), respectively:

$$v_p = \frac{k_{+2}E_T[A]}{K_A\left(1+\frac{\frac{[B]}{K_B}}{1+\frac{[I]}{K_i}}\right)+[A]} \qquad 1)$$

$$v_q = \frac{k_{+4}E_T[B]}{K_B\left(1+\frac{[A]}{K_A}\right)\left(1+\frac{[I]}{K_i}\right)+[B]} \qquad 2)$$

Equation 1 and Equation 2: Kinetic equation for substrate A (i.e., HNE) and substrate B (i.e., glucose) transformation, respectively, when the inhibitor I acts as a competitive ARDI . *KA and KB can be written as $K_A = \frac{k_{-1}+k_{+2}}{k_{+1}}$ and $K_B = \frac{k_{-3}+k_{+4}}{k_{+3}}$, and represent the Michaelis constant of substrate A (i.e., HNE) and B (i.e., glucose), respectively. Ki can be written as $K_i = \frac{[E][I]}{[EI]}$, and represents the dissociation constant of the complex EI.*

The equations 1 and 2 outline two positive effects of competitive ARDIs. Firstly, competitive ARDIs have a direct inhibitory effect on product Q (i.e., sorbitol) generation, which is also impaired by the competitive effect of the agonist substrate A. Secondly, competitive ARDIs apparently enhance the conversion of substrate A (i.e., HNE) because of the decrease of the competition between glucose and HNE [75].

Although “non-complete”, a competitive inhibitor of substrate B (i.e., glucose) can exert DI (namely partial competitive DI) even if the rate of HNE conversion of the ternary complex AKR1B1-ARDI-HNE is impaired in the presence of the competitive ARDI (i.e., $k_{+6} < k_{+2}$) [75]. In this case, the lower is k_{+6} compared to k_{+2}, the most the DI effect is reduced. In addition, a competitive inhibitor of substrate B could affect the ability of substrate A to bind the EI complex. For example, with $k_{+6} < k_{+2}$, if the affinity of the substrate A for EI complex is higher than the affinity for the free biocatalyst, both k_{cat} and K_A^{app} would be decreased [75, 114].
In addition, a DI is possible through uncompetitive and non-competitive inhibition models despite the reaction which should be preserved is partially affected. Admitting that the interaction of a specific substrate with the free biocatalyst induces the exposure of a peculiar binding site for the inhibitor, an uncompetitive inhibitor which binds exclusively the EB complex (i.e., AKR1B1-glucose complex) can exert DI (Figure 3) [75, 114].

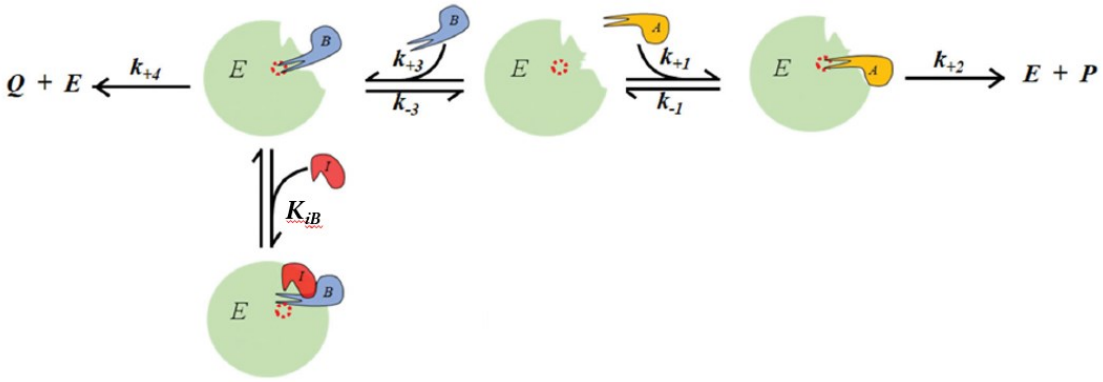

Figure 3. Uncompetitive inhibition model of ARDIs. *The inhibitor I acts as an ARDI and binds to the EB complex (i.e., AKR1B1-glucose). Different kinetic constants k_{+1}, k_{-1}, k_{+2}, k_{+3}, k_{-3}, k_{+4} are related to the formation and dissociation of the complex EB and EA; K_{iB} represents the dissociation constant of the EIB complex. (modified from Cappiello* et al., *2020).*

When analysed in steady-state conditions, the model of uncompetitive DI reported in Figure 3 can be described by the rate equations 3 and 4 expressing the generation of product P (i.e., DHN) and product Q (i.e., sorbitol), respectively:

$$v_p = \frac{k_{+2}E_T[A]}{K_A\left[1+\frac{[B]}{K_B}\left(1+\frac{[I]}{K_{iB}}\right)\right]+[A]} \quad (3$$

$$v_q = \frac{k_{+4}E_T[B]/\left(1+\frac{[I]}{K_{iB}}\right)}{K_B\left(1+\frac{[A]}{K_A}\right)/\left(1+\frac{[I]}{K_{iB}}\right)+[B]} \quad (4$$

Equation 3 and Equation 4: Kinetic equation for substrate A (i.e., HNE) and substrate B (i.e., glucose) transformation, respectively, when the inhibitor I acts as a uncompetitive ARDI. *K_A and K_B can be written as $K_A = \frac{k_{-1}+k_{+2}}{k_{+1}}$ and $K_B = \frac{k_{-3}+k_{+4}}{k_{+3}}$, and represent the Michaelis constant of substrate A (i.e., HNE) and B (i.e., glucose), respectively. K_{iB} can be written as $K_{iB} = \frac{[EB][I]}{[EIB]}$, and represents the dissociation constant of the complex EIB.*

Compared to competitive ARDIs, uncompetitive ARDIs affect the conversion of the substrate B (i.e., glucose) not only in terms of K_m but also in terms of V_{max} (Equation 4). It is noteworthy that, in contrast with the competitive inhibition model, the presence of the agonist substrate A and the presence of the inhibitor exert opposite effects on K_B^{app}, by inducing its increase and decrease, respectively. Most importantly, such model of inhibition partially affects the conversion of substrate A (i.e., HNE), since the formation of ternary complex EIB implies that the free biocatalyst is less available for catalysis (Equation 3).

As above mentioned, a non-competitive inhibitor of B can exert "non-complete" DI (Figure 4). In this case, admitting that the inhibitor does not interfere with the ability of the substrate A to bind the EI complex, the realisation of DI is modulated by the ratio Ki'/Ki, which defines the relative affinity of the inhibitor for the EB complex compared to the free biocatalyst: the highest is the competitive component of the inhibition, the highest is the DI effect [75, 114].

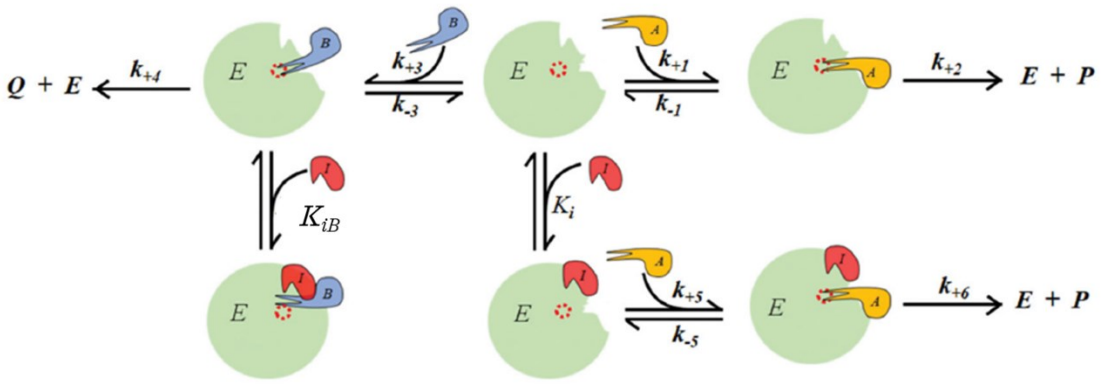

Figure 4. Non-competitive model of action of an ARDI. *The inhibitor I acts as an ARDI and binds to both the EB complex (i.e., AKR1B1-glucose) and the free biocatalyst. Different kinetic constants k_{+1}, k_{-1}, k_{+2}, k_{+3}, k_{-3}, k_{+4}, k_{+5}, k_{-5} and k_{+6} are related to the formation and dissociation of the complex EB, EA, and EIB; K_{iB} represents the dissociation constant of the EIB complex. (modified from Cappiello* et al., *2020).*

The possibility of DI was confirmed by several *in vitro* studies. The first compounds tested for their ability to act as ARDIs, even if not complete, were pyrazolo[1,5-a]pyrimidine synthetic derivatives. Among them, 5e, 4-(4-chlorobenzyl)-7-oxo-4,7-dihydropyrazolo[1,5-a]pyrimidine-6-carboxylic acid has been identified as the most effective ARDI because of its ability to inhibit at greater extent the reduction of L-idose and GS-HNE compared to HNE reduction [115]. However, in recent years the research of ARDIs has been focused on natural sources traditionally known for their beneficial properties. In this regard, the first natural ARDI was isolated from z*olfino* bean, a variety of *Phaseolus vulgaris* L. cultivated in Pratomagno (Tuscany) [116]. Fractionation of methanolic extracts of z*olfino* bean allowed the isolation and characterization of soyasaponins. Among the compounds isolated, soyasaponin Bb (SsBb) is the most promising ARDI acting as a mixed-type inhibitor of glucose reduction and as an uncompetitive inhibitor of HNE. Therefore, although "no complete", in hyperglycaemic conditions SsBb should be able to act as ARDI. In addition, ARDIs were isolated in Green tea, a natural product known for its anti-inflammatory properties. Green tea is reach in catechins, among which Epigallocatechin Gallate (EGCG) is the most abundant. EGCG and its structural moieties epigallocatechin and gallic acid were tested for their ability to act as potential ARDIs. EGCG and its gallate moiety have proved to act as not complete ARDIs, although only EGCG retains the ability to inhibit not only the conversion of glucose, but also on GS-HNE reduction [117].

All together, these findings encourage additional studies to better clarify the structural requirements of ARDIs.

1.6.3 Selective inhibitors

Since AKR1B10 shows high similarity with AKR1B1, it is not surprising that most of the classic ARIs are effective inhibitors of AKR1B10. Accordingly, several ARIs were tested as anti-neoplastic drugs for their ability to inhibit AKR1B10. However, the administration of potent but non-selective inhibitors can cause the onset of adverse effects due to the shutdown of the ubiquitous AKR1B1. Therefore, the administration of selective inhibitors has emerged as a promising tool for cancer therapy.

Comparison of AKR1B10 in holoenzyme conformation and in complex with either ARIs or selective inhibitors outlined two key structural differences with AKR1B1: i) position of Trp112, ii) flexibility of loop A.

i. **Conformation of Trp112 (Trp111 in AKR1B1) [118]**. As shown in Figure 5, in AKR1B1 holoenzyme, Trp111 is located between the anion binding pocket and the specificity pocket, with its side chain always oriented toward the anion binding site (AKR1B1-position). In this conformation, Trp111 is stabilized through hydrophobic interactions with Leu300. By contrast, in AKR1B10 holoenzyme Trp112 side chain points to the specificity pocket (AKR1B10-position), and it is stabilized by a network of hydrogen bond centred on the Gln114.

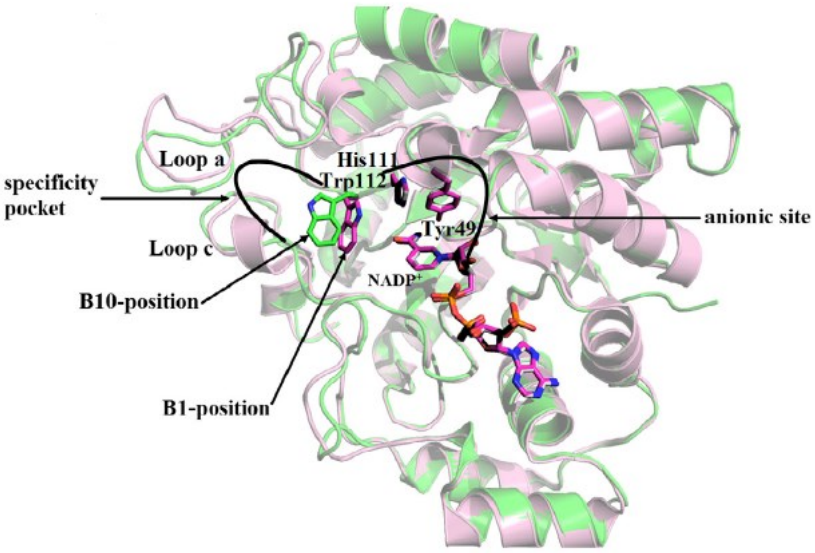

Figure 5. Superimposed holoenzyme structures of AKR1B10 (green) and AKR1B1 (violet). *Trp112 at the AKR1B10-position (green sticks) points to the specificity pocket, while Trp112 (Trp111) at the AKR1B1-position orients to the anionic pocket (Zhang et al. 2013).*

ii. **Flexibility of Loop A** [119]. In AKR1B10, loop A forms a subpocket which can allocate inhibitors or water molecules. In AKR1B1, the loop A is more compact, hydrophobic, and therefore less accessible.

Although *in vitro* screening and crystallographic methods are necessary to determine case-by-case inhibitor-enzyme interactions, three main requirements for AKR1B10 selective inhibition can be outlined [119]:

i. Like ARIs, selective inhibitors of AKR1B10 have an anchoring moiety such as carboxyl acid or acidic hydroxyl functional group. However, inhibitors with cyclic imide compounds need an additional aryl moiety for binding to either the specificity

pocket or loop A subpocket of AKR1B10. For example, *fidarestat*, a well-known cyclic imide ARI which lacks an aryl moiety, is a poor inhibitor of AKR1B10.

ii. Crystallization process of wild type or mutant AKR1B10 with selective inhibitors, determined that selectivity is linked to the presence of AKR1B10-position of Trp112 and/or aryl moieties which provide an optimal filling of the loop A subpocket. Compared to AKR1B1-like conformation, the Trp112 AKR1B10-position reduces the steric hindrance in the anion binding site of AKR1B10, increasing its accessibility to bulky and rigid inhibitors such as oleanolic acid, flufenamic acid, caffeic acid, phenethyl ester and UVI2008 (Figure 6) [118, 120, 121]. By contrast, the binding of non-selective inhibitors like *tolrestat* with AKR1B10 generally forces Trp112 to flip in "AKR1B1-like" position.

iii. Selective inhibitors of AKR1B10 usually do not fit within the specificity pocket of AKR1B1 as occurs for inhibitors with bulky aryl moieties such as JF0049 and MK204 (Figure 6) [122, 123].

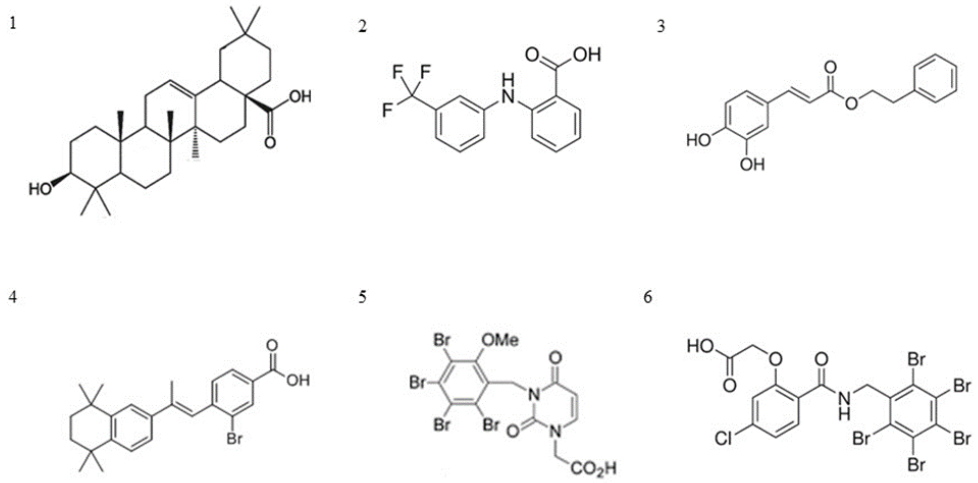

Figure 6 ***Selective inhibitors of AKR1B10****. 1) Oleanolic acid 2) flufenamic acid 3) caffeic acid phenetyl esther 4) UVI2008 5) JF0049 6) MK204.*

Several selective inhibitors of AKR1B10 were tested as antineoplastic compounds in cellular models. Oleanolic acid, CAPE and bisdemethoxycurcumin were able to inhibit isoprenoid metabolism in cancers cells and at least Oleanolic Acid and CAPE reduced cell growth [124-126]. It is noteworthy that Oleanolic acid reduced the growth of mitomycin c-resistant cancer cells [124]. These findings together suggest the antineoplastic effect of AKR1B10 selective

inhibitors and the efficacy of co-administration with anticancer drugs usually used in clinical practice.

2 Aims of the thesis:

In summary, both AKR1B1 and AKR1B10 have a pivotal role as detoxicant enzymes, but their involvement in diabetes and cancer, respectively, strongly suggests that their inhibition could be an effective therapeutic tool. However, several aspects should be considered to overcome failures in clinical trials. The multi-specificity of AKR1B1 requires that its inhibition to counteract secondary diabetes complications should be focused on glucose reduction leaving unaltered or less affected its detoxifying ability. Moreover, considering the AKR1B10 role in cancer development and the overlapping substrate and inhibitor specificities of AKR1B10 and AKR1B1, the administration of selective compounds may be beneficial to hamper the occurrence of side effects linked to off-target inhibition in cancer therapy. In addition, the use of AKR1B10 as a cancer biomarker in liquid biopsy technology could be useful for cancer diagnosis, prognosis and monitoring.

Considering all the abovementioned aspects, the aims of this study were:

i. To identify selective inhibitors of AKR1B10 in *zolfino* beans extract.
ii. To screen synthetic molecules for their ability to inhibit AKR1B1 and AKR1B10.
iii. To optimize a sensitive fluorescent assay for the detection of AKR1B10 in biological samples including small EVs.

3 Materials and Methods

3.1 Materials

Sodium phosphate monobasic, ammonium sulphate, sodium hydroxide, sodium chloride *(J.T. Baker)*; EDTA *(Juoro)*; L-idose, NADPH, *(Carbosynth)*; D, L-gliceraldehyde, bovine serum albumin (BSA), dimethyl sulfoxide (DMSO), D,L-dithiotreitol DTT, PMSF, isopropyl β-D-1-thiogalactopyranoside (IPTG), sodium dodecyl sulphate (SDS), methanol, acetone, yeast extract, Tryptone *(Sigma Aldrich)*; Acrylamide, N,N'-metilen-bis-acrylamide, N,N,N'N'-Tetramethylethylenediamine (TEMED), ammonium persulphate, formaldehyde, SDS, protein assay dye (Bradford reagent), Blue sepharose *(BioRAD Laboratories)*; Tris HCl *(BDH)*; glycerol *(BDH)*; DEAE Sepharose CL-6b e Sephadex G75 *(GE Healthcare)*; Matrex Orange A *(Millipore Amicon).* Prestained Protein Marker (10-175 kDa) (*GE Healthcare Life Sciences*). Expression vector pET30 (*Novagen*); Bondelut C18, solid phase extraction columns, octadecyl sorbent,60 Å pore size, 15 g resin, column volume 25 mL (*UCT Inc.*); YM10 ultrafiltration membranes, Merck-Millipore (Darmstadt,Germany), 4-Methoxy-1-naphtaldehyde (Cymit Quimica), 4-methoxy-1-naphtalenemethanol (Cymit Quimica). A549: Human non-small cell lung cancer: epithelial cell line derived from the lung tissue of an individual with lung cancer (ATCC). All other chemicals were of a reagent grade.

3.2 Methods

3.2.1 Expression, purification, and standard assay of recombinant *h*AKR1B1

3.2.1.1 Expression of recombinant *h*AKR1B1

The pET-30 vector, containing the sequence encoding human AKR1B1 (see Appendix), was used to transform BL21 (DE3) pLysS E. *coli* cells. E. *coli* cells were incubated with the pET-30 vector for 1 h on ice, followed by heat shock treatment for 60 seconds at 42°C and then cooled on ice for 5 minutes. *E. coli* cells were grown overnight at 37°C in 1L of Luria Broth medium supplemented with 30 µg/ml kanamycin. When $O.D._{600\ nm}$ reached a value of 0.8, protein expression was induced by the addition of 0.4 mM IPTG. After overnight incubation at 37 °C, cells were collected by a centrifugation step at 4500 *x* g for 30 min. The resulting pellet was suspended in 10 mM sodium phosphate pH 7 buffer (1 g cells/ ml) supplemented with 0.1 mM EDTA, 2 mM DTT and 1 mM PMSF. Cell lysis was obtained after three freeze-thaw

cycles, followed by ten cycles of sonication (5 W, amplitude 50%). Cell resuspension was centrifuged at 10000*x*g for 30 min at 4 °C and the soluble fraction, namely crude extract, was collected.

3.2.1.2 Purification of recombinant *h*AKR1B1

Purification of AKR1B1 consisted of three column chromatography steps performed at 4 °C. Firstly, the crude extract was applied to an ion exchange DEAE-52 column (3.5 ø *x* 30 cm), which was previously equilibrated in a 10 mM sodium phosphate buffer pH 7 supplemented with 0.1 mM EDTA and 2 mM DTT (standard buffer). The elution was performed at 15 mL/h with the standard buffer until the $O.D._{280\ nm}$ reached a constant baseline value. Then, a linear gradient of NaCl from 0 to 120 mM in standard buffer was applied. Fractions of 4 ml were collected and tested for AKR1B1 activity. Fractions showing AKR1B1 activity were pooled and dialysed against a 10 mM sodium phosphate buffer pH 7 using a YM10 ultrafiltration membrane until the dilution factor of both NaCl and DTT was 1:32. The pool of fractions was concentrated until the volume reached 40 ml and it was applied to a Matrex Orange A affinity chromatography column (3.5 ø *x* 23 cm), which was previously equilibrated in standard buffer deprived of DTT. When the $O.D._{280\ nm}$ reached a constant baseline value, the elution of AKR1B1 was obtained by the addition of 0.1 mM NADPH to the buffer. Fractions showing AKR1B1 activity were pooled and concentrated using a YM10 ultrafiltration membrane until the final volume of 10 ml was reached. The pool of fractions was applied to a molecular exclusion Sephadex G-75 column (2.6 ø *x* 80 cm), which was previously equilibrated in standard buffer. Fractions showing AKR1B1 activity were pooled and concentrated until the final concentration of the enzyme was 0.5 mg/ml. The protein concentration was determined according to Bradford [127], using BSA as a standard protein. AKR1B1 activity and protein concentration of each pool are reported in Table 2. The enzyme was stored in 10 mM sodium phosphate buffer pH 7 supplemented with DTT 2 mM and 33% (v/v) glycerol at -80 °C. The purity of the final enzyme preparation was assessed by SDS-PAGE (Figure 7).

	Volume (ml)	Enzymatic concentration (U/ml)	Protein concentration (mg/ml)	Specific Activity (U/mg)	Total Units (U)	Total Protein (mg)	Purification factor	Yield %
Crude extract	15.0	20.0	11.5	1.7	300.0	173.0	1.0	100
Pool DEAE	42.0	6.0	1.1	5.4	252.0	47.0	3.1	84
Pool Matrex Orange	10	23.9	4.35	5.5	239	43.5	3.2	79
Pool G75	84.0	2.8	0.5	6.0	231.8	38.9	3.4	77

Table 2 AKR1B1 purification Table. *For each purification step, starting from the crude extract (C.E.), volume (ml), enzymatic concentration (expressed as U/ml), total enzyme units (U), protein concentration (mg/ml), total protein (mg), AKR1B1 specific activity (U/mg), purification factor and percent yield are reported.*

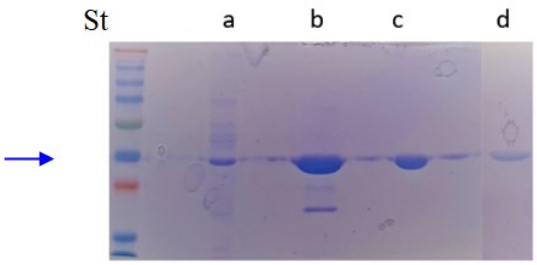

Figure 7 DISC-SDS-PAGE 12%. *Electrophoretic gel of crude extract (a), DEAE 52 pool (b), Matrex Orange Pool (c) and G75 Pool (d). St: standard prestained Sharpmass vii (euroclone). For each sample 10µg of protein was loaded. Blue arrow indicates the molecular weight of 37 KDa, corresponding to the molecular weight of the recombinant hAKR1B1.*

3.2.1.3 Assay of recombinant *h*AKR1B1 activity

Before testing the activity of AKR1B1, the stored enzyme was dialyzed using a YM10 membrane filter against a sodium phosphate buffer pH 7 until the dilution factor of both glycerol and DTT was 1:1000. The standard assay mixture for the detection of AKR1B1 activity contained 0.25 M sodium phosphate buffer pH 6.8, 0.18 mM NADPH, 0.37 M ammonium sulphate, 0.47 mM EDTA and 4 mM D, L-glyceraldehyde in a total volume of 700 µL. The

activity of AKR1B1 was determined at 37 °C by a spectrophotometric assay, monitoring the decrease of absorbance linked to NADPH oxidation at 340 nm (ε_{340nm}= 6.22 $mM^{-1}cm^{-1}$). One unit of enzyme activity is the amount of enzyme that catalyses the conversion of 1 µmol of substrate/min under the above assay conditions. Same assay conditions were adopted during the inhibition studies in the presence of L-Idose and HNE.

3.2.2 Expression, purification, and standard assay of recombinant *h*AKR1B10

3.2.2.1 Expression of recombinant *h*AKR1B10

The pET-30 vector, containing the sequence encoding human AKR1B10 (see Appendix), was used to transform BL21 (DE3) pLysS E. *coli* cells. E. *coli* cells were incubated with the pET-30 vector for 1 h on ice, followed by heat shock treatment for 60 seconds at 42°C and then cooled on ice for 5 minutes. *E. coli* cells were grown overnight at 37°C in 1L of Luria Broth medium supplemented with 30 µg/ml kanamycin. When $O.D._{600\ nm}$ reached a value of 0.8, protein expression was induced by the addition of 0.4 mM IPTG. After overnight incubation at 30 °C, cells were collected by a centrifugation step at 4500*x*g for 30 min at 4 °C. The resulting pellet was resuspended in 50 mM Tris/HCl pH 7.4 buffer (1 g cells/ml) supplemented with 1mM PMSF and 0.5 mM DTT. Cell lysis was obtained after one freeze-thaw cycle, followed by five cycles of sonication (5 W, amplitude 50%). Cell resuspension was centrifuged at 10000 *x*g for 30 min at 4 °C and the soluble fraction, namely crude extract, was collected.

3.2.2.2 Purification of recombinant *h*AKR1B10

Purification of AKR1B10 consisted of two column chromatography steps performed at 4 °C. The crude extract was applied to a DEAE Sepharose CL-6B column (2.5 ø *x* 13 cm), which was previously equilibrated in 50 mM Sodium Phosphate pH 7 buffer supplemented with 2 mM DTT (standard buffer). The elution was performed at 20 ml/h in standard buffer. Fractions of 3.5 ml were collected and tested for AKR1B10 activity. Fractions showing AKR1B10 activity were pooled and dialysed with YM10 ultrafiltration membrane until a final concentration of 0.2 mM DTT was reached. The pool of fractions was then applied to a Blue Sepharose column (1.5 ø *x* 6 cm), which was previously equilibrated with the standard buffer deprived of DTT. The elution was performed at 20 ml/h and fractions of 3.5 ml were collected. When the $O.D._{280nm}$ reached a baseline value, the elution of AKR1B10 was obtained by applying the standard buffer supplemented with 0.1 mM NADPH and 0.37 M NaCl. Fractions showing AKR1B10 activity were pooled and concentrated until a concentration of 2 mg/ml. The protein concentration was

determined according to Bradford [127], using BSA as a standard protein. AKR1B10 activity and protein concentration of each pool are reported in Table 3. The enzyme was stored in 10 mM sodium phosphate buffer pH 7 supplemented with DTT 2 mM and 30% (v/v) glycerol at -20 °C. The purity of the final enzyme preparation was assessed by SDS-PAGE (Figure 8).

	Volume (ml)	Enzymatic concentration (U/ml)	Protein concentration (mg/ml)	Specific Activity (U/mg)	Total Units (U)	Total Protein (mg)	Purification factor	Yield %
Crude extract	21	2.14	13.05	0.16	44.9	274.05	1	100
Pool DEAE	6.5	6.9	7.7	0.89	44.85	50	5.56	100
Pool Blue Sepharose	6.5	4.22	2.49	1.69	27.4	16	10	61

Table 3 AKR1B10 purification Table. *For each purification step, starting from the crude extract (C.E.), volume (ml), enzymatic concentration (expressed as U/ml), total enzyme units (U), protein concentration (mg/ml), total protein (mg), AKR1B10 specific activity (U/mg), purification factor and percent yield are reported.*

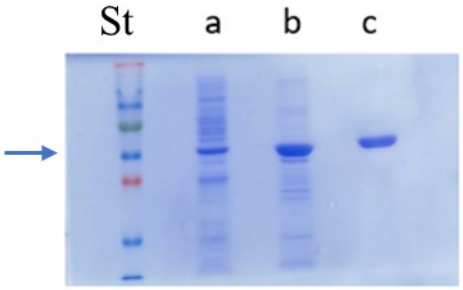

Figure 8 DISC-SDS-PAGE 12%. *Electrophoretic gel of crude extract (a), DEAE pool (b), and Blue Sepharose Pool (c). For each sample 5 µg of protein was loaded. St: standard prestained Sharpmass vii (euroclone). Blue arrow indicates the molecular weight of 37 KDa, corresponding to the molecular weight of the recombinant hAKR1B10.*

3.2.2.3 Activity assay of recombinant *h*AKR1B10

Before testing the activity of AKR1B10, the stored enzyme was dialyzed using a YM10 filter against a sodium phosphate buffer pH 7 supplemented with 0.5 mM DTT until the dilution factor of glycerol was 1:1000. The standard assay mixture for the detection of AKR1B10 activity contained 0.1 M sodium phosphate buffer pH 7, 0.18 mM NADPH, and 15 mM D, L-glyceraldehyde in a total volume of 700 µL. The activity of AKR1B10 was determined at 37 °C by a spectrophotometric assay, monitoring the decrease of absorbance linked to NADPH oxidation at 340 nm (ε_{340nm}= 6.22 $mM^{-1}cm^{-1}$). One unit of enzyme activity is the amount of enzyme that catalyses the conversion of 1 µmol of substrate/min under the assay conditions described above. Same assay conditions were used in inhibition studies in the presence of HNE.

3.2.3 Preparation of HNE

Synthesis of HNE was performed by the Department of Chemistry and Industrial Chemistry, University of Pisa [23]. The compound was synthesized as diethyl-acetal and stored in hexane at -80 °C. The corresponding free aldehyde was obtained by removing the solvent through evaporation and adding 1 mM HCl. After 30 min of in incubation at 4°C, the concentration of the corresponding aldehyde was evaluated by spectrophotometric measurement (ε_{224nm}= 13.75 mM^{-1} cm^{-1}).

3.2.4 Identification of selective inhibitors in *zolfino* bean extract

3.2.4.1 *Zolfino* bean extract preparation

Zolfino bean seeds were incubated at 25°C overnight in ultrapure H_2O (0.5 g/ml). After seeds removal, the medium was boiled for 2h and subsequently centrifuged at 100.000 *xg* for 1 h at 4°C. The supernatant, namely *zolfino* bean extract, was filtered twice through a 0.2 µm PTFE filter and stored at -20 °C.

3.2.4.2 *Zolfino* bean extract fractionation

Fractionation of *zolfino bean* extract was performed by hydrophobic interaction chromatography using a 25 ml *Bondelut C18* column. The *Bondelut C18* column was previously activated by applying the following elution steps: i) 50 ml of acetone at free flow rate, ii) 50 ml of methanol at free flow rate, iii) 100 ml of methanol at a flow rate of 20 ml/h for 5 h, iv) 500 ultrapure H_2O at a flow rate of 20 ml/h. An aliquot of 20 ml of *zolfino* extract was rapidly thawed at room temperature and applied to *BondElut* C18. The separation was performed at a

flow rate of 22 ml/h by applying the following mixtures (v/v) of ultrapure water (solvent A) and methanol (solvent B): i) 200 ml 100% A, ii) 100 ml 25 % B, iii) 100 ml 50% B, iv) 100 ml 100% B. The absorbance was monitored at 265 nm and fractions of 2.2 ml were collected.

3.2.4.3 Mass Spectrometry analysis of fractions of *zolfino* bean extract

Five microliters of each fraction were processed on a Eksigent expert microLC 200 system (Eksigent, AB Sciex, Framingham, MA, USA) and acquired using a 5600+ TripleTOF mass spectrometer (AB Sciex). Samples were separated on a Jupiter 150- 0.3 mm, particle size 4 μm, 90 Å capillary column using 0.1% v/v formic acid in water (buffer A) and 0.1% v/v formic acid in acetonitrile (buffer B) with a linear gradient from 2 to 35% of buffer B in 40 min at a flow rate of 5 μL/min. LC column was directly interfaced with a DuoSpray™ ESI ion source operating in positive mode at 5.5 kV for peptide ionization. We used an information dependent acquisition (IDA) tandem mass spectrometry (MS) for spectral library generation that relies on a survey MS1 scan followed by the selection of a maximum of 20 most abundant precursor ions and their further fragmentation by collisional induced dissociation (CID) using nitrogen N_2 as inert gas to generate MS2 spectra. MS1 survey and MS2 scans were acquired with a resolving power of 30.000 and 25.000 over a mass range of 100–1250 m/z and 50–1250 m/z, respectively. Isolation width for precursor ion selection was set at 0.7 m/z on a Q1. The accumulation time was set to 250 milliseconds for MS1 scans while 100 milliseconds for MS2 scans. Rolling collision energy with a collision energy spread across 5 eV and background subtraction were enabled to achieve the optimal fragmentation according to m/z ratio and charge state and to increase sensitivity.

3.2.5 Detection of *h*AKR1B10 reductase activity by fluorimetric assay

3.2.5.1 Absorbance and fluorescence emission spectra of 4 Methoxy-1-naphtaldehyde and 4-methoxy-1-naphtalene methanol

Stock solution of 3.1 mM 4-Methoxy-1-naphtaldehyde (MONAL-41, Figure 9A) was prepared in a water:acetonitrile solution (2:1) and stored at -20°C. Stock solution of 4-methoxy-1-naphtalenemethanol (MONOL-41, Figure 9B) was prepared in EtOH 100% at a final concentration of 5.86 mM and stored at +4°C.

A B

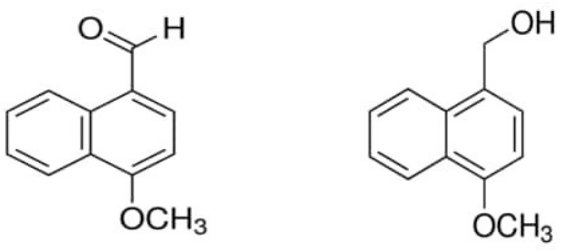

Figure 9 (A) MONAL-41; (B) MONOL-41.

3.2.5.2 Fluorimetric assay of hAKR1B10

Fluorimetric assay of *h*AKR1B10 were performed by FLUOstar OMEGA (BMG Labtech GmbH) in 96-well flat-bottom black Greiner microplates. The assay mixture for the detection of AKR1B10 fluorescent activity contained 0.1 M sodium phosphate buffer pH 7.0, 0.08 mM NADPH, and MONAL-41 in a total volume of 100 µL. To avoid auto-oxidation of the aldehyde, the assay buffer was degassed before use. In addition, to prevent inhibition linked to the acetonitrile, MONAL-41 stock solution was opportunely diluted in the buffer assay before adding to the assay mixtures. The emission of fluorescence of MONOL-41 was followed at 410 nm exciting at 320 nm at 37°C. The absolute reaction rate was calculated as:

$$v = \frac{dF}{dt}\ x\ \frac{1}{slope\ Monol - 41}$$

where $\frac{dF}{dt}$ is the time-dependent fluorescence slope, and "slope MONOL-41" is the slope of the calibration curve of fluorescence of MONOL-41 in 0.1 M sodium phosphate buffer pH 7.0 supplemented with 0.080 mM NADPH.

Same conditions were adopted for inhibition studies in the presence of Oleanolic Acid with the exception that the inhibition assay mixtures contained 0.7% of DMSO.

3.2.5.3 Cell cultures

A549 cell line was grown at 37 °C under a humidified atmosphere of 5% CO_2 and 95% air in DMEM GlutaMAX™ medium in two different conditions: i.) medium was supplemented with 10% FBS which was not previously treated. When cell confluency was 100%, A549 were washed twice in PBS 1x and were grown for 24h in medium without FBS. Cells grown in such

conditions are named “starved”. ii) medium was supplemented with 10% FBS which was previously depleted of bovine small EVs by a differential centrifugation as follows. Firstly, the FBS was centrifuged at 10.000 *x* g for 30 min. The resulting supernatant was collected and subjected to a centrifugation at 100.000 *x* g for 1h. The resulting supernatant (ultracentrifuged FBS) was added to the medium after a filtration with a 0.2 µm filter. Cells grown in such conditions are reported as “not starved”.

3.2.5.4 Extracellular vesicles isolation

Two different methods were performed to isolate small EVs from conditioned medium, namely differential ultracentrifugation and sequential filtration.

Differential ultracentrifugation method: When cell confluency was 100%, the conditioned medium of the “not starved” cell cultures was collected and stored at -20°C. The small extracellular vesicles (EVs) isolation was obtained by differential centrifugation of this medium. After thawing at room temperature, the medium was centrifuged at 2.000 *x* g for 15 min at 4°C. The resulting supernatant was then collected and centrifuged at 10.000 *x* g for 30 min at 4°C. The supernatant was then collected and centrifuged at 100.000 *x* g for 2 h at 4°C. The resulting pellet was resuspended in 0.1 M sodium phosphate pH 7.0 buffer and centrifuged at 100.000 *x* g for 1 h at 4 °C. The resulting pellet is resuspended in 0.1 M sodium phosphate buffer pH 7.0 (250 µl/100 ml of medium centrifuged) and stored at -20°C.

Sequential filtration: Conditioned medium was collected from “starved” A549 cell cultures and applied to a homemade sequential membrane filtration device inspired to ExoTIC [128]. The small EVs were extensively washed during purification with 0.1 M sodium phosphate buffer pH 7.0 and concentrated in Amicon Ultra-filter to a volume of 150 µl.

3.2.5.5 Characterization of EVs

The characterization of small EVs isolated by differential ultracentrifugation method was obtained by using nanoparticle tracking analysis and cryogenic electron transmission microscopy.

Nanoparticle tracking analysis (NTA) was carried out at the external facility Soft Materials Service of ICMAB-CSIC /U6_NANBIOSIS. NTA is based on light-scattering properties and Brownian motion to determine nanoparticle concentration, size, and aggregation state in a liquid suspension. The size and the number of EV obtained by this method were determined by using NanoSight LM10-HS system (Malvern Panalytical) with a tuned 405 nm laser source. Particle-

by particle analysis was performed with the NanoSigth NTA software, by using the Stokes-Einstein equation, to calculate their hydrodynamic diameter.

Cryogenic transmission electron microscopy (cryo-TEM) was performed at the Microscopy Service of the UAB. The EV were visualized to observe their native size and shape. Ten µL of EV were collected and deposited on Formvar-carbon electron microscopy grids to freeze with ethane.

During the whole process, the sample was kept at −182°C. Cryo-TEM images were obtained using the JEOL JEM 2011 electron microscope.

3.2.5.6 Detection of AKR1B10 fluorimetric activity in cell and small EVs extracts

To detect fluorimetric activity of AKR1B10 in cell extracts, cells grown in both conditions described in section 3.2.5.4 were collected and washed with PBS 1x containing 1 mM PMSF, before being stored at -20°C. Then, cells were rapidly thawed at 37°C and lysed with 5 cycles of sonication (impulses of 30 seconds with intervals of 30 seconds, 60% amplitude). Then, cell extracts were centrifuged at 16100 *x g* for 15 min at 4°C to remove cell debris. Same conditions were adopted to lyse the small EVs collected as described in section 3.2.5.4, with the exception that 1 mM PMSF was added after thawing. The total protein concentration in cell extracts and small EVs was determined by Bradford method [127] and Micro BCA™ Protein Assay Kit, respectively.

The assay for fluorimetric detection of AKR1B10 activity in the presence of 7 µM MONAL-41 as substrate was performed as described in section 3.2.5.2, adding either cell extract or small EVs extract in place of the purified protein.

3.2.5.7 Evaluation of the Conversion of MONAL-41 by intact cells

To determine if MONAL-41 is a suitable substrate to follow the reductase activity in A549 cell cultures, cells were treated with MONAL-41, and then MONOL-41 production was monitored by fluorescence emission in conditioned medium. $8x10^5$ cells were seeded on a Petri dish in a final volume of 10 ml of complete medium (DMEM + GlutaMAX™ + 10% (v/v) ultracentrifuged FBS) and incubated at 37°C and 5% CO_2 in air. After overnight incubation, the medium was replaced with 10 mL of complete medium containing 50 µM MONAL-41 or 0.53% (v/v) of acetonitrile (the solvent of MONAL-41) for controls. Detection of MONOL-41 was performed by exciting at 296 nm (pathlength 0.3 cm) the conditioned medium collected at

several time points from cell cultures treated in both conditions. Fluorescence emission spectra were recorded in the 310-500 nm interval. To correct the fluorescence emission spectra of medium obtained from cell cultures treated in both conditions, the fluorescence emission of medium obtained from two Petri dishes without cells treated with complete medium containing 50 μM MONAL-41 or 0.53% (v/v) of acetonitrile was subtracted as a blank.

3.2.5.8 Western blot analysis

Western Blot analysis was performed on small EVs obtained in both conditions described in section 3.2.5.4. Small EVs obtained with the differential centrifugation procedure were lysed with M-PER™ (1:3), and the lysate was centrifuged at 16000 *xg* for 15 minutes at 4°C to remove debris. Then, to concentrate the lysate, it was centrifuged at 14000 *xg* for 5 minutes at 4°C in Amicon Ultra filters with a cut-off of 10 KDa. The lysate was immediately used for Western Blot analysis. Small EVs obtained with the sequential filtration procedure were lysed as described in section 3.2.5.6. The lysate was then centrifuged at 16000 *xg* for 15 minutes at 4°C to remove debris and stored at –20°C.

SDS-page was performed on a 12% (w/v) 0.75 mm polyacrylamide gel using TGX Stain-Free™ Fast Cast™ Acrylamide kit (Biorad). Samples were treated with sample buffer (250 mM Tris-HCl pH 6.8 buffer supplemented with SDS 10% (w/v), glycerol 30% (v/v), bromophenol blue 0.05% (w/v), and 0.7 M β-mercaptoethanol). Samples were incubated for 10 minutes at 70°C. Samples were then loaded on the polyacrylamide gel and the running was performed with a buffer pH 8.8 containing 25 mM Tris, 192 mM glycine, and SDS 1% (w/v) at constant voltage 200V. Gel was then activated for 5 minutes by UV light by ChemiDoc MP Imaging System (Bio-Rad). Proteins were transferred to a 0.2 μM PDVF membrane by Transfer-Blot® Turbo™ (6 minutes at constant 1.3A and at a maximum of 25V). Membrane was then washed for five minutes three times in TBS supplemented with 0.1 % tween®-20 and incubated in TBS supplemented with 0.1% tween®-20 and milk 5% (w/v) for one hour at room temperature. Membrane was then washed for five minutes three times with TBS supplemented with 0.1 % tween®-20. Membrane was then incubated overnight in anti-AKR1B10 antibody (Origene) diluted 1:1000 in TBS supplemented with 0.1% tween®-20 and milk 5% (w/v) at 4°C. Membrane was then washed five minutes three times in TBS supplemented with 0.1% tween®-20 and incubated for one hour in HRP-anti-Rabbit antibody diluted 1:1000 in TBS supplemented with 0.1% tween®-20 and milk 5% (w/v) at room temperature. Membrane was the washed five minutes three times in in TBS supplemented with 0.1% tween®-20 and three

times in TBS. The detection was performed with a solution containing luminol (1:2) and H_2O_2 (1:2) by ChemiDoc MP Imaging System (Bio-Rad).

3.2.6 Kinetic Analysis

The inhibitory effect of commercial standards and of synthetized molecules was determined measuring the reaction rates in the presence of a fixed substrate concentration (2 mM L-idose for AKR1B1 and 0.04 mM HNE for both AKR1B1 and AKR1B10) and increasing inhibitor concentrations. The IC50 (inhibitor concentration able to decrease the enzymatic activity up to 50%) values were determined by non-linear regression analysis fitting experimental data to the following equation:

$$y = \frac{Top - Bottom}{1 + \left(\frac{x}{logIC50}\right)} + Bottom$$

Where "y" is the Residual Activity (%), i.e., the activity measured in the presence of inhibitor normalized on the activity of the controls; "*Top*" and "*Bottom*" represent the plateaus of the fitting curve expressed as Residual Activity (%) and were constrained to values equal to 100 and 0, respectively; "*x*" is the logarithm of inhibitor concentration.

To define the mechanism of action of inhibitors, reaction rates were measured in assay mixtures containing different substrate concentrations (L-idose between 0.8 and 6 mM for AKR1B1 and HNE between 0.03 and 0.08 for both AKR1B1 and AKR1B10) in the absence and in the presence of different inhibitors concentrations. Then, to obtain ${}^{app}V_{max}$ and ${}^{app}K_m$ values, inhibition curves were analysed by non-linear regression fitting the experimental data to the *Michaelis-Menten* equation:

$$y = \frac{V_{max}\, X}{K_m + X}$$

Where "X" represents the concentration of substrate. K_m was constrained to be higher than 0. The apparent dissociation constants *Ki'* (for the ESI complex) and *Ki* (for the EI complex) were then determined from Dixon plots of $1/{}^{app}V_{max}$ and ${}^{app}K_m/{}^{app}V_{max}$ as function of the inhibitor concentration, respectively.

3.2.7 Statistical Analysis

Statistical analysis was performed using Prism Graph-Pad 10 (GraphPad Software, San Diego, CA, USA).

4 Results

4.1 Identification of selective inhibitors in zolfino bean extract

4.1.1 Evaluation of the ability of *zolfino* bean extract to inhibit AKR1B1 and AKR1B10

Zolfino bean extract absorption spectrum was analysed both after preparation and after defrosting to at least preliminarily compare extracts subjected to storage. Although a slight difference in absolute values of absorbance was detected, which can be linked to an intrinsic variability of the analytical method used, the absorption spectra are comparable and show absorption peaks at 265 nm and 340 nm (Figure 10).

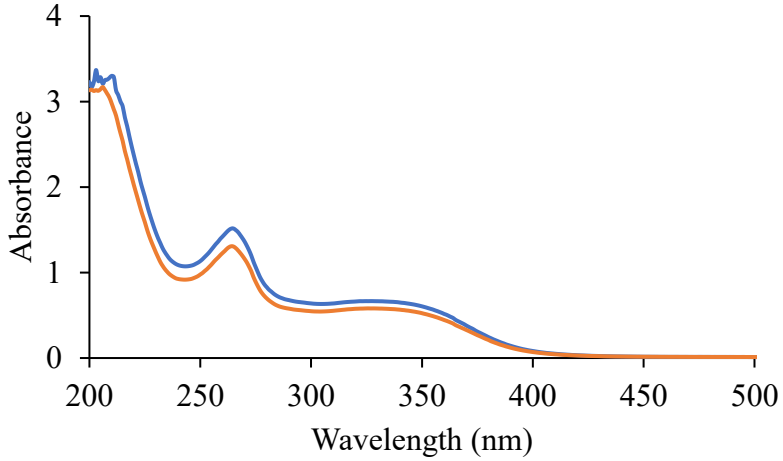

Figure 10 Absorption spectra of zolfino bean extract. *Zolfino* bean extract was diluted 1:10 in milliQ water and evaluated through a spectrophotometric analysis before (blue line) and after (orange line) storage at -20°C.

Fractionation of *zolfino* bean extract was performed on a Bondelut C18 obtained by applying a step wise gradient of methanol, as described in section 3.2.4.2. Fractions were then tested for their ability to inhibit AKR1B1 and AKR1B10 in the presence of 0.04 mM HNE, as a substrate (Figure 11).

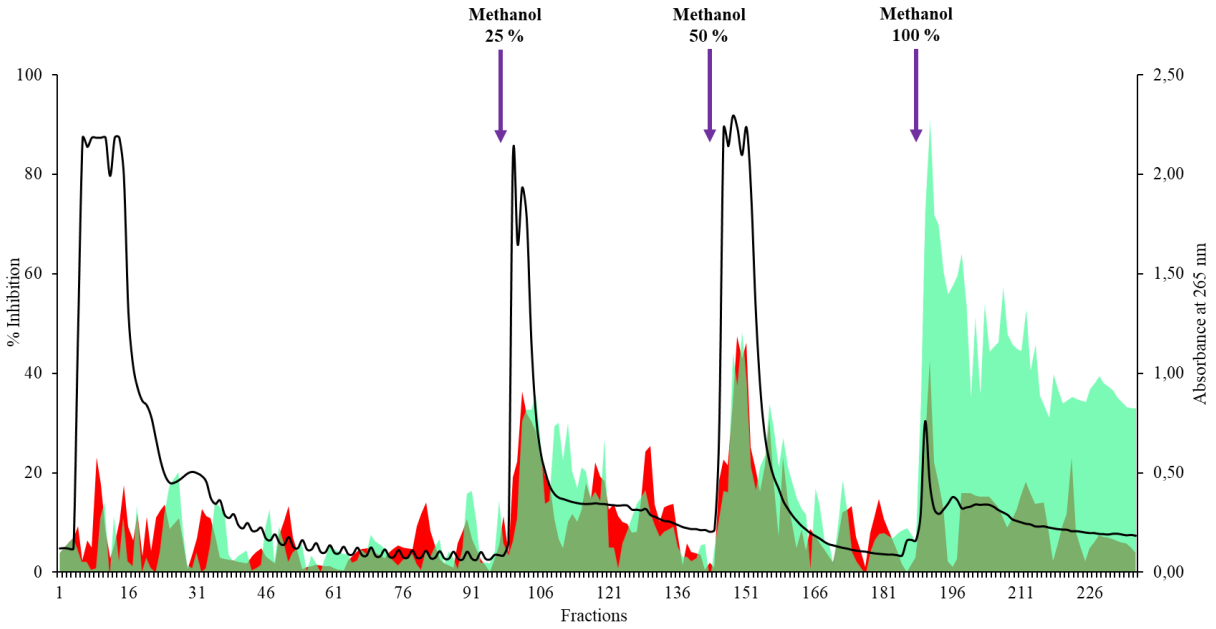

Figure 11: Elution profile of Zolfino beans extract. *The fractionation was obtained by applying 20 ml of zolfino beans extract to a Bondelut C18 column. Fractions were tested for their inhibitory ability on AKR1B1 (red areas) and AKR1B10 (green areas) in the presence of 0.04 mM HNE in at least three independent measurements. 10 mU of AKR1B1 and 5 mU of AKR1B10 were used for inhibition studies. The turquoise area refers to the overlap of red and green areas. Inhibition potential was reported as % Inhibition. The black line indicates the absorbance at 265 nm. The violet arrows indicate the application of Methanol at the reported concentrations.*

To avoid significative inhibition of methanol on both enzymes, the concentration of alcohol in inhibition assay mixtures was kept constant to 1.7% (v/v). Therefore, before testing, fractions eluted in 50% (v/v) methanol and 100% methanol were dried at room temperature in a Speedvac apparatus and resuspended in 1 ml and 0.5 ml of 100% methanol, respectively, while fractions eluted in 100% ultrapure water and in 25% (v/v) methanol were tested without any previous treatment. Then, the following volumes were added to the assay mixtures: i) 50 µl of fractions eluted in 100% ultrapure water and in 25% (v/v) methanol; ii) 25 µl of fractions eluted in 50 % (v/v) methanol; iii) 12 µl of fractions eluted in 100 % methanol. To select the most effective fractions for further analyses through LC-MS, values of selective inhibition (expressed as difference between percentage inhibition exerted on AKR1B10 and percentage inhibition exerted on AKR1B1) were correlated with the percentage inhibition exerted on AKR1B10 (Figure 12). Fractions of interest were 195-197 (figure 12, red circle), eluted in a volume range of 18-24 ml after 100% methanol loading. These fractions combined high inhibitory potential with best AKR1B10 vs AKR1B1 selectivity.

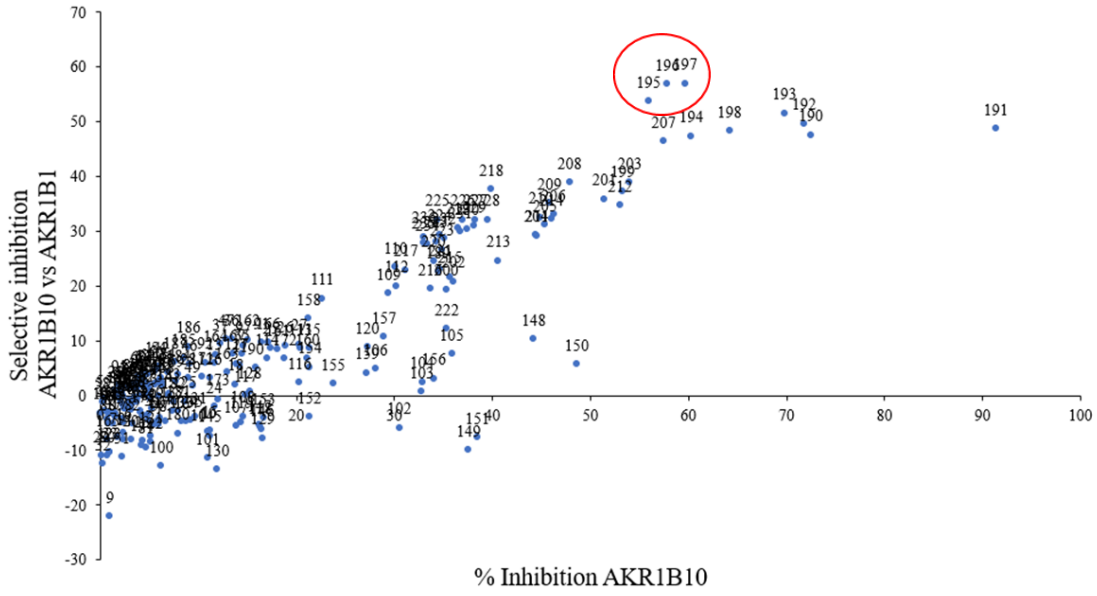

Figure 12. Relationship between selectivity and potency of zolfino beans extract fractions.

4.1.2 Mass spectrometry analysis

The LC-ESI/MS-MS analysis was focused on the subset of four contiguous fractions 195-198, which included fractions with the strongest and most selective inhibitory potential. First, an LC-MS analysis was performed in identical conditions for all the fractions examined, and the 10.000 more represented ion couples were retained in the subsequent analysis.

To identify promising candidates as selective inhibitors of AKR1B10, mass spectra of the examined subset of fractions provided by LC-ESI/MS-MS analysis were filtered according to the following criteria:

i. Fraction 196 was used as a reference since enzymatic assays had identified it as that with the highest selective inhibitory potential.
ii. Intensity of precursor ion peak for the examined compounds must be higher than 10% of the most abundant peak present in the reference fraction.
iii. The precursor ion must be present in the reference fraction.
iv. The relative intensity (%) of the precursor ion must be higher in the reference fraction compared to other fractions of the subset.

These conditions aimed at selecting a subset of molecules present in reasonable abundance in the examined fractions and that are predominantly found in the fraction with the highest and most selective inhibition, under the assumption that the inhibition does not derive from a synergistic or additive effect. To further refine this subset, additional assumptions were made, i.e. that components present in the four analysed fractions are manly different in the relative amount, but not in the identity, of the inhibitors, and that the number of effective inhibitors in the fractions is low. Under these assumptions, inhibition profile observed in the four fractions should match the concentration profile of the molecule in the LC-MS analysis. This was tested by looking for a correlation between the inhibition (%) of AKR1B10 normalized to that of the reference fraction (table 4) and the normalized concentration profile of ions identified by LC-MS (reduced Chi-square test, df = 2).

Fractions	195	196	197	198
Inhibition (%)	54	57	57	48
Normalized inhibition	0.95	1.00	1.00	0.84

Table 4. Normalized inhibitory potential of fractions 195-198, with respect to the inhibitory potential of fraction 196, i.e. the reference fraction. The normalized inhibition values match the expected elution profile of putative strong and selective inhibitors.

According to the above-described data management procedure (reported in figure 13), two precursor ions (fulfilling all the initially posed conditions) matched the elution profile of the subset of fractions ($P_{\chi}\ (\chi^2;\ df = 2) > 0.98$). These ions showed a m/z value of 313.2854 and 359.33 and a retention time of 62.6 and 69.7 min, respectively (figure 14 and 15, respectively). Finally, their fragmentation pattern was compared with publicly available data bases using an online tool (ms.epfl.ch), which allowed the identification of the glycerol-esters of palmitic acid and stearic acid with m/z 313.2854 [M-H_2O^+-H^+] and 359.33 [M^+-H^+], respectively (Figure 16).

RAW data

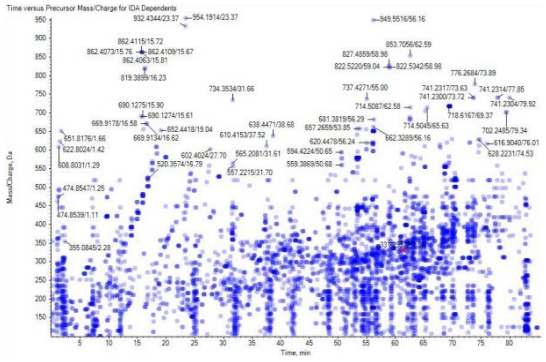

Representative example of LCMS peaks in one fraction
Each dot represents a single molecule in the analyzed fraction

Peak Filtering

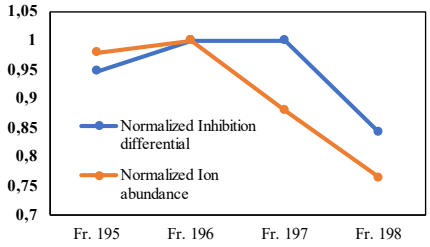

Profile matching between differential inhibition and ion concentration in the fractions.

m/z peaks filter criteria

(1) Fraction 196 used as reference

(2) Intensity greater than 10% of the most intense peak in chromatogram

(3) Relative intensity (%) of the precursor ion higher in the reference fraction compared with other fractions

MS/MS spectra extraction

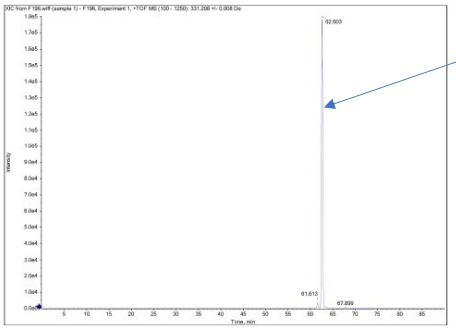

Extraction of Selected Ion Chromatogram

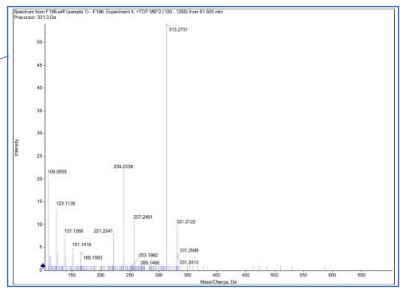

Recovery of MS/MS spectra

MSTools

Identification by comparison with spectral libraries (ms.epfl.ch)

Figure 13. Data management procedure of LC-ESI-MS/MS results.

A

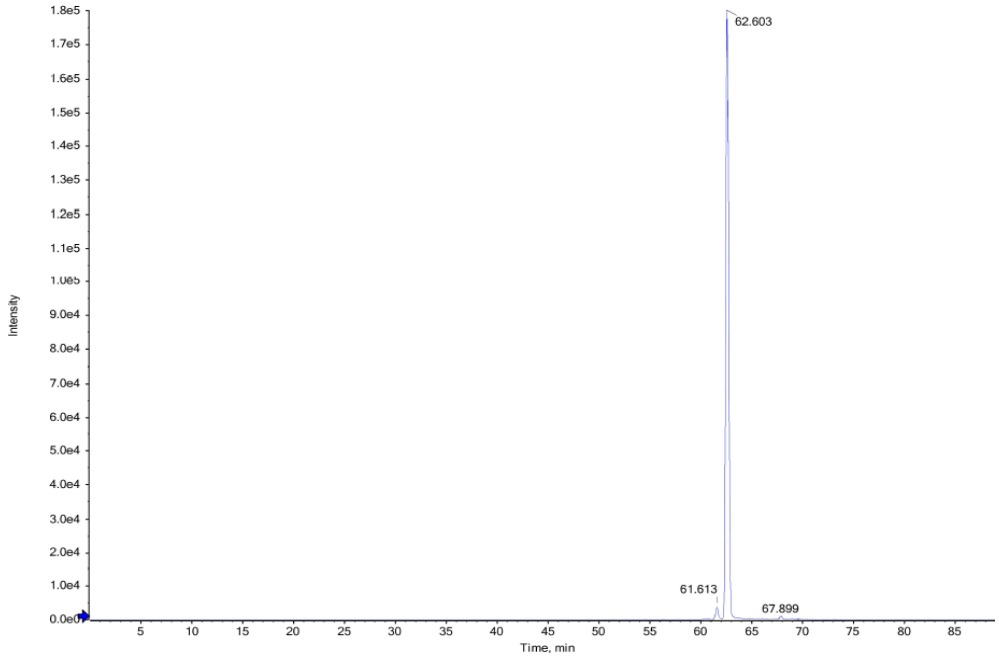

B

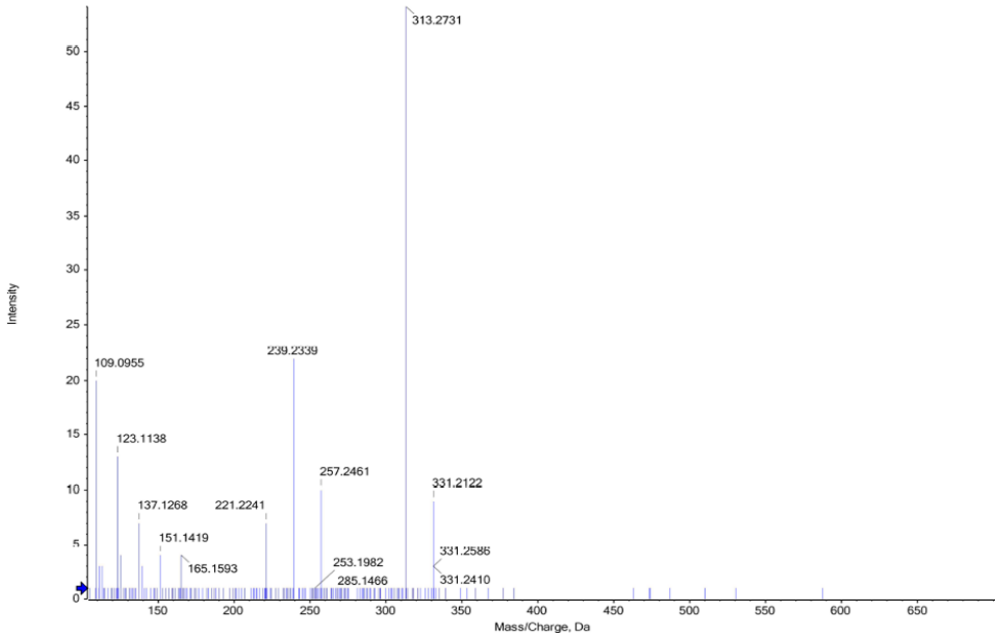

Figure 14. **Panel (A):** Extracted Ion chromatogram of compound with m/z 313.2854 [M-H2O^{+}-H^{+}]; **Panel (B)**: Fragmentation spectrum.

A

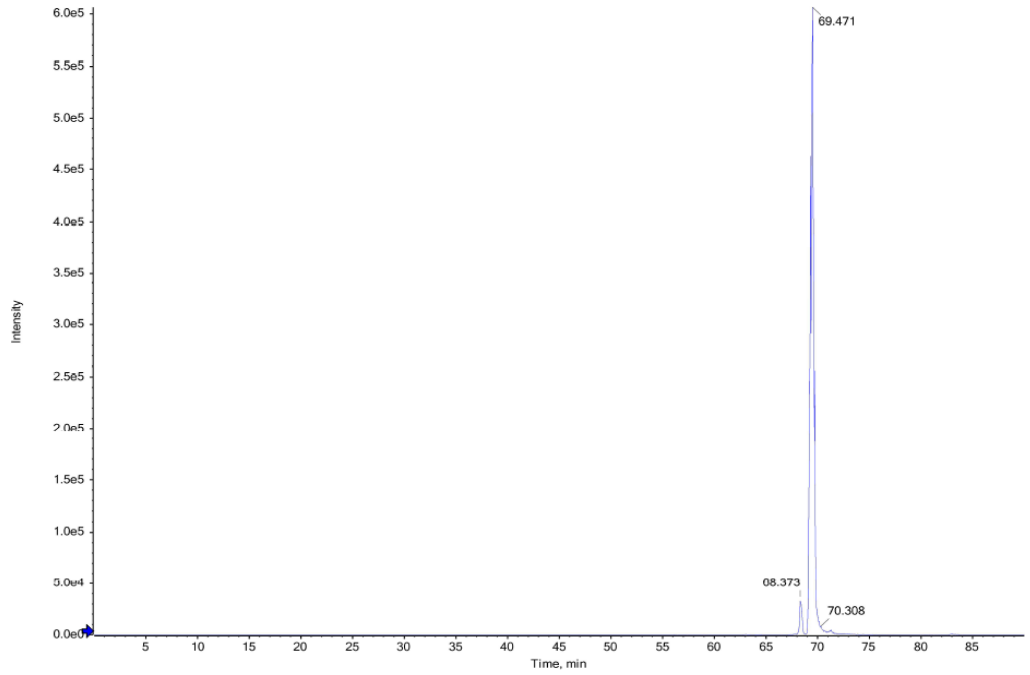

B

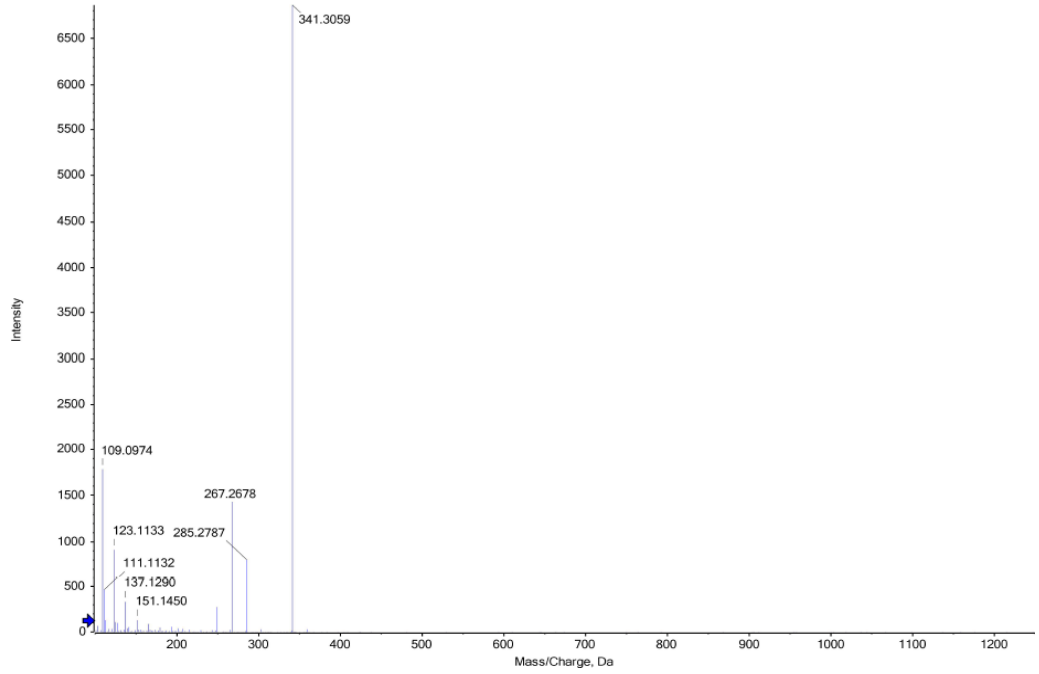

Figure 156. **Panel (A):** Extracted Ion chromatogram of compound with m/z 359.33 [M^+-H^+]; **Panel (B)**: Fragmentation spectrum.

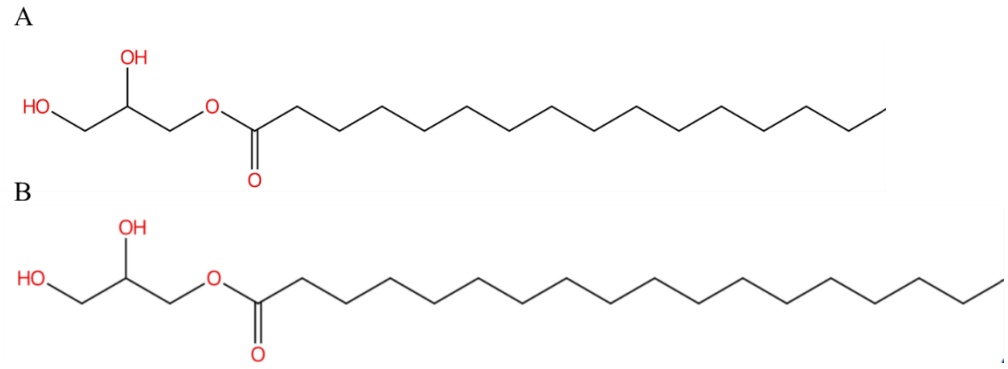

Figure 16. Glycerol-1-palmitate (alpha-palmitin) (A) and Glycerol-1-stearate (B).

4.1.3 Palmitic acid as a selective inhibitor of AKR1B10

The inhibition study was preliminary focused on alpha-palmitin. To determine the ability of alpha-palmitin to exert selective inhibition on AKR1B10 with respect to AKR1B1, inhibition studies were performed in the presence of 0.04 mM HNE. The assay mixtures contained 1.7% (v/v) of methanol.

Residual activity of AKR1B10 and AKR1B1 measured in the presence of 22 µM commercial alpha-palmitin, the highest concentration under which it was soluble in the inhibition assay, were 88% (± 4, n=12) and 97% (±3, n=5), respectively. These results hampered further characterization of inhibition properties of alpha-palmitin. In addition, given the strong similarity between the structures of alpha-palmitin and Glycerol-1-stearate, similar solubility issues are expected with the latter. Therefore, and despite the potentially promising selectivity, the analysis of this molecule was shelved.

However, both saturated and unsaturated fatty acids with long chains are reported to be inhibitors of the dehydrogenase activity of AKR1B10 [129]. Therefore, the ability of the fatty acid fragment of alpha-palmitin (PA) to act as a selective inhibitor of AKR1B10 was further explored. Preliminary studies showed that an inhibitor concentration of 22 µM commercial PA did not impair the activity of AKR1B1 neither in the presence of 0.04 mM HNE nor in the presence of 0.8 mM L-Idose, while the residual activity of AKR1B10 was 40% (± 7, n= 4) in the presence of 0.04 mM HNE. PA showed significative inhibitory potential against AKR1B10 with a value of IC50 of 2.23 µM (confidence interval 95%: 1.59 to 3.11) (figure 17). Therefore, it is possible to conclude that PA acts as a selective inhibitor of AKR1B10 with respect to AKR1B1 in the presence of HNE as a substrate.

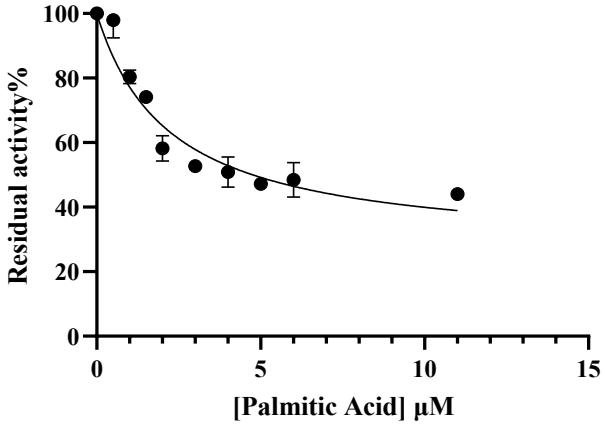

Figure 17. Residual Activity (%) of 4.5 mU AKR1B10 in the presence of HNE 0.04 mM at the indicated concentrations of PA*. Assay mixtures contained 1.7% (v/v) of methanol. Error bars (when not visible are in the symbol size) represent the standard deviation of the mean of at least three measurements.*

To determine inhibition mechanism of PA, kinetic characterization was performed (figure 18). Values of ^{app}Ki' and ^{app}Ki were 2.91±0.15 µM and 4.7±0.9 µM, respectively. Since values of ^{app}Ki' and ^{app}Ki were not significative different, PA acts as a purely non-competitive inhibitor for AKR1B10 when HNE is used as a substrate.

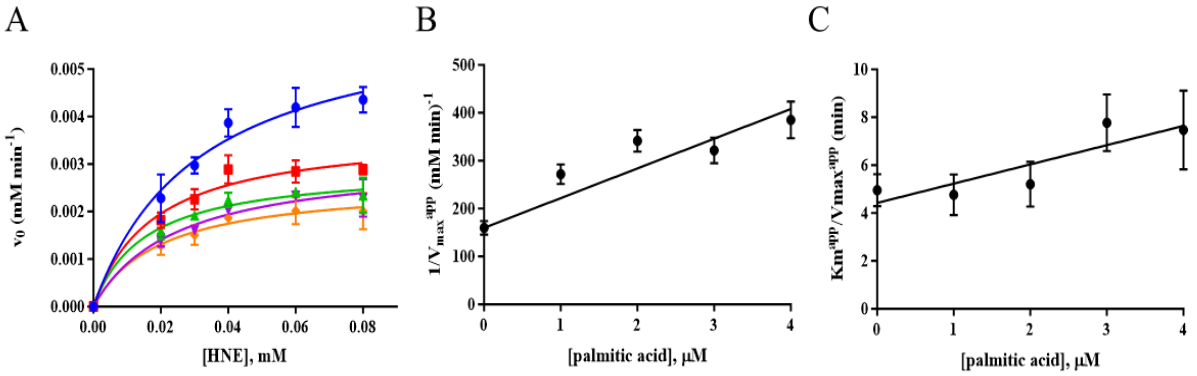

Figure 18. Kinetic characterization of PA as inhibitor of AKR1B10*. Non-linear regression plot of AKR1B10 (4,5 mU) activity at the indicated HNE concentrations (panel A) in the presence of PA at the concentrations: 4 µM (orange diamonds), 3 µM (purple triangles), 2 µM (green triangles), 1 µM (red squares), and 0 (blue circles). Panels (B) and (C): Dixon plots of $1/^{app}V_{max}$ and of $^{app}K_m/^{app}V_{max}$, respectively, obtained through the non-linear regression analysis (panel A), as a function of PA concentration. Assay mixtures contained 1.7% (v/v) of methanol. Error bars (when not visible, are within the symbols' size) represent the standard deviations of the mean of at least three measurements.*

4.2 Identification of novel synthetic compounds as ARDIs and selective inhibitors of AKR1B10

4.2.1 Preliminary screening of synthetic molecules for their ability to exert inhibition on AKR1B1 and AKR1B10

In collaboration with CHIBIOFARAM Department (University of Messina), novel compounds were synthetized in order to establish their effectiveness on AKR1B1 and AKR1B10 activity. Structures are shown in Figure 19, and 20.

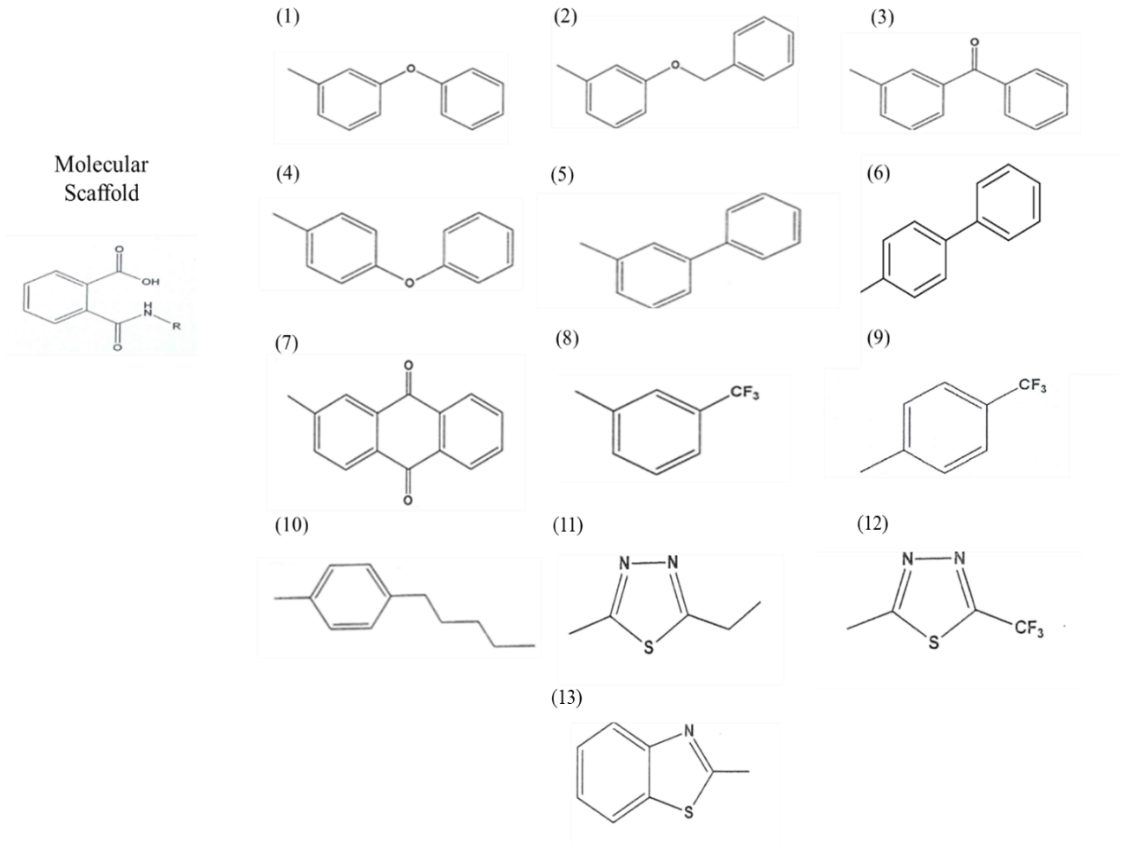

Figure 19. Novel compounds synthesized and provided by CHIBIOFARAM Department (University of Messina). *On the left: Molecular Scaffold. On the right R substituents: (1) FR1, (2) FR2, (3) FR3, (4) FR4, (5) FR5, (6) FR6, (7) MC1, (8) MC3, (9) MC4, (10) MC5, (11) MC6, (12) MC7, (13) MC8.*

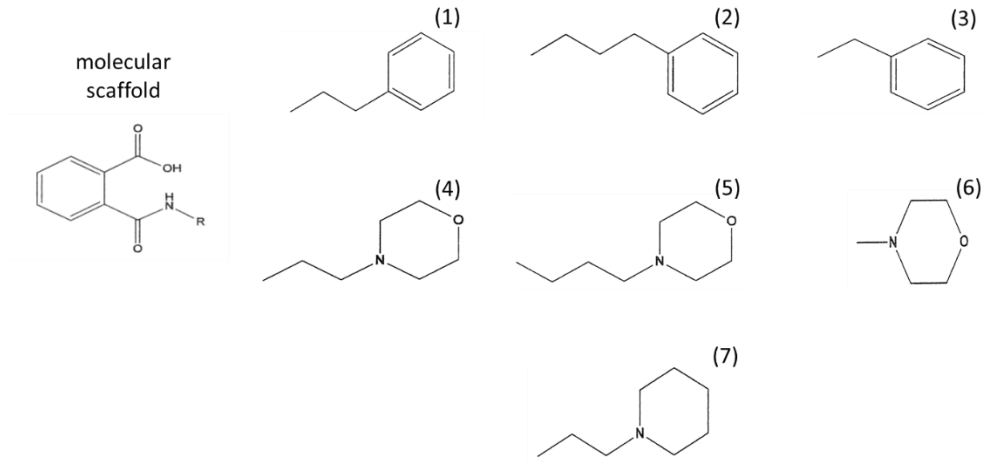

Figure 20. Novel compounds synthesized and provided by CHIBIOFARAM Department (University of Messina). *On the left: Molecular Scaffold. On the right R substituents: (1) LM1, (2) LM2, (3) LM3, (4) LM4, (5) LM5, (6) LM6 (7) LM7.*

Molecules were screened for their ability to inhibit AKR1B10 and AKR1B1 in the presence of HNE and in the presence of either HNE or L-Idose as substrates, respectively. Since molecules were dissolved in 100% DMSO, to avoid significative DMSO-mediated inhibition of both enzymes, the concentration of DMSO was kept constant to a value of 0.7% in all inhibition assay mixtures [130]. As a preliminary test, the inhibitory ability of molecules was analysed at the highest concentration under which they were soluble in assay mixtures (Table 5). Molecules not able to exert more than 30% inhibition were not used for further analyses. Molecules belonging to the LM series and MC3, MC4, MC6, and MC7 were ineffective on both AKR1B1 and AKR1B10. In addition, FR3, FR5 and MC8 were able to inhibit AKR1B1 but they were ineffective on AKR1B10. Conversely, molecules able to overcome this cut-off were used to determine the IC50 values reported in table 6 and their inhibitory potential is discussed in the following sections.

	AKR1B1 L-Idose	AKR1B1 HNE	AKR1B10 HNE
LM1	90% (0.285mM)	98% (0.285mM)	78% (0.285mM)
LM2	82% (0.285mM)	85% (0.285mM)	100% (0.285mM)
LM3	100% (0.285mM)	96% (0.285mM)	100% (0.285mM)
LM4	87,5% (0.285mM)	100% (0.285mM)	85% (0.285mM)
LM5	93% (0.285mM)	97% (0.285mM)	97% (0.285mM)
LM6	83% (0.285mM)	90% (0.285mM)	100% (0.285mM)
LM7	95% (0.285mM)	100% (0.285mM)	100% (0.285mM)
FR1	< 70%	< 70%	< 70%
FR2	< 70%	< 70%	< 70%
FR3	< 70%	< 70%	90% (0.057mM)
FR4	< 70%	< 70%	< 70%
FR5	< 70%	< 70%	77% (0.285mM)
FR6	< 70%	< 70%	< 70%
MC1	< 70%	< 70%	< 70%
MC3	74% (0.142mM)	82% (0.142mM)	94% (0.285mM)
MC4	71% (0.142mM)	83% (0.142mM)	100% (0.285mM)
MC5	< 70%	< 70%	< 70%
MC6	95% (0.142mM)	90% (0.142mM)	100% (0.142mM)
MC7	83% (0.142mM)	74% (0.142mM)	100% (0.142mM)
MC8	< 70%	< 70%	70% (0.285mM)

Table 5: Residual activity (%) of AKR1B1 and AKR1B10. The concentration of the inhibitor used for testing is reported in brackets. Inhibition studies of AKR1B1 were performed in the presence of 2 mM L-Idose or 0.04 mM HNE. Inhibition studies of AKR1B10 were performed in the presence of 0.04 mM HNE. In all assay mixtures 10 mU of AKR1B1 or AKR1B10 were used. "< 70%" means that molecules whose inhibitory potential resulted in a residual activity of AKR1B10 lower than 70 %, were further analysed to determine the IC50 values reported in table 6. n=3.

4.2.2 AKR1B1 differential inhibitors

To identify molecules able to inhibit AKR1B1, IC50 values were calculated from inhibition curves (Figure 21) in the presence of either L-Idose or HNE. The IC50 values showed approximately the same order of magnitude (table 6). Among molecules belonging to FR series, FR3 and FR5 showed the highest inhibition potency: the IC50 of both inhibitors was lower than 0.1 mM in the presence of L-idose, but only FR3 showed an IC50 value lower than 0.1 mM in the presence of HNE. Among molecules belonging to MC series, MC1 and MC8 showed the highest inhibitory potential in the presence of both L-Idose and HNE with an IC50 value lower than 0.05 mM.

Inhibitor	Substrate	IC50 (mM)	Confidence Interval 95%	R square
FR1	L-Idose	**0.151**	0.122 – 0.186	0.972
	HNE	**0.244***	0.210 – 0.283	0.997
FR2	L-Idose	**0.138**	0.098 – 0.197	0.922
	HNE	**0.199**	0.167 – 0.235	0.983
FR3	L-Idose	**0.070**	0.061 – 0.081	0.997
	HNE	**0.045***	0.038 – 0.052	0.998
FR4	L-Idose	**0.144**	0.119 – 0.175	0.965
	HNE	**0.185**	0.148 – 0.231	0.954
FR5	L-Idose	**0.086**	0.068 – 0.109	0.973
	HNE	**0.138**	0.104 – 0.182	0.961
FR6	L-Idose	**0.094**	0.072 – 0.122	0.942
	HNE	**0.179***	0.152 – 0.211	0.975
MC1	L-Idose	**0.024**	0.014 – 0.039	0.921
	HNE	**0.045**	0.038 – 0.054	0.979
MC5	L-Idose	**0.105**	0.082 – 0.135	0.989
	HNE	**0.140**	0.126 – 0.155	0.998
MC8	L-Idose	**0.020**	0.017 – 0.023	0.992
	HNE	**0.015**	0.010 – 0.020	0.995

Table 6 IC50 values of tested molecules. IC50 values were obtained by applying the non-linear regression analysis to the inhibition curves reported in figure 21. The significative difference of IC50 in the presence of 2 mM L-Idose and 0.04 mM HNE is reported (*= $p < 0.05$).

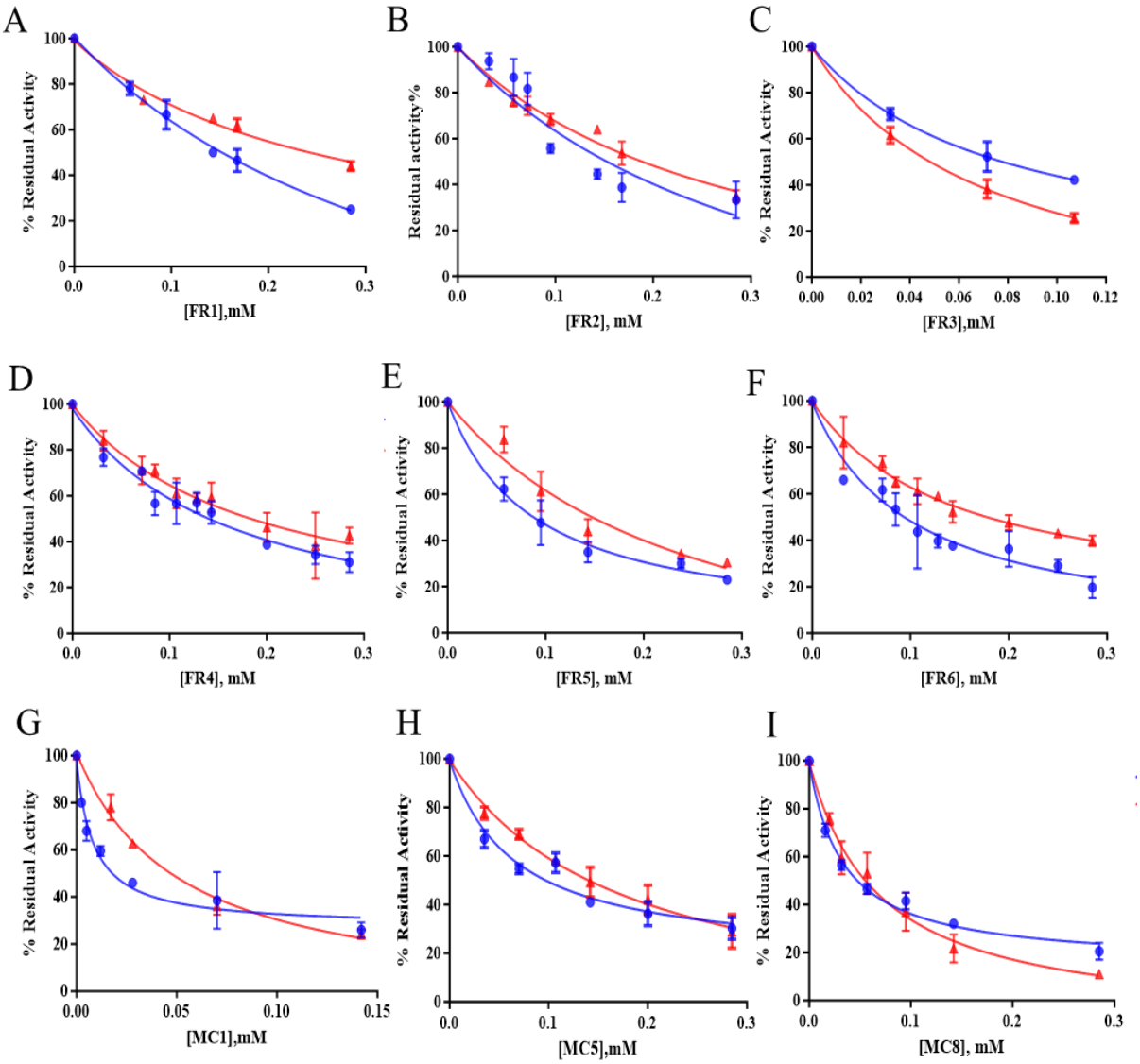

Figure 21. Residual activity (%) of AKR1B1 (10mU) in the presence of 2 mM L-Idose (blue circles) and 0.04 mM HNE (red triangles) as a function of inhibitor concentration: *FR1 (panel A), FR2 (panel B), FR3 (panel C), FR4 (panel D), FR5 (panel E), FR6 (panel F), MC1 (panel G), MC8 (panel H,) and MC8 (panel I). Error bars represent the standard deviation of the mean of at least three independent measurements (when not visible, are within the symbols 'size).*

As reported in section 1.6.2, a molecule is defined as DI if it inhibits the catalyst depending on the substrate the enzyme is working on. To determine the ability of molecules to exert DI when L-Idose and HNE are used as substrates, IC50 values were compared by applying *Welch's test of Unpaired T test*. The comparison of IC50 values showed that L-Idose reduction was more susceptible to inhibition than HNE reduction in the presence of FR1 ($p < 0.05$) and FR6 ($p < 0.05$), whereas FR3 showed higher inhibitory potency when HNE was used as substrate with respect to L-Idose ($p < 0.05$). Therefore, as emerged from these results, FR1 and FR6 act as interesting differential inhibitors able to preferentially inhibit the polyol pathway affecting at lesser extent the detoxifying activity of AKR1B1. On the contrary, the differential action of FR3, which inhibits HNE reduction at greater extent with respect to L-idose reduction, seems undesirable.

4.2.3 Kinetic characterization of AKR1B1 DIs

Since their ability to exert DI (in terms of preferential inhibition on L-idose compared to HNE) on AKR1B1, kinetic characterization was performed on the FR1 and FR6 to elucidate their inhibitory mechanism (figure 22 and figure 23, respectively).

Values of $^{app}K'_i$ (0.34 ± 0.04 mM) and $^{app}K_i$ (0.142 ± 0.0054 mM) obtained in the presence of L-Idose, indicated that FR1 acts as mixed-type inhibitor with a significant ($p < 0.01$) preference toward the free enzyme with respect to the ES complex. Similarly, values of $^{app}K'_i$ (0.145 ± 0.0146 mM) and $^{app}K_i$ (0.069 ± 0.0036 mM) indicated that FR1 acts as a mixed-type inhibitor also in the presence of HNE with a prevalence of the competitive component ($p < 0.05$).

Values of $^{app}K_i'$ (0.159± 0.023 mM) and $^{app}K_i$ (0.080± 0.004 mM) suggest that FR6 acts as a mixed-type inhibitor with a prevalence of the competitive component ($p < 0.05$) in the presence of L-Idose as a substrate. However, $^{app}K_i'$ (0.154± 0.001 mM) and $^{app}K_i$ (0.180± 0.021 mM) inhibitor constant values are not significantly different when HNE is used as a substrate, therefore suggesting that FR6 acts as a pure non-competitive inhibitor in the presence of HNE.

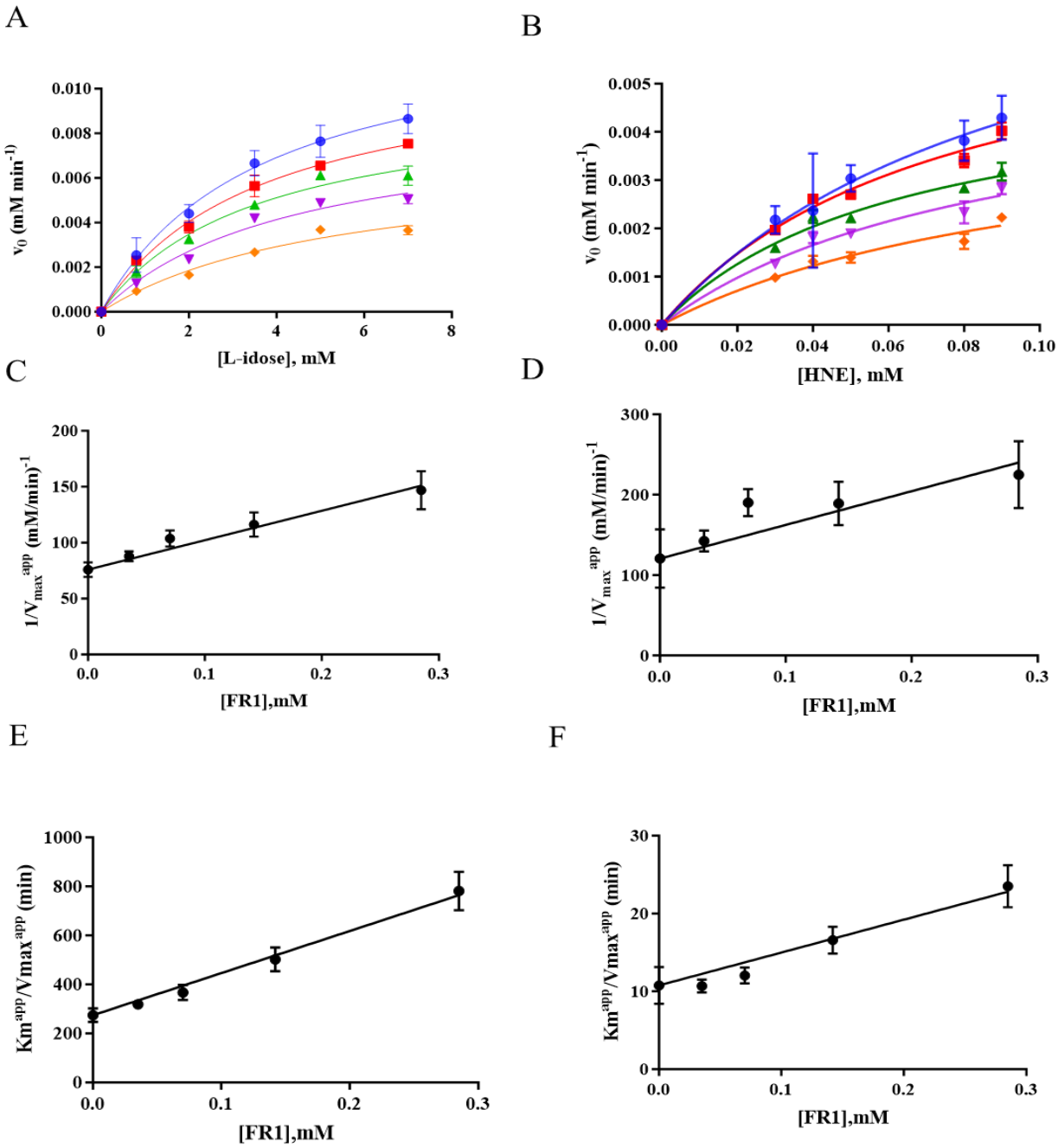

Figure 22. Kinetic characterization of FR1 as inhibitor of AKR1B1. *Non-linear regression plot of AKR1B1 activity at the indicated L-Idose (Panel A) and HNE (panel B) concentrations in the presence of FR1 at the indicated concentrations: 0.285 mM (orange diamonds), 0.142 mM (purple triangles), 0.071 mM (green triangles), 0.035 mM (red squares), and 0 (blue circles). Error bars (when not visible, are within the symbols' size) represent the standard deviations of the mean of at least three measurements. Panels (C) and (E): Dixon plots of* $^{app}K_m/^{app}V_{max}$ *and of* $1/^{app}V_{max}$*, respectively, obtained through the non-linear regression analysis (panel A), as a function of FR1 concentration. Panels (D) and (F Dixon plots of* $^{app}K_m/^{app}V_{max}$ *and of* $1/^{app}V_{max}$*, respectively, obtained through the non-linear regression analysis (panel B), as a function of FR1 concentration.*

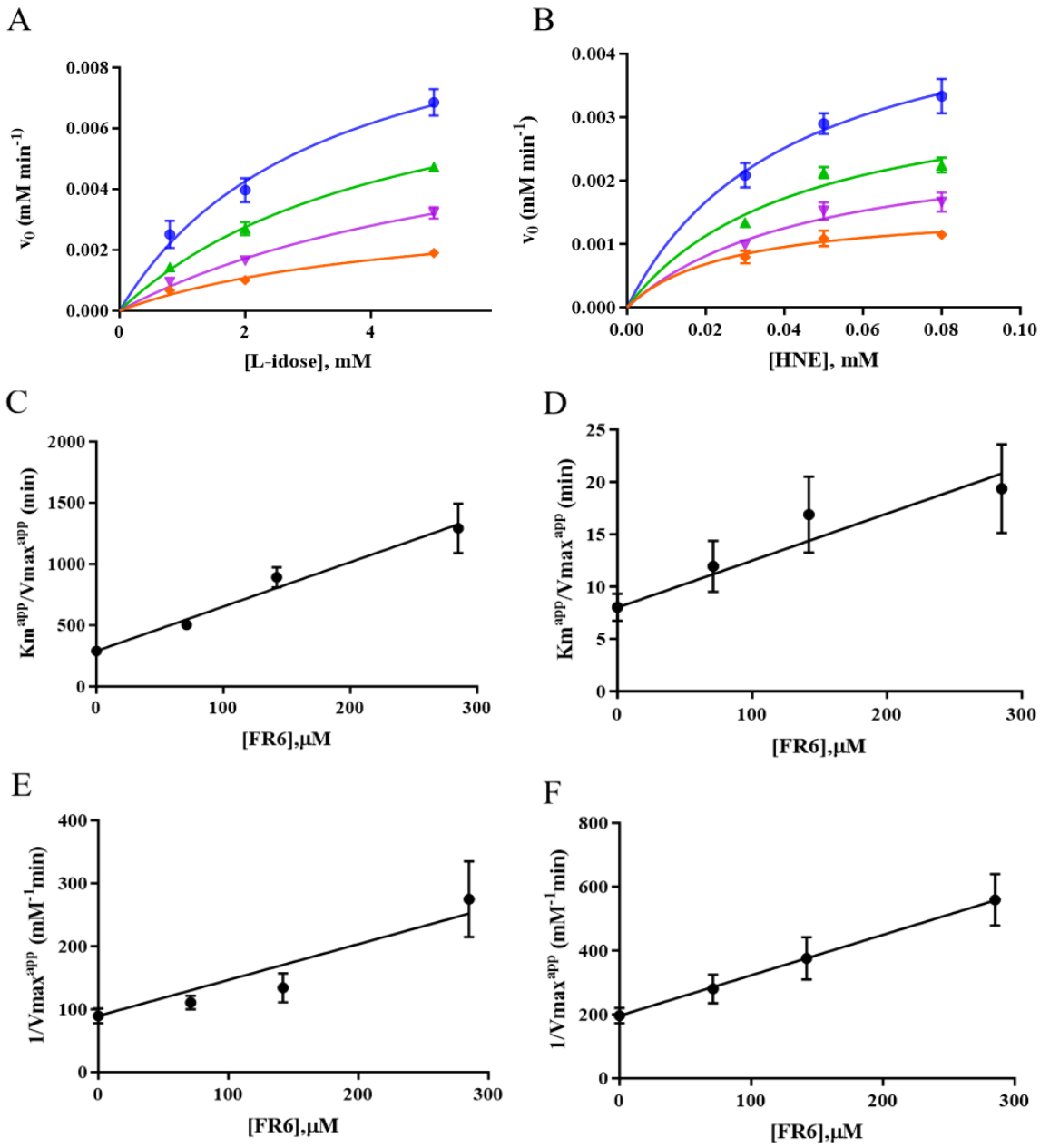

Figure 23. Kinetic characterization of FR6 as inhibitor of AKR1B1. *Non-linear regression plot of AKR1B1 (10 mU) activity at the indicated L-Idose (Panel A) and HNE (panel B) concentrations in the presence of FR6 at the concentrations: 0.285 mM (orange diamonds), 0.142 mM (purple triangles), 0.071 mM (green triangles), and 0 (blue circles). Error bars (when not visible, are within the symbols' size) represent mean of at least three measurements. Panels (C) and (E): Dixon plots of* $^{app}K_m/^{app}V_{max}$ *and of* $1/^{app}V_{max}$*, respectively, obtained through the non-linear regression analysis (panel A), as a function of FR6 concentration. Panels (D) and (F): Dixon plots of* $^{app}K_m/^{app}V_{max}$ *and of* $1/^{app}V_{max}$*, respectively, obtained through the non-linear regression analysis (panel B), as a function of FR6 concentration.*

4.2.4 Selective inhibitors of AKR1B10

As previously reported, IC50 values were determined for molecules able to exert at least an inhibition of 30% at the highest concentration under which they were soluble in assay mixtures (Table 7). The inhibition curves are reported in Figure 24. Among these molecules, FR1, MC5, and FR4 are the most potent inhibitors (Table 7). Comparison of IC50 values obtained for AKR1B1 and AKR1B10 in the presence of 0.04 mM HNE allowed to identify selective inhibitors (Figure 25). FR1 significantly inhibited AKR1B10 at greater extent than AKR1B1. Conversely, FR6 showed the opposite behaviour since it exerted higher impact on AKR1B1 with respect to AKR1B10. Regarding to the other molecules tested (FR2, FR4, MC1 and MC5), no significative selective inhibition was determined. However, considering data presented in table 5, it should be noted that FR3, FR5 and MC8 were not able to inhibit AKR1B10 activity more than 30% at the highest concentration under which they were soluble in assay mixtures. Conversely, IC50 values of these compounds were determined for AKR1B1. Therefore, these three inhibitors represent the most selective inhibitors for AKR1B1.

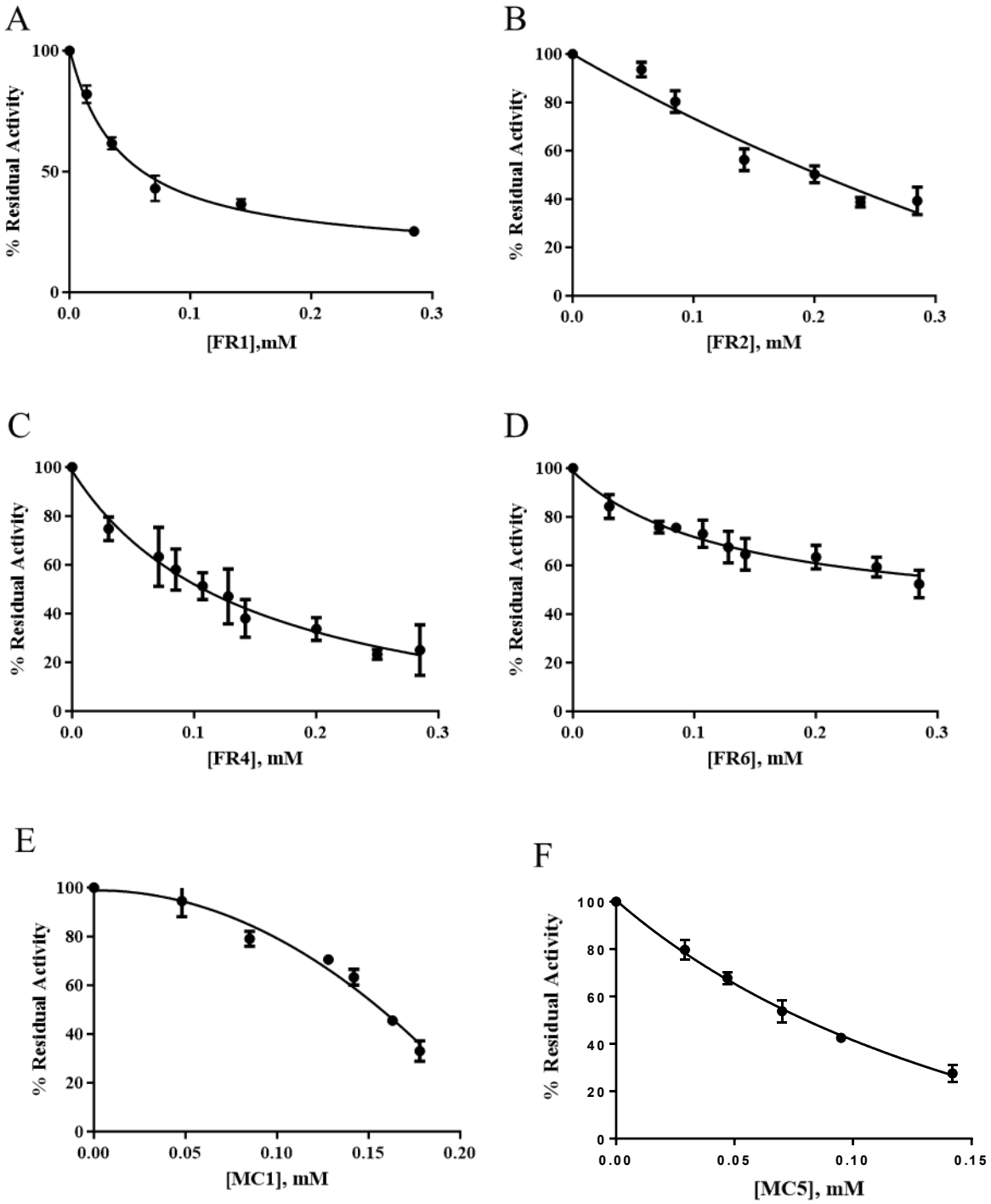

Figure 24. Residual activity (%) of AKR1B10 (10mU) in the presence of 0.04 mM HNE as a function of inhibitor concentration*: FR1 (panel A), FR2 (panel B), FR4 (panel C), FR6 (panel D), MC1 (panel E) and MC5 (panel F). Error bars represent the deviation standard of the of at least three independent measurements (when not visible, are located within the of the size of the symbol).*

Inhibitor	IC50 (mM)	Confidence Interval 95 %	R square
FR1	**0.062**	0.045 – 0.085	0.976
FR2	**0.192**	0.144 – 0.255	0.949
FR4	**0.107**	0.082 – 0.141	0.938
FR6	**0.345**	0.279 – 0.425	0.964
MC1	**0.176**	0.116 – 0.265	0.893
MC5	**0.209**	0.138 – 0.366	0.986

Table 7. IC50 values of tested molecules. *IC50 values were obtained by applying the non-linear regression analysis to the inhibition curves reported in figure 24.*

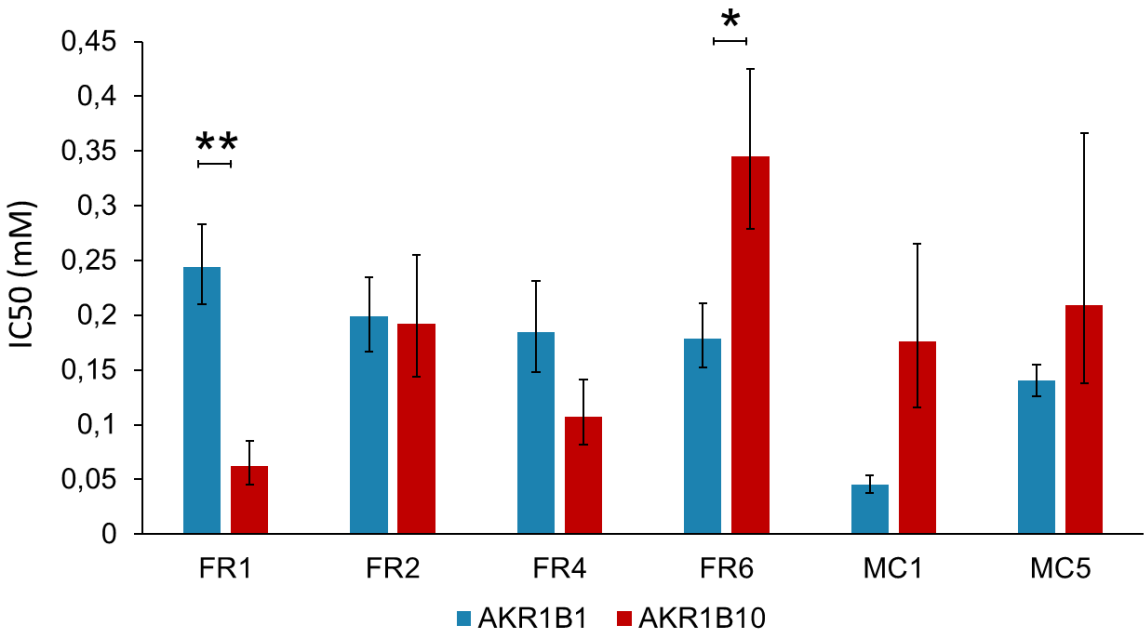

Figure 25. Selective inhibition of tested molecules between AKR1B1 and AKR1B10). Histograms represent the IC50 values obtained in the presence of 0.04 mM HNE. The error bars represent minimum and maximum values of the confidence interval of IC50 values. Unpaired T-test with Welch's correction. n=3; ** $p \leq 0.01$; * $p < 0.05$.

To determine the inhibitory mechanism of FR1 which acts as the most powerful inhibitor on AKR1B10 and is also selective compared to AKR1B1, the kinetic characterization of this compound was performed in the presence of HNE (figure 26). Values of $^{app}K'i$ (0.10 ± 0.003 mM) and ^{app}Ki (0.55± 0.077 mM) suggested that FR1 acts as mixed-type inhibitor on AKR1B10 with a significant preference toward the ES complex with respect to the free enzyme ($p < 0.05$).

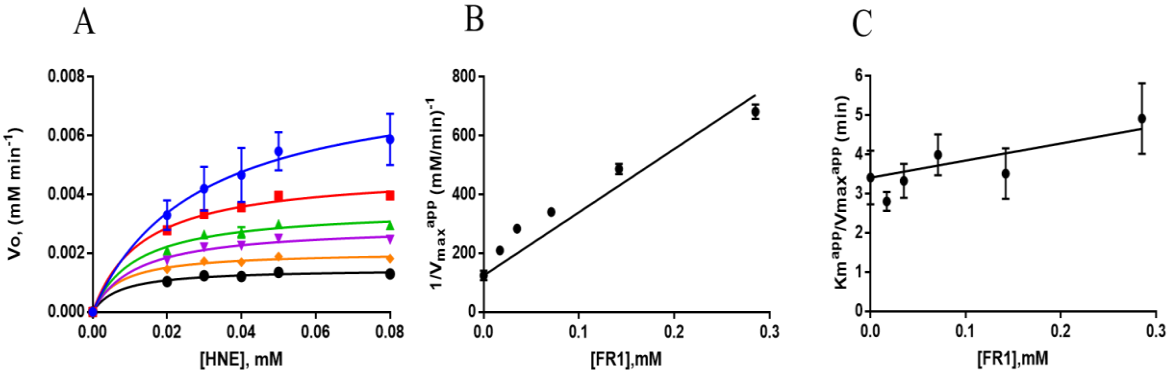

Figure 26. Kinetic characterization of FR1 as inhibitor of AKR1B10*. Non-linear regression plot of AKR1B10 (10 mU) activity at the indicated HNE concentrations in the presence of FR1 (panel A) at the concentrations: 0.285 mM (black circles), 0.142 mM (orange diamonds), 0.071 mM (purple triangles), 0.035 mM (green triangles), 0.017 mM (red squares), and 0 (blue circles). Panels (B) and (C): Dixon plots of $1/^{app}V_{max}$ and of $^{app}K_m/^{app}V_{max}$, obtained through the non-linear regression analysis (panel A). Error bars (when not visible, are within the symbols' size) represent mean of at least three measurements.*

4.2.5 Selective inhibitors of AKR1B1

FR3, FR5 and MC8 represent the most selective inhibitors for AKR1B1 as discussed in section 4.2.4. Considering the most powerful effect exerted by MC8 on AKR1B1 activity for HNE reduction (IC50 value three times and nine times lower for FR3 and FR5 respectively), the kinetic characterization of this compound was performed in the presence of HNE (figure 27). Values of $^{app}K'i$ (0.09 ± 0.015 mM) and ^{app}Ki (0.07± 0.006 mM) indicated that MC8 acts as a pure non-competitive inhibitor on AKR1B1 as the inhibitor constant were not significantly different.

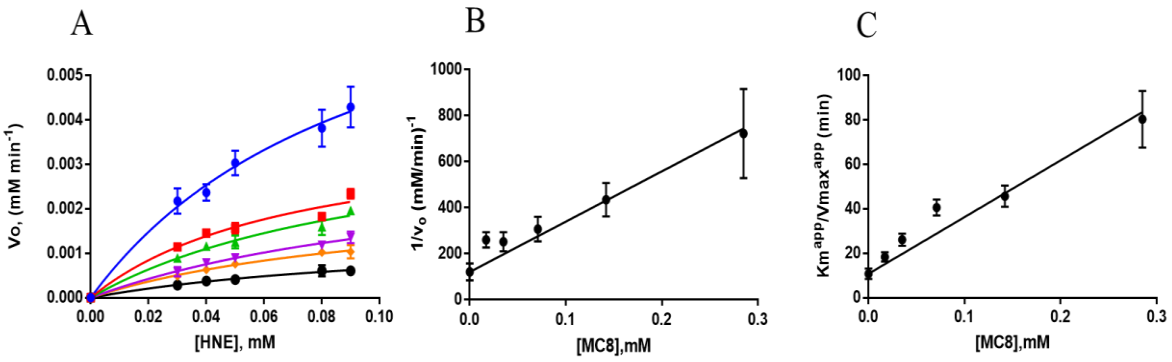

Figure 27. Kinetic characterization of MC8 as inhibitor of AKR1B1*. Non-linear regression plot of AKR1B1 (10 mU) activity at the indicated HNE concentrations in the presence of MC8 (panel A) at the concentrations: 0.285 mM (black circles), 0.142 mM (orange diamonds), 0.071 mM (purple triangles), 0.035 mM (green triangles), 0.017 mM (red squares), and 0 (blue circles). Panels (B) and (C): Dixon plots of* $1/^{app}V_{max}$ *and of* $^{app}K_m/^{app}V_{max}$*, obtained through the non-linear regression analysis (panel A). Error bars (when not visible, are within the symbols' size) represent mean of at least three measurements.*

4.3 Fluorimetric assay for the detection of AKR1B10 reductase activity

This study was partially performed during the 6 months stage at the Department of Biochemistry and Molecular Biology, Faculty of Biosciences, Universitat Autònoma de Barcelona, Spain, under the supervision of Prof. Jaume Farrés.

4.3.1 Fluorescence properties of MONAL-41 and MONOL-41

MONAL-41 and MONOL-41 spectral properties were investigated and are reported in table 8.

	Absorption		**Fluorescence**
	λ max (nm)	**ε ($mM^{-1}cm^{-1}$)**	**λ max (nm)**
MONOL-41	296	7.1	380
MONAL-41	333	12.81	420

Table 8 MONAL-41 and MONOL-41 spectral properties.

These results are in good agreement with Wierzchowski *et al.* [131], except for MONOL-41 millimolar extinction coefficient (ε). However, measures of MONOL-41 reported by Wierzchowski *et al.* [131] were conducted in aqueous media. By contrast, here the analyses of MONOL-41 were performed in ethanol 100%, therefore it is not possible to exclude that this discrepancy is related to the effect of the solvent. The fluorescence quantum yield of MONAL-41 is negligible (Φ = 0.003), but its corresponding alcohol shows an intense fluorescence spectrum (Φ = 0.36) [131].

4.3.2 Optimization of a fluorimetric assay for the detection of AKR1B10 activity

Since the assay mixtures to detect AKR1B10-reductase activity contain NADPH and MONAL-41, interferences on MONOL-41 fluorescence emission linked to their presence were investigated. Absorption spectra of MONOL-41, MONAL-41 and NADPH are partially overlapped (Panel A, figure 28). The highest value of absorption of MONOL-41 and the lowest value of micromolar extinction coefficients ratios of both MONAL-41 and NADPH with respect to MONOL-41 are registered at 296 nm (Panel B, Figure 28). When these compounds at the same concentrations are excited at 296 nm, MONOL-41 shows a peak of fluorescence emission at 380 nm, whereas MONAL-41 and NADPH fluorescence emission is undetectable (Panel C, figure 28). Therefore, the optimal set-up to follow the reduction of MONAL-41 is to excite at 296 nm and detect the fluorescence emission at 380 nm.

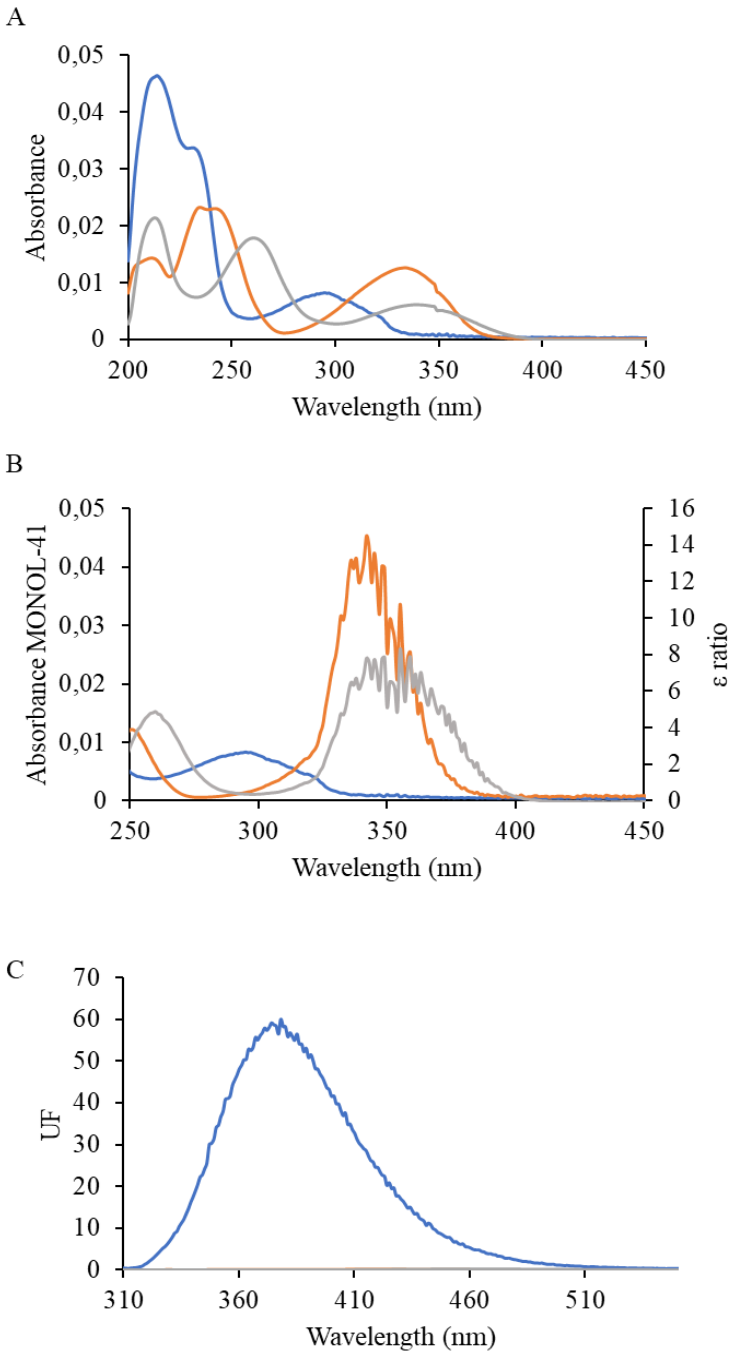

Figure 28. Evaluation of the optimal set-up for the evaluation of MONAL-41 reduction. Panel A: Absorption spectra of 1 µM MONOL-41(blue line), 1 µM MONAL-41 (orange line) and 1 µM NADPH (grey line). Panel B: Comparison of the absorption spectrum of 1 µM MONOL-41 (blue line) with micromolar coefficient ratios (ε) MONAL-41/MONOL-41 (orange line) and NADPH/MONOL-41 (grey line) with respect to MONOL-41. Panel C: Emission spectra of 1 µM MONOL-41 (blue line), 1 µM MONAL-41 and 1 µM NADPH, when exciting at 296 nm (MONAL-41 and NADPH emission spectra are undetectable in these conditions).

However, in enzymatic assay mixtures the concentration of NADPH needs to be saturating. The usual NADPH concentration used for spectrophotometric assays is around 0.15-0.2 mM, which would hamper a proper measurement due to inner filter effect in fluorimetric assays. Thus, to avoid the inner filter effect, two precautions were taken: i. the concentration of NADPH in assay mixtures was fixed at 0.08 mM, which anyway is still eight times higher than the K_m of NADPH for *h*AKR1B10 [132]; ii. the path-length was considerably reduced by performing the fluorimetric assay in 96-well microplates in a total volume of 100 µl.

As above-mentioned, the optimal set-up to detect the enzymatic reduction of MONAL-41 is to excite at 296 nm and follow the fluorescence emission linked to the production of MONOL-41 at 380 nm. However, the use of a plate reader, which is equipped with specific absorption and emission filters, forced the use of a different combination of excitation and emission wavelengths, i.e., bandwidth 310-350 nm and 410-425 nm, respectively. Since this combination of excitation and emission wavelengths overlaps with the optimal set-up for NADPH fluorescence detection (i.e., excitation at 355 nm and emission at 460 nm), the interference of NADPH on MONOL-41 fluorescence emission was investigated. The variation of the units of fluorescence (UF) obtained at different concentrations of MONOL-41 in the presence of 0.08 mM NADPH was compared to the variation of UF obtained at different concentrations of NADPH in the presence of 1.58 µM MONOL-41, exciting at 310-350 nm and detecting the emission at 410-425 nm (figure 29). It is possible to conclude that the variation of fluorescence linked to NADPH oxidation has a slight impact (approximately 1.3%) on the variation of fluorescence emission linked to the production of MONOL-41. In addition, results showed in figure 29 demonstrate that the limit of detection of MONOL-41 in assay conditions is approximately 150 nM.

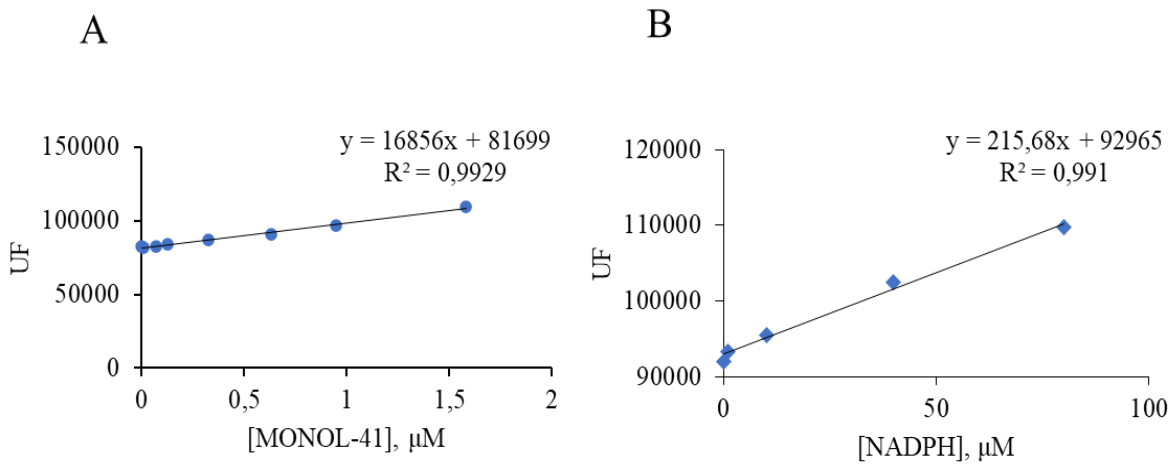

Figure 29. *Calibration curve obtained by exciting at 320 nm and detecting the emission fluorescence at 410-10 nm of MONOL-41 in the presence of 80 µM NADPH (panel A) and the emission fluorescence of NADPH in the presence of 1.58 µM MONOL-41 (panel B).*

4.3.3 Characterization of MONAL-41 as substrate of AKR1B10

Before performing the fluorescent assay, purified enzyme activity was analysed by the standard assay as described in section 3.2.2.3. Then, the fluorescent activity of 0.12 mU of AKR1B10 was tested in the presence of different concentrations of MONAL-41. The rate of transformation of MONAL-41 is progressively inhibited as the concentration of the substrate is increased (Panel A, Figure 30). The inhibitory effect at higher concentrations could be linked to the increase of absorbance, therefore in a decrease of sensitivity due to inner filter effect and reabsorption [133], albeit a contribution of inhibition by substrate cannot be ruled out.

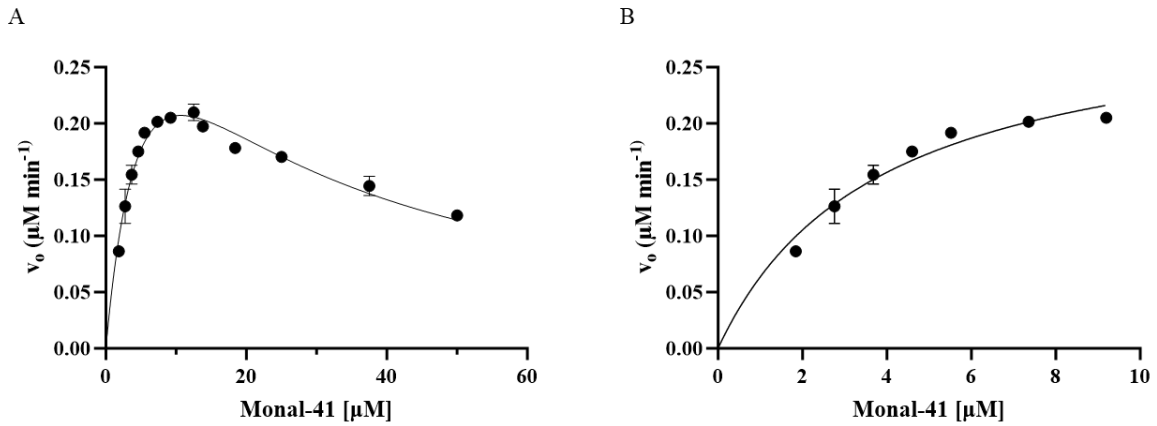

Figure 30. Dependence of AKR1B10 reaction rate on MONAL-41 concentration.

Inhibitory effect on AKR1B10 activity at high concentrations of MONAL-41 (panel A). Fit of experimental points into Michaelis and Menten equation (panel B). Error bars (when not visible, are within the symbols' size) represent mean of at least three measurements

Therefore, kinetic parameters reported in Table 9 were determined by fitting the experimental data points obtained in the presence of MONAL-41 2-9 µM into *Michaelis* and *Menten* equation (panel B, figure 30).

	Average	Standard error
K_m (µM)	3.81	0.50
K_{cat} (min^{-1})	14.54	0.81
K_{cat}/K_m (μM^{-1} min^{-1})	3.82	0.55

Table 9 Kinetic parameters of AKR1B10 for MONAL-41.

In addition, as a preliminary test, the activity of 20 mU of AKR1B1 was fluorimetrically detected in an assay mixture containing 0.25 M sodium phosphate pH 6.8 buffer, 0.47 mM EDTA, 0.1 M ammonium sulphate, NADPH 0.08 mM and 5 µM MONAL-41 as a substrate. In these assay conditions, the initial velocity was 0.22 µM min^{-1} (± 0.022). Similar initial velocity values are obtained with 0.12 mU in the presence of 5.5 – 9 µM. Although a complete substrate curve was not performed for AKR1B1, the initial velocity of 0.22 µM min^{-1} registered for AKR1B1 was obtained in the presence of an amount of enzyme 167 higher than the amount of enzyme used for the experimental procedures with AKR1B10, therefore indicating that this substrate is selective for AKR1B10 detection.

Aldehydic substrates commonly used in the research field for both enzymes are D,L-glyceraldehyde, p-nitrobenzaldehyde (PNB) and HNE. As reported in table 10, V_{max} values are comparable for both enzymes. As regards to K_m, values referring to D,L-glyceraldehyde and PNB are higher and lower, respectively, for AKR1B10 compared to AKR1B1, whereas values referring to HNE are comparable. These results were obtained in the presence of 5 mU of both enzymes.

Substrate	Kinetic value	AKR1B1	AKR1B10
D,L-glyceraldehyde	K_m (mM)	0.12 ± 0.014	1.057 ± 0.16
	V_{max} (mM min^{-1})	0.009 ± 0.0002	0.008 ± 0.0003
PNB	K_m (µM)	58.64 ± 11.14	6.68 ± 1.04
	V_{max} (mM min^{-1})	0.009 ± 0.0007	0.009 ± 0.0009
HNE	K_m (mM)	0.054 ± 0.0056	0.049 ± 0.0099
	V_{max} (mM min^{-1})	0.004 ± 0.0002	0.007 ± 0.0006

Table 10. Kinetic values of AKR1B10 and AKR1B1 for D,L-glyceraldehyde, PNB, and HNE obtained in the presence of 5 mU of both enzymes by spectrophotometric assay in the standard assay conditions. *Results reported are best-fit values with the corresponding standard error of experimental data points fitted into Michaelis and Menten equation. (Data not published).*

All together these results indicate that in these conditions, MONAL-41 is a good substrate for AKR1B10 activity detection, and it would be selective for AKR1B10 with respect to AKR1B1.

4.3.4 Determination of the half-inhibitory concentration of Oleanolic Acid

Since the goal of the study is to detect the fluorescent activity of AKR1B10 in biological samples (i.e., cells and small EVs) the combined use of MONAL-41, as substrate, and of a selective inhibitor could be useful to discern the activity of AKR1B10 from aspecific MONAL-41-reductase activities present in the extracts. In this regard, Oleanolic acid was used in inhibition assays since it is one of the most efficient selective inhibitors of AKR1B10 with respect to AKR1B1 (IC50 ratio AKR1B1/AKR1B10 equal to 1370) [124]. The IC50 of Oleanolic Acid determined in the presence of 4 μM MONAL-41 was 6.99 μM (CI 95% 4.79 to 10.14) (figure 31).

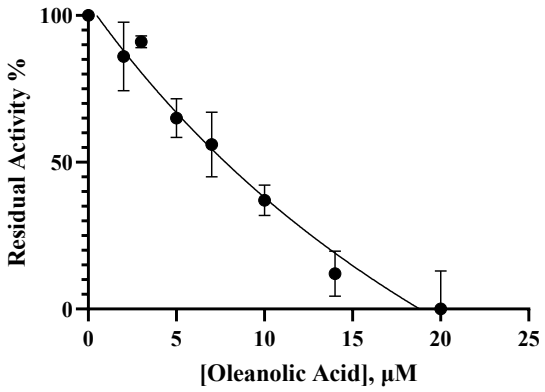

Figure 31. *Residual Activity (%) of 0.12 mU AKR1B10 in the presence of 4 μM MONAL-41 at the indicated concentrations of Oleanolic Acid. Error bars (when not visible, are within the symbols' size) represent mean of at least three measurements.*

4.3.5 Characterization EVs by NTA and Cryo-TEM

After EV isolation through differential centrifugation, characterization was performed by using NTA. The batch contained 3.92e+10 (+/- 1.92e+09) particles/ml clustered on a monodisperse peak at 145 nm, with particles of about 186.6 +/- 1.9 nm in diameter (mean +/- standard error) (Figure 32, Panel A). The observation of EV under Cryo-TEM showed spherically shaped membranes composed of a lipid bilayer (Figure 32, panel B).

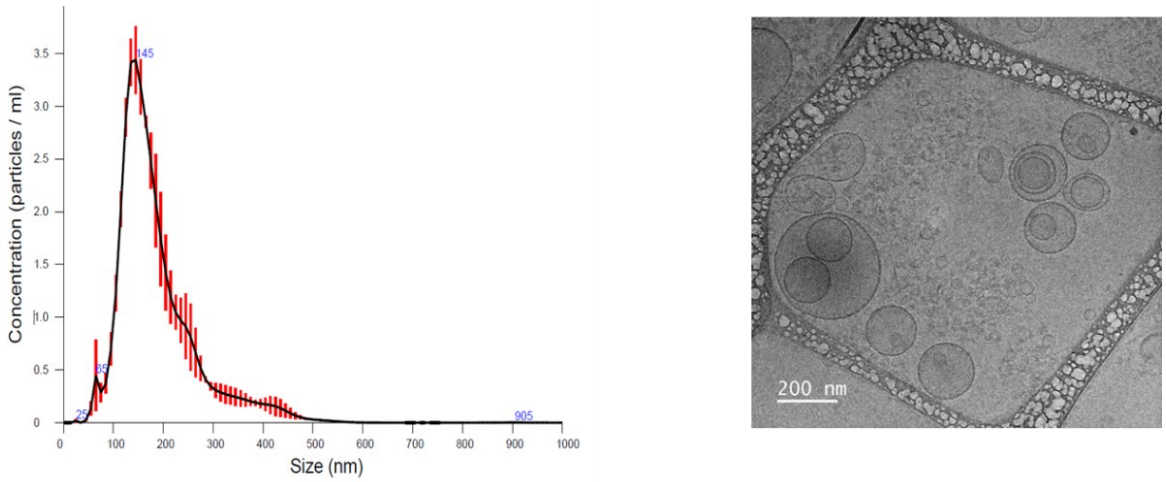

Figure 32. *(A) Size distribution of A549 EV by nanoparticle tracking analysis; Visualization of A549 EV size and morphology by cryo-TEM; Representative images of (B) scale bar: 200 nm.*

4.3.6 Detection of AKR1B10 activity in cells and small EVs extracts

The detection of AKR1B10 activity in cells and small EVs extracts was performed as described in section 3.2.5.6. The activities were measured in small EVs extracts and in their corresponding cell cultures grown in conditions described in section 3.2.5.3. To avoid the inner filter effect linked to MONAL-41 higher concentrations, reductase activities of extracts were analysed in the presence of 7 μM MONAL-41. Table 11 reports the specific activities expressed as U/mg of cell extracts. For comparison the specific activity of the recombinant purified *h*AKR1B10 is also reported.

	Specific activity (U/mg)
Recombinant purified *h*AKR1B10	0.47 (± 0.0162)
Cell extract of "starved" A549	0.020 (± 0.0004)
Cell extract of "not starved" A549	0.024 (± 0.0017)

Table 11 *Specific activity of recombinant purified hAKR1B10 and cell extracts of both starved and nt starved A549 measured in the presence of 7 μM MONAL-41. Results are reported as means and standard deviations of at least three measurements.*

One-way ANOVA test with Brown-Forsythe and Welch's correction showed that the specific activity of both cell extracts is comparable; as expected, it is significantly lower than the specific activity of the recombinant enzyme ($p < 0.0001$).

Considering that AKR1B10 and AKR1B1 are highly expressed in A549 cell line (normalized transcript per million values are 3299.7 and 1579, respectively [134]), the residual activity of cell extracts in the presence of 20 μM Oleanolic acid and 7 μM MONAL-41 was investigated. The residual activity of both cell extracts and the purified recombinant enzyme is reported in Table 12.

	Residual Activity %
Cell extract of starved A549	57.49 (±3.84)
Cell extract of not starved A549	62.19 (±0.73)

Table 12. *Residual Activity (%) of recombinant purified hAKR1B10 and cell extracts of both "starved" and "not starved" A549 measured in the presence of 7 μM MONAL-41 and 20 μM Oleanolic Acid. Results are reported as means and standard deviations of at least three measurements.*

The residual activity of MONAL-41 reduction in the presence of Oleanolic Acid of "starved" and "not starved" cell extracts is approximately 57% and 62%, respectively, which indicates an unaltered effect of the starvation condition on the residual activity. The inhibitory effect of Oleanolic acid on recombinant purified *h*AKR1B10 is different (approximately 17%), as expected considering that the analysis conditions in the presence of a recombinant purified enzyme are obviously different than those in the presence of cell extracts. Although the Oleanolic Acid is a selective inhibitor of AKR1B10 with respect to AKR1B1, it is a multifunctional molecule able to bind other targets [124]. In addition, it is not possible to rule out the presence of other enzymes able to reduce MONAL-41. However, the high selectivity between AKR1B1 and AKR1B10 (section 4.3.3), and the high expression of these two enzymes in the chosen cell line compared with other reductases might suggest that the MONAL-41 reduction is largely performed by AKR1B10.

As regards the extracts of small EVs collected from cell cultures as described in section 3.2.5.4, no MONAL-41-reductase activity was detected.

Western blot analysis was performed on small EVs extracts as described in section 3.2.5.8 to detect *h*AKR1B10 (figure 33). In addition, a lane of the polyacrylamide gel was loaded with the purified recombinant *h*AKR1B10 extensively dialysed in 10 mM sodium phosphate buffer (figure 33). The molecular weight of the recombinant protein obtained from several analysis was in a range of 40-44 KDa. The analysis of western blots of the small EVs extracts showed the presence of a band corresponding to the molecular weight of the purified protein. However, other aspecific bands are visible in the lanes of the small EVs extracts, probably linked to the use of a polyclonal antibody (figure 33).

All together these results suggest that the AKR1B10 could be present in the small EVs but the inability to detect its activity paves the way for several hypotheses: i. the enzyme is secreted in the small EVs as an inactivated form, ii. the enzyme in the small EVs was inactivated during

the procedures of small EVs collection and/or storage; iii. the small EVs contain inhibitors of MONAL-41 reductase activity.

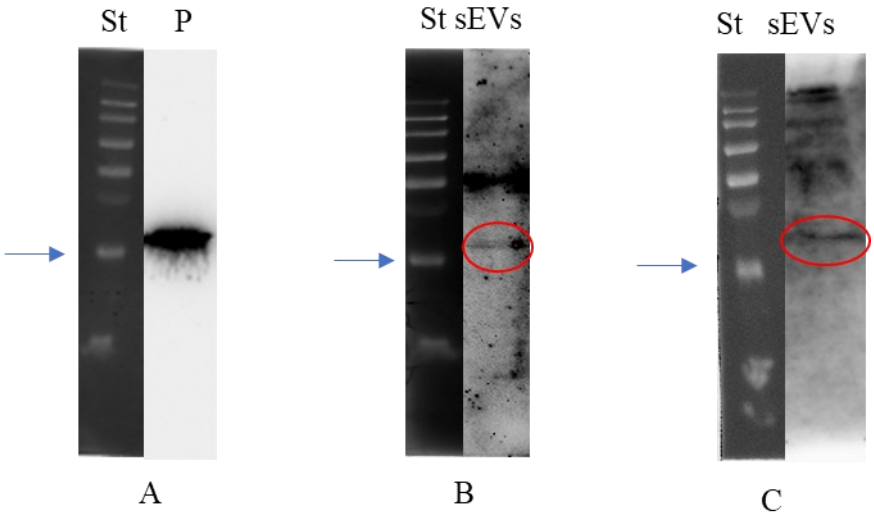

Figure 33. Western Blot analysis*:* (A) 0.5 µg of purified recombinant *h*AKR1B10; (B) 10 µg of extract of small EVs collected through differential centrifugation; (C) 14.5 µg of extract of small EVs collected through sequential filtration. St: standard prestained Sharpmass vii (Euroclone); P: purified recombinant *h*AKR1B10; s EVs: small EVs extract; Blue arrows indicate the molecular weight of 37 KDa. Red circles indicate the band corresponding to the hAKR1B10 detected with anti-body.

4.3.7 Detection of MONOL-41 in conditioned medium of A549 cell cultures

As a preliminary test to evaluate if MONAL-41 is suitable for monitoring the reductase activity in cell cultures, the detection of MONOL-41 in conditioned medium obtained from cell cultures treated with MONAL-41 was investigated. A549 cells were treated with 50 µM MONAL-41 for 4 hours. The reduction of MONAL-41 was evaluated in the conditioned medium at several time points. Statistical significance was performed by two-way ANOVA test with Tukey's correction for multiple comparisons. As shown in Figure 34, the conditioned medium of cells treated with MONAL-41 showed a time-dependent significative increase in emission of fluorescence. In addition, treated cells showed a significantly higher emission of fluorescence compared to control cells for each timepoint. This preliminary test paves the way for several scenarios: i. MONAL-41 enters cell membranes, and/or ii. MONAL-41 enters the EVs membranes, it is then converted to MONOL-41, which is finally released in the medium; iii. MONAL-41 is converted to MONOL-41 by enzymes which were released in the conditioned medium. Although further analyses are needed to determine the uptake/influx pathway of MONAL-41 and to determine whether cells, EVs and/or enzymes released in the conditioned

medium reduced MONAL-41, this result demonstrated that the aldehyde reduction activity of cell cultures can be easily monitored by using MONAL-41 as a substrate.

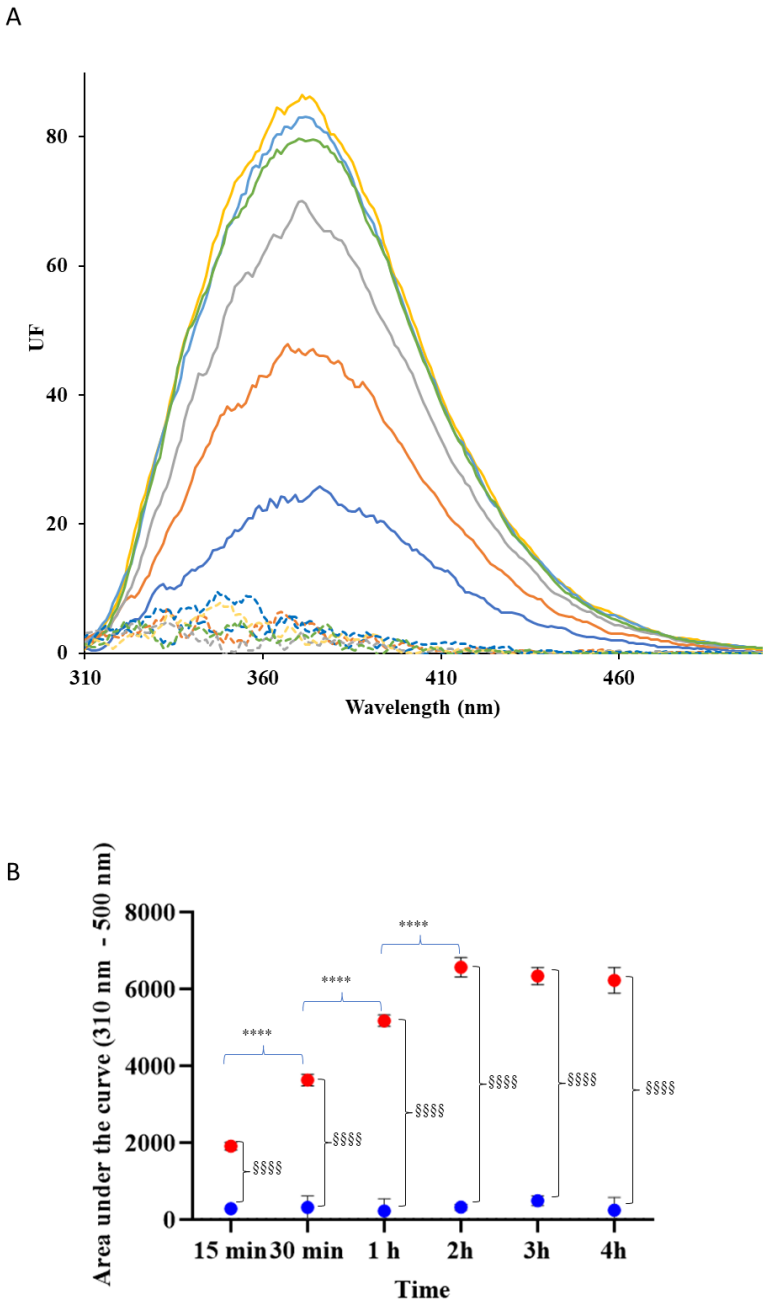

Figure 34. Detection of MONOl-41 in conditioned medium of A549 cell cultures by exciting at 296 nm. Panel(A)*: Representative example of cells treated with 0.53 % (v/v) as controls (dashed lines) and cells treated with 50 µM MONAL-41(continuous lines) fluorescence emission spectra at 15 min (dark blue), 30 min (orange), 1 hour (grey), 2 hours (yellow), 3 hours (light blue), 4 hours (green).* ***Panel (B)****: Area under the curve of fluorescence emission peaks represented in panel (A): cells treated with 50 µM MONAL-41 (red dots) and cells treated with 0.53% (v/v) acetonitrile (blue dots). Error bars (when not visible, are within the symbols' size) represent mean of three measurements (****= p<0.0001, refers to different timepoints of treated cells; §§§§= p<0.0001, refers to difference between controls and treated cells at each timepoint.)*

Discussion

AKR1B1 and AKR1B10 are two NADPH-dependent reductases with high homology sequence and overlapping substrate specificity.

AKR1B10 plays a relevant role as detoxifying enzyme in gastrointestinal tissues. However, it is overexpressed in several tumours and supports cancer progression through several mechanism including cytotoxic aldehydes detoxification, chemoresistance, activation of procarcinogens, and regulation of retinoic acid. Therefore, AKR1B10 is considered as an antineoplastic target. However, the high structural similarity with AKR1B1 may compromise the effectiveness of anticancer treatments based on non-selective inhibitors. Therefore, the research of compounds able to discriminate between AKR1B10 and AKR1B1 has emerged as an innovative tool in cancer therapy to avoid the complications of classic inhibitors.

On the other hand, for decades AKR1B1 has been studied as a target for anti-diabetes treatments because of its role as the first enzyme of the polyol-pathway. The activation of the polyol-pathway in diabetes is considered as a trigger of several damaging processes which concur to the onset secondary diabetes complications. However, in physiologic conditions AKR1B1 plays a relevant role as detoxicant enzyme. The inhibition of the detoxicant activity of AKR1B1 may partially explain the failure of AKR1B1 classic inhibitors as anti-diabetes adjuvants. In this regard, the application of ARDIs able to inhibit the glucose-reductase activity of AKR1B1 without affecting or affecting at lesser extent its detoxifying ability may be determinant to overcome the side effects of classic inhibitors.

The inhibitory ability against AKR1B1 and AKR1B10 of novel synthetic compounds provided by CHIBIOFARAM department (University of Messina) was investigated. The ability to act as ARDIs was tested in the presence of L-Idose (an epimer of glucose) and in the presence of HNE. Among the compounds tested, molecules belonging to LM series and MC3, MC4, MC6, and MC7 were poor inhibitors of AKR1B1. Conversely, FR5, MC1, and MC8 showed high inhibitory potential in the presence of both substrates, but not DI ability. On the other hand, although their inhibitory potential was less effective compared to the afore-mentioned compounds, FR1 and FR6 acted as non-complete ARDIs. FR1 acted as mixed-type inhibitor with a prevalence of the competitive component in the presence of both L-Idose and HNE. FR6 acted as mixed-type inhibitor with a prevalence of the competitive component in the presence of L-Idose and as pure non-competitive inhibitor in the presence of HNE. In addition, FR3 shows the undesirable effect of inhibiting at higher extent HNE reduction with respect to L-

Idose. However, a caveat is needed. These molecules were tested in the presence of one substrate at time. Therefore, the optimization of an assay able to detect the inhibitory potential of a compound when both substrates are simultaneously present may be useful to predict with more accuracy the inhibitory action of the identified ARDIs *in vivo* conditions. However, results of kinetic characterization suggest that the hyperglycaemic conditions occurring in diabetes should favour the action of FR1 and FR6 on glucose reduction, affecting at lesser extent the reduction of HNE.

In addition, the ability of these synthetic compounds to discriminate between AKR1B1 and AKR1B10 was investigated in the presence of HNE. Similar to the effect exerted on AKR1B1, compounds of LM series and MC3, MC4, MC6, and MC7 had no significative effect on AKR1B10. Conversely, FR1 was detected as a selective inhibitor of AKR1B10. On the contrary, FR3, FR5, FR6 and MC8 acted as selective inhibitors of AKR1B1. Modelling studies are necessary to deep the knowledge about the correlations between the inhibitory potential of the tested molecules and the interaction patterns of molecules functional groups with the binding site of the enzyme. However, it is possible to make some considerations about essential structural features to exert DI and/or selective inhibition. Compounds that show an alkylphenyl ring, a 4-alkyl-morpholine ring, a trifluoromethylphenyl ring, a thiadiazole ring or a 1-propylpiperidine ring are poor inhibitors of both enzymes. Although, FR1 and FR4 are isomers with a methyldiphenyl ether group, they show different inhibitory potential. FR1 summarizes the desired features described until now, since it is both an ARDI and a selective and powerful inhibitor of AKR1B10. Conversely, even if a strong inhibitor of AKR1B10, FR4 does not exert any selectivity or differential inhibitory ability. Compounds with a 2-Methylbenzothiazole (MC8), a 3-Methylbenzophenone (FR3) or a Methyldiphenyl (FR5 and FR6) group are selective inhibitors of AKR1B1. In addition, although FR5 and FR6 are isomers, only FR6 acts as an ARDI. Although this research is still in its early stages, these findings could possibly support future modelling analyses and the synthesis of new drug candidates.

As evinced from the above reported results, synthesis of large libraries with high chemical diversity is a valuable approach to identify new lead compounds. However, the research of bioactive compounds in natural sources offer some advantages: i. natural products often show novel scaffolds and structure complexity, which can be used as a starting point for drug design; ii. bioactive compounds found in edible vegetables confer them nutraceutical properties, therefore contributing to promote their use as functional food. *Zolfino* bean extract is a natural source known for being rich in AKR1B1 inhibitors including ARDIs [116]. In this study the

isolation and the identification of promising candidates able to exert selective inhibition on AKR1B10 from a crude *zolfino* extract is reported. The fractionation of the crude extract through hydrophobic interaction chromatography and the inhibition studies performed on fractions allowed to identify fractions with the highest and most selective inhibitory potential toward AKR1B10 with respect to AKR1B1. Glycerol esters of palmitic acid (also known as alpha-palmitin) and stearic acid were identified as putative selective inhibitors through LC-MS analysis. Given the structural similarity of the identified compounds, inhibition studies were performed on alpha-palmitin. In the adopted assay conditions, solubility issues hampered a full characterization of alpha-palmitin, which showed poor inhibitory potential on AKR1B10 and no effect on AKR1B1. However, "disassembling" compounds to evaluate the inhibitory ability of the fragments is a common practice in enzymatic inhibition studies. In addition, the ability of saturated and unsaturated fatty acids to inhibit AKR1B10 was reported [129]. Hara *et al*. screened saturated and unsaturated fatty acids for their ability to inhibit the dehydrogenase activity of AKR1B10 in the presence of geraniol as a substrate. The inhibitory potential of saturated fatty acid was strictly correlated to their hydrocarbon chain length: the potency increased with the increase of chains length 9:0 to 14:0 [129]. However, palmitic acid and stearic acid (16:0 and 18:0, respectively) showed low inhibitory potential. Conversely, their derivatives with a cis-unsaturated bond (palmitoleic acid and oleic acid, respectively) and cis-polyunsaturated fatty acids, regardless of differences in length of the hydrocarbon chain and in number and/or position of the unsaturated bonds, significantly inhibited the dehydrogenase activity of the enzyme [129]. Hara *et al*. tested fatty acids with the highest inhibitory potential toward AKR1B10 dehydrogenase-activity to assess their selectivity on pyrimidine-3-aldehyde-reductase activity of AKR1B10 with respect to AKR1B1, therefore excluding palmitic and stearic acid from selectivity inhibition studies. In the present study, the inhibitory potential of palmitic acid toward AKR1B1 and AKR1B10 was investigated. Palmitic acid had no effect on AKR1B1 in the presence of HNE and L-Idose. Conversely, Palmitic acid was highly effective on AKR1B10 in the presence of HNE (IC50 2.23 μM) and its characterization showed a purely non-competitive mode of action. Based on the information reported in literature, this is the first study in which the inhibitory ability of palmitic acid was investigated in the presence of HNE as a substrate. The inhibition percentage of 20 μM of palmitic acid on the dehydrogenase activity of AKR1B10 in the presence of 25 μM geraniol as a substrate was 33% [129]. The discrepancy in the effect exerted by palmitic acid on AKR1B10 in the presence of geraniol and in the presence of HNE (as here reported) are probably related to the differences in chemical structure of the two substrates. Again, modelling analyses are needed to explain the interaction

patterns between palmitic acid and the binding site, which are essential to exert selectivity toward AKR1B10 with respect to AKR1B1 in the presence of HNE. However, these results are a solid starting point that paves the way for new candidates for selective inhibition of AKR1B10.

Finally, results reported in this study showed that a fluorescent assay for the detection of AKR1B10 was successfully optimized. The assay is based on the detection of the fluorescent compound MONOL-4 as a product of the NADPH-dependent reduction of MONAL-41. Results revealed that MONAL-41 is a good substrate of AKR1B10, since its K_m is approximately 3.8 μM, which is lower than the K_m of the substrates commonly used in the research field. The use of MONAL-41 as a substrate in combination with the use of a plate reader offers some advantages in terms of sensitivity and time/cost management: the activity assay requires a very small amount of enzyme, and it is possible to run 96 assays simultaneously.

The fluorescent assays performed in the presence of both MONAL-41 as a substrate and oleanolic acid as an inhibitor of AKR1B10, showed that the residual activity of cell extracts is higher than the residual activity detected with the recombinant enzyme. This effect can be the result of the binding of oleanolic acid to other targets, which reduces the availability of the inhibitor and consequently its efficacy on AKR1B10. Moreover, although preliminary tests indicated that the affinity of MONAL-41 is higher for AKR1B10 compared to AKR1B1, it is not possible to exclude the contribution of other NADPH-dependent reductases able to convert MONAL-41 in cell extracts. Finally, no MONAL-41-reductase activity was detected in small EVs extracts, although the protein was detected in these samples through Western Blot analyses. However, these results do not exclude an inactivation of AKR1B10 which could occur during the EVs collection and/or storage procedures or before the secretion of the enzyme in small EVs. In addition, it cannot be excluded the presence in small EVs of compounds which can interfere with AKR1B10 activity detection. However, the presence of AKR1B10 either as an active or as an inactive form in small EVs obtained from A549 cell cultures rises several questions about its role as a secreted protein, which needs to be deeply investigated. Treatment of A549 cell cultures with MONAL-41 showed that reductase activity of cell cultures can be easily monitored through the detection of MONOL-41 in the conditioned medium. However, this preliminary test hampered the discrimination of the effectors of MONOL-41 production, which can be theoretically linked to cells, EVs or even enzymes released in the medium. All together these results suggested that several further analyses are needed to have a

comprehensive view of MONAL-41 application for the detection of AKR1B10 activity in cell cultures and extracts of both cells and EVs: i. MONAL-41 specificity should be verified with other reductases present in A549 cell extracts; ii. to verify that the procedures of collection and storage do not inactivate AKR1B10; iii. to verify if MONAL-41 is reduced by cells, EVs and/or enzymes released in the conditioned medium of cell cultures. To ascertain if MONAL-41 is specific for AKR1B10 and to elucidate how MONAL-41 is converted in cell cultures would promote the use of MONAL-41 to monitor AKR1B10 in biological extracts as well as in cell cultures.

Appendix

Figure 1A: pET-30a (+) vector (Novagen). The pET-30a(+) vector carries an N-terminal His•Tag®/thrombin/S•Tag™/enterokinase configuration plus an optional C-terminal His•Tag sequence. Unique sites are shown on the circle map. The T7 expression region is reversed on the circular map. The cloning/expression region of the coding strand transcribed by T7 RNA polymerase is shown below.

pET-30a(+) sequence landmarks	
T7 promoter	419-435
T7 transcription start	418
His•Tag coding sequence	327-344
S•Tag coding sequence	249-293
Multiple cloning sites	
(*Nco* I - *Xho* I)	158-217
His•Tag coding sequence	140-157
T7 terminator	26-72
lacI coding sequence	826-1905
pBR322 origin	3339
Kan coding sequence	4048-4860
f1 origin	4956-5411

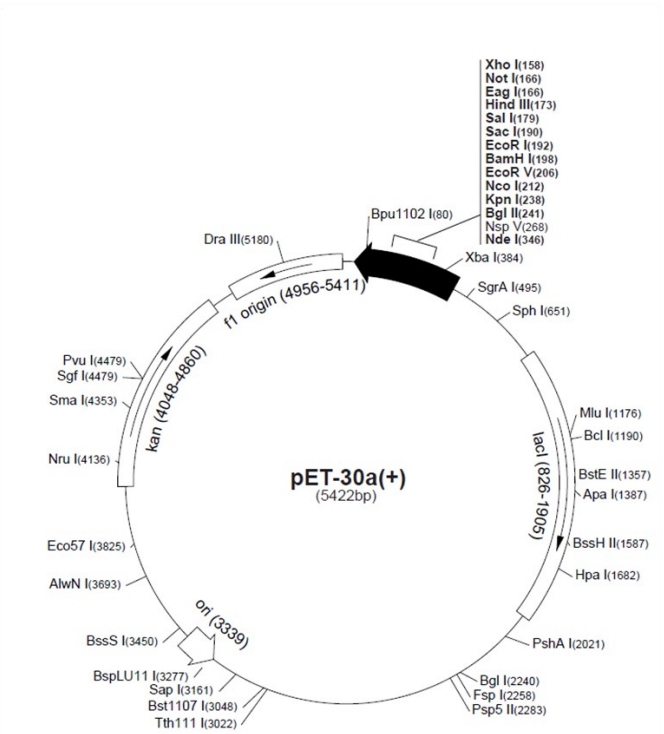

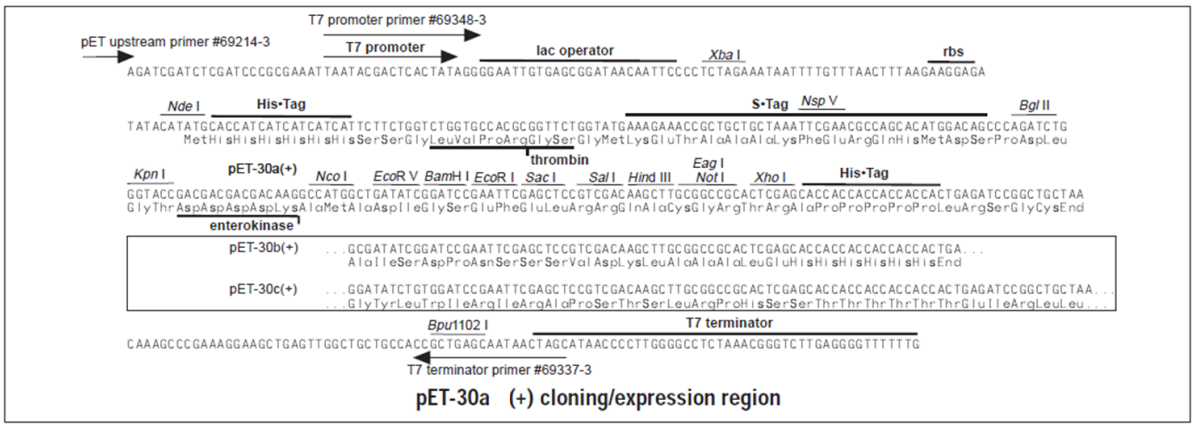

Figure 2A: coding sequence of AKR1B1.

ATGGCAAGCCGTCTCCTGCTCAACAACGGCGCCAAGATGCCCATCCTGGGGTTGGGTACC
TGGAAGTCCCCTCCAGGGCAGGTGACTGAGGCCGTGAAGGTGGCCATTGACGTCGGGTAC
CGCCACATCGACTGTGCCCATGTGTACCAGAATGAGAATGAGGTGGGGGTGGCCATTCAG
GAGAAGCTCAGGGAGCAGGTGGTGAAGCGTGAGGAGCTCTTCATCGTCAGCAAGCTGTGG
TGCACGTACCATGAGAAGGGCCTGGTGAAAGGAGCCTGCCAGAAGACACTCAGCGACCTG
AAGCTGGACTACCTGGACCTCTACCTTATTCACTGGCCGACTGGCTTTAAGCCTGGGAAG
GAATTTTTCCCATTGGATGAGTCGGGCAATGTGGTTCCCAGTGACACCAACATTCTGGAC
ACGTGGGCGGCCATGGAAGAGCTGGTGGATGAAGGGCTGGTGAAAGCTATTGGCATCTCC
AACTTCAACCATCTCCAGGTGGAGATGATCTTAAACAAACCTGGCTTGAAGTATAAGCCT
GCAGTTAACCAGATTGAGTGCCACCCATATCTCACTCAGGAGAAGTTAATCCAGTACTGC
CAGTCCAAAGGCATCGTGGTGACCGCCTACAGCCCCCTCGGCTCTCCTGACAGGCCCTGG
GCCAAGCCCGAGGACCCTTCTCTCCTGGAGGATCCCAGGATCAAGGCGATCGCAGCCAAG
CACAATAAAACTACAGCCCAGGTCCTGATCCGGTTCCCCATGCAGAGGAACTTGGTGGTG
ATCCCCAAGTCTGTGACACCAGAACGCATTGCTGAGAACTTTAAGGTCTTTGACTTTGAA
CTGAGCAGCCAGGATATGACCACCTTACTCAGCTACAACAGGAACTGGAGGGTCTGTGCC
TTGTTGAGCTGTACCTCCCACAAGGATTACCCCTTCCATGAAGAGTTTTGA

Figure 3A: coding sequence of AKR1B10.

ATGGCCACGTTTGTGGAGCTCAGTACCAAAGCCAAGATGCCCATTGTGGGCCTGGGCACT
TGGAAGTCTCCTCTTGGCAAAGTGAAAGAAGCAGTGAAGGTGGCCATTGATGCAGGATAT
CGGCACATTGACTGTGCCTATGTCTATCAGAATGAACATGAAGTGGGGGAAGCCATCCAA
GAGAAGATCCAAGAGAAGGCTGTGAAGCGGGAGGACCTGTTCATCGTCAGCAAGTTGTGG
CCCACTTTCTTTGAGAGACCCCTTGTGAGGAAAGCCTTTGAGAAGACCCTCAAGGACCTG
AAGCTGAGCTATCTGGACGTCTATCTTATTCACTGGCCACAGGGATTCAAGTCTGGGGAT
GACCTTTTCCCCAAAGATGATAAAGGTAATGCCATCGGTGGAAAAGCAACGTTCTTGGAT
GCCTGGGAGGCCATGGAGGAGCTGGTGGATGAGGGGCTGGTGAAAGCCCTTGGGGTCTCC
AATTTCAGCCACTTCCAGATCGAGAAGCTCTTGAACAAACCTGGACTGAAATATAAACCA
GTGACTAACCAGGTTGAGTGTCACCCATACCTCACACAGGAGAAACTGATCCAGTACTGC
CACTCCAAGGGCATCACCGTTACGGCCTACAGCCCCCTGGGCTCTCCGGATAGACCTTGG
GCCAAGCCAGAAGACCCTTCCCTGCTGGAGGATCCCAAGATTAAGGAGATTGCTGCAAAG
CACAAAAAAACCGCAGCCCAGGTTCTGATCCGTTTCCATATCCAGAGGAATGTGATTGTC
ATCCCCAAGTCTGTGACACCAGCACGCATTGTTGAGAACATTCAGGTCTTTGACTTTAAA
TTGAGTGATGAGGAGATGGCAACCATACTCAGCTTCAACAGAAACTGGAGGGCCTGTAAC
GTGTTGCAATCCTCTCATTTGGAAGACTATCCCTTCAATGCAGAATATTGA

References

1. Penning, T.M., *The aldo-keto reductases (AKRs): Overview.* Chem Biol Interact, 2015. **234**: p. 236-46.
2. Cao, D., S.T. Fan, and S.S. Chung, *Identification and characterization of a novel human aldose reductase-like gene.* J Biol Chem, 1998. **273**(19): p. 11429-35.
3. Tarle, I., et al., *Probing the active site of human aldose reductase. Site-directed mutagenesis of Asp-43, Tyr-48, Lys-77, and His-110.* J Biol Chem, 1993. **268**(34): p. 25687-93.
4. Sotriffer, C.A., O. Krämer, and G. Klebe, *Probing flexibility and "induced-fit" phenomena in aldose reductase by comparative crystal structure analysis and molecular dynamics simulations.* Proteins, 2004. **56**(1): p. 52-66.
5. Bohren, K.M., et al., *Tyrosine-48 is the proton donor and histidine-110 directs substrate stereochemical selectivity in the reduction reaction of human aldose reductase: enzyme kinetics and crystal structure of the Y48H mutant enzyme.* Biochemistry, 1994. **33**(8): p. 2021-32.
6. Borhani, D.W., T.M. Harter, and J.M. Petrash, *The crystal structure of the aldose reductase.NADPH binary complex.* J Biol Chem, 1992. **267**(34): p. 24841-7.
7. Urzhumtsev, A., et al., *A 'specificity' pocket inferred from the crystal structures of the complexes of aldose reductase with the pharmaceutically important inhibitors tolrestat and sorbinil.* Structure, 1997. **5**(5): p. 601-12.
8. Shen, Y., et al., *Human aldo-keto reductases 1B1 and 1B10: a comparative study on their enzyme activity toward electrophilic carbonyl compounds.* Chem Biol Interact, 2011. **191**(1-3): p. 192-8.
9. Srivastava, S., et al., *Structural and kinetic determinants of aldehyde reduction by aldose reductase.* Biochemistry, 1999. **38**(1): p. 42-54.
10. Srivastava, S., et al., *Lipid peroxidation product, 4-hydroxynonenal and its conjugate with GSH are excellent substrates of bovine lens aldose reductase.* Biochem Biophys Res Commun, 1995. **217**(3): p. 741-6.
11. Zhong, L., et al., *Aldo-keto reductase family 1 B10 protein detoxifies dietary and lipid-derived alpha, beta-unsaturated carbonyls at physiological levels.* Biochem Biophys Res Commun, 2009. **387**(2): p. 245-50.
12. Martin, H.J. and E. Maser, *Role of human aldo-keto-reductase AKR1B10 in the protection against toxic aldehydes.* Chem Biol Interact, 2009. **178**(1-3): p. 145-50.
13. Hirosawa, K., et al., *Quantitative analysis of mRNA and protein expression levels of aldo-keto reductase and short-chain dehydrogenase/reductase isoforms in the human intestine.* Drug Metab Dispos, 2023.
14. Petersen, D.R. and J.A. Doorn, *Reactions of 4-hydroxynonenal with proteins and cellular targets.* Free Radic Biol Med, 2004. **37**(7): p. 937-45.
15. Schaur, R.J., et al., *4-Hydroxy-nonenal-A Bioactive Lipid Peroxidation Product.* Biomolecules, 2015. **5**(4): p. 2247-337.
16. Nègre-Salvayre, A., et al., *Proatherogenic effects of 4-hydroxynonenal.* Free Radic Biol Med, 2017. **111**: p. 127-139.
17. Di Domenico, F., A. Tramutola, and D.A. Butterfield, *Role of 4-hydroxy-2-nonenal (HNE) in the pathogenesis of alzheimer disease and other selected age-related neurodegenerative disorders.* Free Radic Biol Med, 2017. **111**: p. 253-261.
18. Zarkovic, K., A. Jakovcevic, and N. Zarkovic, *Contribution of the HNE-immunohistochemistry to modern pathological concepts of major human diseases.* Free Radic Biol Med, 2017. **111**: p. 110-126.

19. Yoval-Sánchez, B. and J.S. Rodríguez-Zavala, *Differences in susceptibility to inactivation of human aldehyde dehydrogenases by lipid peroxidation byproducts.* Chem Res Toxicol, 2012. **25**(3): p. 722-9.
20. Li, D., et al., *Protective effect of inducible aldo-keto reductases on 4-hydroxynonenal-induced hepatotoxicity.* Chem Biol Interact, 2019. **304**: p. 124-130.
21. Lyon, R.C., et al., *Aldo-keto reductases mediate constitutive and inducible protection against aldehyde toxicity in human neuroblastoma SH-SY5Y cells.* Neurochem Int, 2013. **62**(1): p. 113-21.
22. Balogh, L.M. and W.M. Atkins, *Interactions of glutathione transferases with 4-hydroxynonenal.* Drug Metab Rev, 2011. **43**(2): p. 165-78.
23. Balestri, F., et al., *Stereoselectivity of Aldose Reductase in the Reduction of Glutathionyl-Hydroxynonanal Adduct.* Antioxidants (Basel), 2019. **8**(10).
24. Shen, Y., et al., *Impaired self-renewal and increased colitis and dysplastic lesions in colonic mucosa of AKR1B8-deficient mice.* Clin Cancer Res, 2015. **21**(6): p. 1466-76.
25. Zu, X., et al., *Aldo-keto reductase 1B10 protects human colon cells from DNA damage induced by electrophilic carbonyl compounds.* Mol Carcinog, 2017. **56**(1): p. 118-129.
26. Morikawa, Y., et al., *Protective Effect of Aldo-keto Reductase 1B1 Against Neuronal Cell Damage Elicited by 4'-Fluoro-α-pyrrolidinononanophenone.* Neurotox Res, 2021. **39**(4): p. 1360-1371.
27. Sonowal, H. and K.V. Ramana, *4-Hydroxy-Trans-2-Nonenal in the Regulation of Anti-Oxidative and Pro-Inflammatory Signaling Pathways.* Oxid Med Cell Longev, 2019. **2019**: p. 5937326.
28. Ramana, K.V., et al., *Mitogenic responses of vascular smooth muscle cells to lipid peroxidation-derived aldehyde 4-hydroxy-trans-2-nonenal (HNE): role of aldose reductase-catalyzed reduction of the HNE-glutathione conjugates in regulating cell growth.* J Biol Chem, 2006. **281**(26): p. 17652-60.
29. Ramana, K.V. and S.K. Srivastava, *Mediation of aldose reductase in lipopolysaccharide-induced inflammatory signals in mouse peritoneal macrophages.* Cytokine, 2006. **36**(3-4): p. 115-22.
30. Miláčková, I., et al., *Artichoke Leaf Extract Inhibits AKR1B1 and Reduces NF-κB Activity in Human Leukemic Cells.* Phytother Res, 2017. **31**(3): p. 488-496.
31. Ma, J., et al., *AKR1B10 overexpression in breast cancer: association with tumor size, lymph node metastasis and patient survival and its potential as a novel serum marker.* Int J Cancer, 2012. **131**(6): p. E862-71.
32. Shi, J., et al., *Aldo-Keto Reductase Family 1 Member B10 (AKR1B10) overexpression in tumors predicts worse overall survival in hepatocellular carcinoma.* J Cancer, 2019. **10**(20): p. 4892-4901.
33. He, Y.C., et al., *Overexpression of AKR1B10 in nasopharyngeal carcinoma as a potential biomarker.* Cancer Biomark, 2016. **16**(1): p. 127-35.
34. Fang, C.Y., Y.H. Lin, and C.L. Chen, *Overexpression of AKR1B10 predicts tumor recurrence and short survival in oral squamous cell carcinoma patients.* J Oral Pathol Med, 2019. **48**(8): p. 712-719.
35. Chung, Y.T., et al., *Overexpression and oncogenic function of aldo-keto reductase family 1B10 (AKR1B10) in pancreatic carcinoma.* Mod Pathol, 2012. **25**(5): p. 758-66.
36. Fukumoto, S., et al., *Overexpression of the aldo-keto reductase family protein AKR1B10 is highly correlated with smokers' non-small cell lung carcinomas.* Clin Cancer Res, 2005. **11**(5): p. 1776-85.
37. Yan, R., et al., *Aldo-keto reductase family 1 B10 gene silencing results in growth inhibition of colorectal cancer cells: Implication for cancer intervention.* Int J Cancer, 2007. **121**(10): p. 2301-6.

38. Liu, Y., et al., *Compensatory upregulation of aldo-keto reductase 1B10 to protect hepatocytes against oxidative stress during hepatocarcinogenesis.* Am J Cancer Res, 2019. **9**(12): p. 2730-2748.
39. Matsunaga, T., et al., *Aldo-keto reductase 1B10 promotes development of cisplatin resistance in gastrointestinal cancer cells through down-regulating peroxisome proliferator-activated receptor-γ-dependent mechanism.* Chem Biol Interact, 2016. **256**: p. 142-53.
40. Nishinaka, T., et al., *Regulation of aldo-keto reductase AKR1B10 gene expression: involvement of transcription factor Nrf2.* Chem Biol Interact, 2011. **191**(1-3): p. 185-91.
41. Torres-Mena, J.E., et al., *Aldo-Keto Reductases as Early Biomarkers of Hepatocellular Carcinoma: A Comparison Between Animal Models and Human HCC.* Dig Dis Sci, 2018. **63**(4): p. 934-944.
42. Matsunaga, T., et al., *Involvement of the aldo-keto reductase, AKR1B10, in mitomycin-c resistance through reactive oxygen species-dependent mechanisms.* Anticancer Drugs, 2011. **22**(5): p. 402-8.
43. Matsunaga, T., et al., *Pathophysiological roles of autophagy and aldo-keto reductases in development of doxorubicin resistance in gastrointestinal cancer cells.* Chem Biol Interact, 2019. **314**: p. 108839.
44. Carazo, A., et al., *Vitamin A Update: Forms, Sources, Kinetics, Detection, Function, Deficiency, Therapeutic Use and Toxicity.* Nutrients, 2021. **13**(5).
45. Jin, Y., et al., *Retinoids as anti-cancer agents and their mechanisms of action.* Am J Cancer Res, 2022. **12**(3): p. 938-960.
46. Endo, S., T. Matsunaga, and T. Nishinaka, *The Role of AKR1B10 in Physiology and Pathophysiology.* Metabolites, 2021. **11**(6).
47. Gallego, O., et al., *Comparative functional analysis of human medium-chain dehydrogenases, short-chain dehydrogenases/reductases and aldo-keto reductases with retinoids.* Biochem J, 2006. **399**(1): p. 101-9.
48. Ruiz, F.X., et al., *Aldo-keto reductases from the AKR1B subfamily: retinoid specificity and control of cellular retinoic acid levels.* Chem Biol Interact, 2009. **178**(1-3): p. 171-7.
49. Endo, S., et al., *Roles of rat and human aldo-keto reductases in metabolism of farnesol and geranylgeraniol.* Chem Biol Interact, 2011. **191**(1-3): p. 261-8.
50. Endo, S., et al., *Kinetic studies of AKR1B10, human aldose reductase-like protein: endogenous substrates and inhibition by steroids.* Arch Biochem Biophys, 2009. **487**(1): p. 1-9.
51. Zhang, W., et al., *Knockdown or inhibition of aldo-keto reductase 1B10 inhibits pancreatic carcinoma growth via modulating Kras-E-cadherin pathway.* Cancer Lett, 2014. **355**(2): p. 273-80.
52. Zhong, L., et al., *AKR1B10 induces cell resistance to daunorubicin and idarubicin by reducing C13 ketonic group.* Toxicol Appl Pharmacol, 2011. **255**(1): p. 40-7.
53. Bains, O.S., et al., *A correlation between cytotoxicity and reductase-mediated metabolism in cell lines treated with doxorubicin and daunorubicin.* J Pharmacol Exp Ther, 2013. **347**(2): p. 375-87.
54. Heibein, A.D., et al., *Role of aldo-keto reductases and other doxorubicin pharmacokinetic genes in doxorubicin resistance, DNA binding, and subcellular localization.* BMC Cancer, 2012. **12**: p. 381.
55. Hintzpeter, J., et al., *Inhibition of human anthracycline reductases by emodin - A possible remedy for anthracycline resistance.* Toxicol Appl Pharmacol, 2016. **293**: p. 21-9.

56. Büküm, N., et al., *Inhibition of AKR1B10-mediated metabolism of daunorubicin as a novel off-target effect for the Bcr-Abl tyrosine kinase inhibitor dasatinib.* Biochem Pharmacol, 2021. **192**: p. 114710.
57. Bhagat, A. and E.S. Kleinerman, *Anthracycline-Induced Cardiotoxicity: Causes, Mechanisms, and Prevention.* Adv Exp Med Biol, 2020. **1257**: p. 181-192.
58. Piska, K., et al., *Metabolic carbonyl reduction of anthracyclines - role in cardiotoxicity and cancer resistance. Reducing enzymes as putative targets for novel cardioprotective and chemosensitizing agents.* Invest New Drugs, 2017. **35**(3): p. 375-385.
59. Zhao, F., et al., *Amentoflavone-loaded nanoparticles enhanced chemotherapy efficacy by inhibition of AKR1B10.* Nanotechnology, 2022. **33**(38).
60. Quinn, A.M., R.G. Harvey, and T.M. Penning, *Oxidation of PAH trans-dihydrodiols by human aldo-keto reductase AKR1B10.* Chem Res Toxicol, 2008. **21**(11): p. 2207-15.
61. Zhang, L., et al., *Impact of smoking cessation on global gene expression in the bronchial epithelium of chronic smokers.* Cancer Prev Res (Phila), 2008. **1**(2): p. 112-8.
62. Wang, R., et al., *Smoking-induced upregulation of AKR1B10 expression in the airway epithelium of healthy individuals.* Chest, 2010. **138**(6): p. 1402-10.
63. Kang, M.W., et al., *AKR1B10 is associated with smoking and smoking-related non-small-cell lung cancer.* J Int Med Res, 2011. **39**(1): p. 78-85.
64. Woenckhaus, M., et al., *Smoking and cancer-related gene expression in bronchial epithelium and non-small-cell lung cancers.* J Pathol, 2006. **210**(2): p. 192-204.
65. Du, Z., et al., *Quantitative proteomics identifies a plasma multi-protein model for detection of hepatocellular carcinoma.* Sci Rep, 2020. **10**(1): p. 15552.
66. Cao, Z., et al., *AKR1B10 as a Potential Novel Serum Biomarker for Breast Cancer: A Pilot Study.* Front Oncol, 2022. **12**: p. 727505.
67. Luo, D.X., et al., *Aldo-keto reductase family 1, member B10 is secreted through a lysosome-mediated non-classical pathway.* Biochem J, 2011. **438**(1): p. 71-80.
68. Luo, D., et al., *Heat shock protein 90-α mediates aldo-keto reductase 1B10 (AKR1B10) protein secretion through secretory lysosomes.* J Biol Chem, 2013. **288**(51): p. 36733-40.
69. Vesiclepedia. http://microvesicles.org/gene_summary?gene_id=57016.
70. Mashouri, L., et al., *Exosomes: composition, biogenesis, and mechanisms in cancer metastasis and drug resistance.* Mol Cancer, 2019. **18**(1): p. 75.
71. Palazzolo, S., et al., *Cancer Extracellular Vesicles: Next-Generation Diagnostic and Drug Delivery Nanotools.* Cancers (Basel), 2020. **12**(11).
72. Zhang, L. and D. Yu, *Exosomes in cancer development, metastasis, and immunity.* Biochim Biophys Acta Rev Cancer, 2019. **1871**(2): p. 455-468.
73. Chabert, C., et al., *AKR1B10, One of the Triggers of Cytokine Storm in SARS-CoV2 Severe Acute Respiratory Syndrome.* Int J Mol Sci, 2022. **23**(3).
74. Li, W., et al., *Liquid biopsy in lung cancer: significance in diagnostics, prediction, and treatment monitoring.* Mol Cancer, 2022. **21**(1): p. 25.
75. Cappiello, M., et al., *Intra-site differential inhibition of multi-specific enzymes.* J Enzyme Inhib Med Chem, 2020. **35**(1): p. 840-846.
76. Inagaki, K., I. Miwa, and J. Okuda, *Affinity purification and glucose specificity of aldose reductase from bovine lens.* Arch Biochem Biophys, 1982. **216**(1): p. 337-44.
77. Dworkin, J.P. and S.L. Miller, *A kinetic estimate of the free aldehyde content of aldoses.* Carbohydr Res, 2000. **329**(2): p. 359-65.

78. Balestri, F., et al., *L-Idose: an attractive substrate alternative to D-glucose for measuring aldose reductase activity.* Biochem Biophys Res Commun, 2015. **456**(4): p. 891-5.
79. Balestri, F., et al., *Modulation of aldose reductase activity by aldose hemiacetals.* Biochim Biophys Acta, 2015. **1850**(11): p. 2329-39.
80. Del Corso, A., M. Cappiello, and U. Mura, *From a dull enzyme to something else: facts and perspectives regarding aldose reductase.* Curr Med Chem, 2008. **15**(15): p. 1452-61.
81. Ramana, K.V., et al., *Nitric oxide regulates the polyol pathway of glucose metabolism in vascular smooth muscle cells.* Faseb j, 2003. **17**(3): p. 417-25.
82. Zopf, S., et al., *Localization of the polyol pathway in the human kidney.* Histol Histopathol, 2009. **24**(4): p. 447-55.
83. Beck, F.X. and W. Neuhofer, *Cell volume regulation in the renal papilla.* Contrib Nephrol, 2006. **152**: p. 181-197.
84. Ko, B.C., et al., *Identification and characterization of multiple osmotic response sequences in the human aldose reductase gene.* J Biol Chem, 1997. **272**(26): p. 16431-7.
85. King, G.L., et al., *Cellular and molecular abnormalities in the vascular endothelium of diabetes mellitus.* Annu Rev Med, 1994. **45**: p. 179-88.
86. Hashim, Z. and S. Zarina, *Osmotic stress induced oxidative damage: possible mechanism of cataract formation in diabetes.* J Diabetes Complications, 2012. **26**(4): p. 275-9.
87. Kinoshita, J.H., L.O. Merola, and E. Dikmak, *Osmotic changes in experimental galactose cataracts.* Exp Eye Res, 1962. **1**: p. 405-10.
88. Kinoshita, J.H. and C. Nishimura, *The involvement of aldose reductase in diabetic complications.* Diabetes Metab Rev, 1988. **4**(4): p. 323-37.
89. Banditelli, S., et al., *A new approach against sugar cataract through aldose reductase inhibitors.* Exp Eye Res, 1999. **69**(5): p. 533-8.
90. Lee, A.Y., S.K. Chung, and S.S. Chung, *Demonstration that polyol accumulation is responsible for diabetic cataract by the use of transgenic mice expressing the aldose reductase gene in the lens.* Proc Natl Acad Sci U S A, 1995. **92**(7): p. 2780-4.
91. Ansari, N.H., et al., *Trolox protects hyperglycemia-induced cataractogenesis in cultured rat lens.* Res Commun Chem Pathol Pharmacol, 1994. **84**(1): p. 93-104.
92. Srivastava, S.K. and N.H. Ansari, *Prevention of sugar-induced cataractogenesis in rats by butylated hydroxytoluene.* Diabetes, 1988. **37**(11): p. 1505-8.
93. Wu, J., Z. Jin, and L.J. Yan, *Redox imbalance and mitochondrial abnormalities in the diabetic lung.* Redox Biol, 2017. **11**: p. 51-59.
94. Wu, J., et al., *Pancreatic mitochondrial complex I exhibits aberrant hyperactivity in diabetes.* Biochem Biophys Rep, 2017. **11**: p. 119-129.
95. Couto, N., J. Wood, and J. Barber, *The role of glutathione reductase and related enzymes on cellular redox homoeostasis network.* Free Radic Biol Med, 2016. **95**: p. 27-42.
96. Aouacheri, O., et al., *The investigation of the oxidative stress-related parameters in type 2 diabetes mellitus.* Can J Diabetes, 2015. **39**(1): p. 44-9.
97. Obrosova, I.G., et al., *An aldose reductase inhibitor reverses early diabetes-induced changes in peripheral nerve function, metabolism, and antioxidative defense.* Faseb j, 2002. **16**(1): p. 123-5.
98. Kuzumoto, Y., et al., *Effect of the aldose reductase inhibitor fidarestat on experimental diabetic neuropathy in the rat.* Diabetologia, 2006. **49**(12): p. 3085-93.
99. De Mattia, G., et al., *Effect of aldose reductase inhibition on glutathione redox status in erythrocytes of diabetic patients.* Metabolism, 1994. **43**(8): p. 965-8.

100. Shen, C.Y., et al., *The Development of Maillard Reaction, and Advanced Glycation End Product (AGE)-Receptor for AGE (RAGE) Signaling Inhibitors as Novel Therapeutic Strategies for Patients with AGE-Related Diseases.* Molecules, 2020. **25**(23).
101. Ighodaro, O.M., *Molecular pathways associated with oxidative stress in diabetes mellitus.* Biomed Pharmacother, 2018. **108**: p. 656-662.
102. Jubaidi, F.F., et al., *The Role of PKC-MAPK Signalling Pathways in the Development of Hyperglycemia-Induced Cardiovascular Complications.* Int J Mol Sci, 2022. **23**(15).
103. Geraldes, P. and G.L. King, *Activation of protein kinase C isoforms and its impact on diabetic complications.* Circ Res, 2010. **106**(8): p. 1319-31.
104. Peterson, M.J., et al., *CP-45,634: a novel aldose reductase inhibitor that inhibits polyol pathway activity in diabetic and galactosemic rats.* Metabolism, 1979. **28**(4 Suppl 1): p. 456-61.
105. Kern, T.S. and R.L. Engerman, *Aldose reductase and the development of renal disease in diabetic dogs.* J Diabetes Complications, 1999. **13**(1): p. 10-6.
106. Spielberg, S.P., et al., *In-vitro assessment of a hypersensitivity syndrome associated with sorbinil.* Ann Intern Med, 1991. **114**(9): p. 720-4.
107. de la Fuente, J.A. and S. Manzanaro, *Aldose reductase inhibitors from natural sources.* Nat Prod Rep, 2003. **20**(2): p. 243-51.
108. Quattrini, L. and C. La Motta, *Aldose reductase inhibitors: 2013-present.* Expert Opin Ther Pat, 2019. **29**(3): p. 199-213.
109. Vincent, T.E., S. Mendiratta, and J.M. May, *Inhibition of aldose reductase in human erythrocytes by vitamin C.* Diabetes Res Clin Pract, 1999. **43**(1): p. 1-8.
110. Cunningham, J.J., P.L. Mearkle, and R.G. Brown, *Vitamin C: an aldose reductase inhibitor that normalizes erythrocyte sorbitol in insulin-dependent diabetes mellitus.* J Am Coll Nutr, 1994. **13**(4): p. 344-50.
111. Patil, K.K. and R.N. Gacche, *Inhibition of glycation and aldose reductase activity using dietary flavonoids: A lens organ culture studies.* Int J Biol Macromol, 2017. **98**: p. 730-738.
112. Fallahzadeh, M.K., et al., *Effect of addition of silymarin to renin-angiotensin system inhibitors on proteinuria in type 2 diabetic patients with overt nephropathy: a randomized, double-blind, placebo-controlled trial.* Am J Kidney Dis, 2012. **60**(6): p. 896-903.
113. Del-Corso, A., et al., *A new approach to control the enigmatic activity of aldose reductase.* PLoS One, 2013. **8**(9): p. e74076.
114. Cappiello, M., et al., *Basic models for differential inhibition of enzymes.* Biochem Biophys Res Commun, 2014. **445**(3): p. 556-60.
115. Balestri, F., et al., *Acid Derivatives of Pyrazolo[1,5-a]pyrimidine as Aldose Reductase Differential Inhibitors.* Cell Chem Biol, 2018. **25**(11): p. 1414-1418.e3.
116. Balestri, F., et al., *Soyasaponins from Zolfino bean as aldose reductase differential inhibitors.* J Enzyme Inhib Med Chem, 2019. **34**(1): p. 350-360.
117. Balestri, F., et al., *Aldose Reductase Differential Inhibitors in Green Tea.* Biomolecules, 2020. **10**(7).
118. Zhang, L., et al., *Inhibitor selectivity between aldo-keto reductase superfamily members AKR1B10 and AKR1B1: role of Trp112 (Trp111).* FEBS Lett, 2013. **587**(22): p. 3681-6.
119. Ruiz, F.X., X. Parés, and J. Farrés, *Perspective on the Structural Basis for Human Aldo-Keto Reductase 1B10 Inhibition.* Metabolites, 2021. **11**(12).
120. Zhang, L., et al., *Structural basis for the inhibition of AKR1B10 by caffeic acid phenethyl ester (CAPE).* ChemMedChem, 2014. **9**(4): p. 706-9.

121. Ruiz, F.X., et al., *Structural basis for the inhibition of AKR1B10 by the C3 brominated TTNPB derivative UVI2008.* Chem Biol Interact, 2017. **276**: p. 174-181.
122. Ruiz, F.X., et al., *Structural Determinants of the Selectivity of 3-Benzyluracil-1-acetic Acids toward Human Enzymes Aldose Reductase and AKR1B10.* ChemMedChem, 2015. **10**(12): p. 1989-2003.
123. Cousido-Siah, A., et al., *IDD388 Polyhalogenated Derivatives as Probes for an Improved Structure-Based Selectivity of AKR1B10 Inhibitors.* ACS Chem Biol, 2016. **11**(10): p. 2693-2705.
124. Takemura, M., et al., *Selective inhibition of the tumor marker aldo-keto reductase family member 1B10 by oleanolic acid.* J Nat Prod, 2011. **74**(5): p. 1201-6.
125. Matsunaga, T., et al., *Potent and selective inhibition of the tumor marker AKR1B10 by bisdemethoxycurcumin: probing the active site of the enzyme with molecular modeling and site-directed mutagenesis.* Biochem Biophys Res Commun, 2009. **389**(1): p. 128-32.
126. Soda, M., et al., *Design, synthesis and evaluation of caffeic acid phenethyl ester-based inhibitors targeting a selectivity pocket in the active site of human aldo-keto reductase 1B10.* Eur J Med Chem, 2012. **48**: p. 321-9.
127. Bradford, M.M., *A rapid and sensitive method for the quantitation of microgram quantities of protein utilizing the principle of protein-dye binding.* Anal Biochem, 1976. **72**: p. 248-54.
128. Liu, F., et al., *The Exosome Total Isolation Chip.* ACS Nano, 2017. **11**(11): p. 10712-10723.
129. Hara, A., et al., *Inhibition of aldo-keto reductase family 1 member B10 by unsaturated fatty acids.* Arch Biochem Biophys, 2016. **609**: p. 69-76.
130. Misuri, L., et al., *The use of dimethylsulfoxide as a solvent in enzyme inhibition studies: the case of aldose reductase.* J Enzyme Inhib Med Chem, 2017. **32**(1): p. 1152-1158.
131. Wierzchowski, J., et al., *Fluorometric assays for isozymes of human alcohol dehydrogenase.* Anal Biochem, 1989. **178**(1): p. 57-62.
132. Giménez-Dejoz, J., et al., *Engineering aldo-keto reductase 1B10 to mimic the distinct 1B15 topology and specificity towards inhibitors and substrates, including retinoids and steroids.* Chem Biol Interact, 2019. **307**: p. 186-194.
133. Wierzchowski, J., B. Holmquist, and B.L. Vallee, *Determination of human serum alcohol dehydrogenase using isozyme-specific fluorescent substrates.* Anal Chem, 1992. **64**(2): p. 181-6.
134. *The Human Protein Atlas.* https://www.proteinatlas.org/.

5 Academic contributions of the Doctoral candidate in the thematic area of the dissertation

1. Casertano M, Genovese M, **Piazza L**, Balestri F, Del Corso A, Vito A, Paoli P, Santi A, Imperatore C, Menna M. Identifying Human PTP1B Enzyme Inhibitors from Marine Natural Products: Perspectives for Developing of Novel Insulin-Mimetic Drugs. Pharmaceuticals (Basel). 2022 Mar 8;15(3):325. doi: 10.3390/ph15030325. PMID: 35337123; PMCID: PMC8950868.
2. Balestri F, Poli G, **Piazza L**, Cappiello M, Moschini R, Signore G, Tuccinardi T, Mura U, Del Corso A. Dissecting the Activity of Catechins as Incomplete Aldose Reductase Differential Inhibitors through Kinetic and Computational Approaches. Biology (Basel). 2022 Sep 6;11(9):1324. doi: 10.3390/biology11091324. PMID: 36138801; PMCID: PMC9495972.
3. Casertano M, Genovese M, Santi A, Pranzini E, Balestri F, **Piazza L**, Del Corso A, Avunduk S, Imperatore C, Menna M, Paoli P. Evidence of Insulin-Sensitizing and Mimetic Activity of the Sesquiterpene Quinone Avarone, a Protein Tyrosine Phosphatase 1B and Aldose Reductase Dual Targeting Agent from the Marine Sponge *Dysidea avara*. Pharmaceutics. 2023 Feb 4;15(2):528. doi: 10.3390/pharmaceutics15020528. PMID: 36839851; PMCID: PMC9964544.
4. Genovese M, Imperatore C, Casertano M, Aiello A, Balestri F, **Piazza L**, Menna M, Del Corso A, Paoli P. Dual Targeting of PTP1B and Aldose Reductase with Marine Drug Phosphoeleganin: A Promising Strategy for Treatment of Type 2 Diabetes. Mar Drugs. 2021 Sep 24;19(10):535. doi: 10.3390/md19100535. PMID: 34677434; PMCID: PMC8540617.